공학박사 학위논문

Robust and Interference-Resilient MAC/PHY Layer Strategies for WLANs

WLAN의 신뢰성 및 간섭 회피를 위한 MAC/PHY 기법

2018년 2월

서울대학교 대학원

전기·컴퓨터공학부

변 성 호

Abstract

Thanks to the explosive growth of mobile devices such as smartphones and tablet PCs, IEEE 802.11 wireless local area network (WLAN), often referred to as WiFi, has become one of the most successful wireless access technologies, supporting ever increasing demand for high data rates at relatively low cost. Encouraged by this remarkable success, the state-of-the-art IEEE 802.11 WLAN provides a physical layer (PHY) data rate of Gb/s to a single user in the 5 GHz unlicensed band, by enabling multi-input and multi-output (MIMO) technology, which utilizes multiple antennas at both transmitter and receiver, and channel bonding which aggregates multiple 20 MHz channels up to 160 MHz bandwidth. Furthermore, as a key feature to enhance medium access control (MAC) efficiency, IEEE 802.11 standard defines frame aggregation called aggregate MAC protocol data unit (A-MPDU), which amortizes PHY protocol overhead over multiple frames by packing several MPDUs into a single frame.

In this dissertation, we propose the following three strategies to enhance throughput performance in practice: (1) Mobility-aware PHY rate and A-MPDU length control, (2) Receiver-driven operating channel width adaptation, and (3) Receive architecture for eliminating time-domain interference not overlapping with the desired signal in frequency-domain.

Firstly, a significant growth of mobile data traffic volume, primarily generated by portable devices, has led to a change of WLAN communication environments; the wireless channel condition in WLAN system is no longer quasi-stationary over the duration of a single frame reception. Especially, frame aggregation, i.e., A-MPDU, which lengthens frame duration significantly, causes the channel state information (CSI) obtained at the preamble can be no longer valid for successfully decoding the latter part of A-MPDUs, when the channel condition substantially changes during the A-MPDU reception. To cope with this problem, we analyze the wireless channel dynamics con-

sidering mobility through extensive measurements, and we then build a model which represents the impact of mobility with a noise vector in the I-Q plane, to investigate how the mobility affects the A-MPDU reception performance. Based on our analysis, we develop *STRALE*, a ***st***andard-compliant and mobility-aware PHY ***ra***te and A-MPDU ***le***ngth adaptation scheme with ease of implementation. Through extensive simulations with 802.11ac using ns-3 and prototype implementation with commercial 802.11n devices, we demonstrate that *STRALE* achieves up to 2.9× higher throughput, compared to a fixed duration setting according to IEEE 802.11 standard. *STRALE* simply requires to update device driver only at one end of the wireless link (i.e., transmitter), thus allowing it to be applicable to any kind of platforms.

Second, IEEE 802.11ac supports bandwidth of 20, 40, and 80 MHz as a mandatory feature, and optionally supports 160 MHz bandwidth. To transmit and receive packets using such wide bandwidth, the 802.11ac devices need to increase the size of fast Fourier transform (FFT), equivalently, the baseband bandwidth, referred to as *operating channel width* (OCW). However, our experiment results reveal various situations where bandwidth adaptation without changing the receiver's OCW, leads to poor reception performance due surprisingly to *time-domain interference* not overlapping with the incoming desired signal in frequency domain. To cope with this problem, we develop *RECONN*, a standard-compliant and receiver-driven OCW adaptation scheme with ease of implementation. Our prototype implementation in commercial 802.11ac devices shows that *RECONN* achieves up to 1.85× higher throughput by completely eliminating time-domain interference. To our best knowledge, this is the first work to discover the time-domain interference problem, and to develop OCW adaptation scheme in 802.11ac system.

Finally, based on the observation that time-domain interference causes 1) *packet detection and synchronization failure*, 2) *undesirable receive locking problem*, and 3) *automatic gain control (AGC) failure*, we propose a receive architecture called *REAC-*

TER to eliminate the impact of time-domain interference: *REACTER* digitally extracts the desired preamble signal not affected by time-domain interference, and provides interference-resilient A-MPDU reception performance by real-time AGC level adaptation during A-MPDU reception. The proposed receive architecture extensively evaluated via IT++ based link-level simulator, and the simulation results show that *REACTER* significantly improves the frame reception performance by completely eliminates the impact of time-domain interference.

In summary, we identify the two existing problems through the extensive measurement and simulations, and we then propose compelling algorithms to improve the throughput performance. We demonstrate the feasibility of our approaches by implementing prototypes in off-the-shelf commercial 802.11n/ac devices, showing that our proposed algorithms fully comply with the 802.11 MAC and requires no PHY modification such that it can be applicable to the existing hardware platform by simply updating the device driver only at one end of the wireless link. Furthermore, we present a novel receive architecture which shows the ability to fundamentally enhance the performance of wide bandwidth operation with very low cost and complexity.

Keywords: IEEE 802.11 wireless local area network (WLAN), Wi-Fi, aggregate MPDU (A-MPDU), mobility, channel estimation, baseband, operating channel width, automatic gain control (AGC), prototype design

Student number: 2013-30965

Robust and Interference-Resilient MAC/PHY Layer Strategies for WLANs

Contents

Abstract **i**

Contents **iv**

List of Tables **viii**

List of Figures **ix**

1 Introduction **1**

1.1 Motivation 1

1.2 Overview of Existing Approach 3

1.2.1 A-MPDU Length Adaptation 3

1.2.2 Wide Bandwidth Operation in IEEE 802.11ac WLANs 4

1.2.3 Receive Architecture for WLAN Devices 5

1.3 Main Contributions 6

1.3.1 Mobility-Aware PHY Rate and A-MPDU Length Adaptation . 6

1.3.2 Receiver-Driven Operating Channel Width Adaptation 7

1.3.3 Rx Architecture for Eliminating Time-Domain Interference . 7

1.4 Organization of the Dissertation 8

2 *STRALE*: Mobility-Aware PHY Rate and A-MPDU Length Adaptation in IEEE 802.11 WLANs **10**

2.1 Introduction 10

2.2 Preliminaries . . . 12
2.2.1 Channel Estimation and Compensation . . . 12
2.2.2 Frame Aggregation . . . 14
2.2.3 Modulation and Coding Schemes . . . 15
2.2.4 MIMO, SM, STBC and channel bonding . . . 15
2.3 Case Study . . . 16
2.3.1 Experimental Setting . . . 16
2.3.2 Temporal Selectivity . . . 17
2.3.3 Impact of Mobility . . . 18
2.3.4 Impact of MCSs . . . 21
2.3.5 IEEE 802.11n/ac Features . . . 22
2.3.6 Rate Adaptation: *Minstrel* . . . 23
2.4 Caudal Noise Model . . . 25
2.4.1 Caudal Noise Modeling for $n \times n$ MIMO Channel . . . 26
2.4.2 Impact of Caudal Noise . . . 28
2.5 *STRALE*: Proposed Algorithm . . . 30
2.5.1 Possible Solutions for Caudal Loss Problem . . . 31
2.5.2 Operation of *STRALE* . . . 32
2.6 Performance Evaluation . . . 37
2.6.1 Methodology . . . 37
2.6.2 Simulation Results . . . 39
2.6.3 Prototype Implementation . . . 44
2.7 Summary . . . 46

3 *RECONN*: Receiver-Driven Operating Channel Width Adaptation in IEEE 802.11ac WLANs 48

3.1 Introduction . . . 48
3.2 Preliminaries . . . 51
3.2.1 Packet Detection and Initial Synchronization . . . 51

3.2.2 Wide Bandwidth Operation 52
3.3 Cast Study 53
3.3.1 Motivation 55
3.3.2 Packet Detection and Synchronization Failure 57
3.3.3 Receive Locking to Interference Signal 59
3.3.4 AGC Failure 61
3.4 *RECONN*: Proposed Algorithm 64
3.4.1 Possible Solutions 64
3.4.2 *RECONN* 67
3.5 Performance Evaluation 70
3.5.1 One-to-One Scenario 72
3.5.2 Multi-station Scenario 74
3.6 Summary 75

4 *REACTER*: Receive Architecture for Eliminating Time-Domain Interference 76

4.1 Introduction 76
4.2 Preliminaries 78
4.2.1 Packet Detection and Synchronization 78
4.2.2 Automatic Gain Control in IEEE 802.11 WLAN 80
4.3 *REACTER*: Proposed Architecture 80
4.3.1 Simulation Methodology 80
4.3.2 Digital Low Pass Filter (DLPF) 82
4.3.3 Real-Time AGC 89
4.3.4 Structure of *REACTER* 96
4.4 Performance Evaluation 100
4.5 Summary 101

5 Concluding Remarks **102**

5.1 Research Contributions 102

5.2 Future Work 103

Abstract (In Korean) **112**

감사의 글 **115**

List of Tables

2.1 MCS information. 21
2.2 Throughput and SFER using *Minstrel* 23

List of Figures

2.1 IEEE 802.11n/ac PPDU (mixed) frame format of A-MPDU. A receiver estimates the channel conditions to obtain CSI by using training symbols. 13

2.2 A-MPDU and BlockAck exchange. BlockAck can acknowledge up to 64 consecutive MPDUs with a fixed-size bitmap. 15

2.3 Floor plan (22 m $\times$ 14 m). 16

2.4 CDF of the normalized amplitude changes with varying time gap, τ. . 17

2.5 Impact of mobility. We calculate BER using the fixed subframe length and SFER statistics obtained from the experiments. 19

2.6 SFER according to subframe location. 21

2.7 SFER of various 802.11n/ac features. 22

2.8 Rate distribution on *Minstrel*. Because we use the 802.11n NIC, MCS notation, in this figure, follows the definition from IEEE 802.11n standard: for exmaple, MCS 15 matches to 64-QAM with 5/6-code rate using two spatial streams. 24

2.9 Error vector caused by mobility in the I-Q plane. 26

2.10 WINNER channel model II simulation results according to user mobility (different marks) and SNR at the PLCP preamble (different colors) 29

2.11 BER comparison between simulation and measurement results from Atheros AR9380 and Intel IWL5300 NICs. 30

2.12 The optimal PHY rate (dotted line) and A-MPDU length (line) for the given user mobility and CSIs. 31
2.13 Detailed operation of *STRALE*. 34
2.14 Simulation results for one-to-one scenario: *STRALE* shows the best throughput performance under any circumstances, when user moves 0.8 m/s. 38
2.15 MCS and spatial stream (SS) distribution used at 30 m distance. . . . 40
2.16 Simulation results of multiple station scenario: *STRALE* provides 59.9% and 14.3% higher throughput than those of baseline 802.11ac and *MoFA*. 41
2.17 Experiment results: *STRALE* shows the best performance by jointly adapting PHY rate and A-MPDU length according to the degree of user mobility. 43
2.18 PHY rate distribution measured between P1 and P2. 45

3.1 Spectrum example in which the time-domain interference degrades reception performance. Time-domain interference can be eliminated by reducing OCW to 40 MHz. 49
3.2 Structure of the legacy preamble identical to 802.11a preamble. 51
3.3 Floor plan of our experiments (22 m $\times$ 12 m). Each point represents locations where devices are deployed. 53
3.4 Uplink throughput obtained by AC3200 and AC2600 according to tSIR. The interference is generated by NI USRP with 802.11 AF, where no frequency overlapping exists. 54
3.5 Average packet detection and time/frequency synchronization measurement results obtained by NI USRP based on Schmidl and Cox algorithm. 57
3.6 Normalized auto-correlation magnitude according to time sample index measured by NI USRP. 58

3.7 Uplink throughput and two types of error rate according to the different interference patterns when tSIR is 6 dB. 60
3.8 Uplink throughput and two types of error rate measured by using AC2600, according to three different interference patterns. 62
3.9 CDF of duration in which subframe errors occur within an A-MPDU. 63
3.10 Example of decreasing OCW due to time-domain interference: A-MPDU loss triggers spectral scan, while A-MPDU reception continues. If the receiver detects the interference, in this case, at the secondary 40 MHz channel, it sends an operating mode notification frame to the transmitter prior to reducing OCW to 40 MHz. After receiving 40 MHz A-MPDU, the receiver finally reduces OCW in order to receive A-MPDUs scheduled to be transmitted over 80 MHz channels. . 65
3.11 Example of increasing OCW: Expiration of N_{wnd} triggers probing, where the receiver increases OCW to 80 MHz, and conducts spectral scan. Because time-domain interference does not exist, the receiver decides to remain on 80 MHz OCW, and hence, sends a operating mode notification frame to the transmitter. 66
3.12 Implementation structure of *RECONN*. 70
3.13 Measurement results obtained by the receiver according to tSIR. The transmitter is AC2600 and the interference is generated by NI USRP. . 71
3.14 Snapshot of instantaneous throughput when tSIR is -12 dB. Interference is turned on at 9 s and turned off between 18 s and 19 s. 73
3.15 Multi-station environment. *RECONN* achieves 1.49$\times$ higher network throughput than that of *Baseline*, when the interference exists. 74

4.1 Structure of the legacy preamble identical to 802.11a preamble. 79
4.2 Structure of IT++ based IEEE 802.11ac link-level simulator. 81

4.3 Spectrum usage for our simulation. The 20 MHz time-domain interference signal is generated on channel 48 (i.e., on the 20 MHz channel within the secondary 40 MHz channels). 82
4.4 Packet detection and synchronization performance according to SNR, when the transmission bandwidth is 20 MHz. 83
4.5 Packet detection and synchronization performance according to SNR, when the transmission bandwidth is 80 MHz. 84
4.6 Time-domain interference causes undesirable packet detection and synchronization failure, when time-domain interference arrives first. In this scenario, extracting the primary channel using 20 MHz DLPF can effectively eliminate the impact of time-domain interference. 86
4.7 Packet detection and synchronization performance according to tSIR. 87
4.8 Time-domain interference causes clipping, exceeding ADC dynamic range. 90
4.9 ADC noise contributions. 91
4.10 SFER and the number of clipping results according to tSIR, when time-domain interference overlaps with the desired A-MPDU reception. 92
4.11 Average SFER according to subframe index, when time-domain interference entirely or partly overlaps with the desired A-MPDU. 93
4.12 Normalized pEVM and pEVP according to OFDM symbol index, when tSIR is -10 dB. 94
4.13 Structure of *REACTER*. Digital time-domain samples pass DLPF of 20 MHz for packet detection and synchronization. Based on clipping feedback from ADC and the measured time-samples power, AGC level is adjusted in real-time. 95

4.14 SFER and the number of clipping events for according to tSIR, when time-domain interference partly or entirely overlaps with the desired A-MPDU. 98
4.15 Average SFER according to subframe index, when time-domain interference partly overlaps with the desired A-MPDU from the 13-th subframe to 48-th subframe. 99

Chapter 1

Introduction

1.1 Motivation

Over the last few years, with the dramatic growth of mobile devices such as smartphones and table PCs, IEEE 802.11 wireless local area network (WLAN), often referred to as WiFi, has become an essential and indispensable part of our everyday life, supporting ever increasing demand of users for various types of services. Encouraged by this remarkable success, state-of-the-art IEEE 802.11ac WLAN provides a physical layer (PHY) data rate of Gb/s to a single user in the 5 GHz unlicensed band [1].

As key features to enhance throughput performance, IEEE 802.11 specifications defines two types of aggregation techniques in either *time and/or frequency* domain: (1) frame aggregation called aggregate MAC protocol data unit (A-MPDU) to enhance medium access control (MAC) efficiency which amortizes protocol overhead over multiple MPDUs in time-domain, and (2) wide bandwidth operation called channel bonding, to increase the number of data subcarriers by aggregating several 20 MHz channels up to 160 MHz bandwidth in frequency domain. Although the aggregation in time and frequency provides the higher achievable throughput, we have shown the real-world limitations of the new features as follows.

Frame aggregation in time-domain: Designed primarily for indoor and nomadic

environments, where the wireless channel does not dynamically change during a single frame reception, WLAN receiver conducts the channel estimation only once during the preamble reception (i.e., at the beginning of a frame). However, a significant growth of mobile data traffic volume, primarily generated by portable devices, has led to a change of WLAN communication environments; the wireless channel condition in WLAN system is no longer quasi-stationary over the duration of a single frame reception. Especially, frame aggregation, which lengthens frame duration significantly, causes the channel state information (CSI) obtained at the preamble can be no longer valid for successfully decoding the latter part of A-MPDUs, when the channel condition substantially changes during the A-MPDU reception. In such cases, subframe error rate (SFER) significantly increases as the time gap between the preamble and subframe increases. This is referred to as *caudal loss* [2, 3].

Channel bonding in frequency-domain: To transmit and receive packets using such wide bandwidth, 802.11ac devices need to increase the size of fast Fourier transform (FFT), equivalently, twice the baseband bandwidth, referred to as *operating channel width* (OCW), without changing the data subcarrier spacing of 312.5 kHz. Understandingly, it is possible to transmit and receive a packet using the bandwidth less than or equal to OCW.[1] Therefore, the use of wide channel bandwidth has greatly contributed to throughput performance improvement, but our experiment results have revealed strong evidence that using the bandwidth less than OCW causes *time-domain interference problem*, not overlapping with the desired signal in frequency-domain, but leading to poor throughput performance. More seriously, changing the baseband bandwidth for every packet is impossible in WLAN system, since the switching delay is known to be several tens of microseconds due to the reconfiguration delay of hardware such as RF front end [4]. This problem might become severer in coexistence with other emerging technologies such as IEEE 802.11ax or LTE-LAA, as well as due to bandwidth heterogeneity of the existing WLAN devices [5, 6].

[1] Given that, once OCW is set, it is hardly changed.

1.2 Overview of Existing Approach

1.2.1 A-MPDU Length Adaptation

There have been several studies on frame aggregation in the literature. An analytical framework to evaluate the performance of the 802.11n frame aggregation is presented in [7]. In [8, 9], the authors propose algorithms to optimize A-MPDU subframe length according to the channel condition. However, all these studies are based on an impractical assumption that all subframes experience the same signal-to-noise ratio (SNR) distribution, and hence, aggregating more subframes into an A-MPDU always results in higher throughput.

In [2], we have proposed a mobility-aware frame length adaptation algorithm, which dynamically adapts A-MPDU length during run-time by observing the increase of SFER in the latter part of A-MPDU. However, this scheme does not take PHY rate adaptation into account, while we have found that using lower modulation and coding scheme (MCS) index often enhances the throughput performance in mobile environments, by making transmission more robust to caudal loss as well as channel degradation. On the other hand, Lee *et al.* propose an intra-frame rate control algorithm to alleviate caudal loss in fast time-varying environments [10]. However, not only a single MCS index can be assigned to a single frame in IEEE 802.11 system, but also decision on when and how to decrease MCS index within an A-MPDU is still complicate.

Additionally, robust channel estimation techniques are proposed in [3, 11]. The former proposes mid-amble aided channel estimation technique for long frames in high mobility vehicular radio channel, and the latter proposes a practical channel estimation and tracking scheme for WLAN receivers. However, these approaches are costly and impractical for large-scale adoption, because they incur additional protocol/computational overhead, and/or do not comply with the existing hardware, which are undesirable for practical WLAN systems.

1.2.2 Wide Bandwidth Operation in IEEE 802.11ac WLANs

Since the publication of IEEE 802.11ac standard [1], several papers have provided an overview of 802.11ac amendment. In [12] and [13], the authors have introduced the core 802.11ac technologies, especially, wide bandwidth operation and multi-user multiple input multiple output (MU-MIMO). The work in [14] provides an insight of the necessity of dynamic bandwidth switching through simulation results. In [15], Gong *et al*. propose a MAC protection scheme that combats hidden nodes on secondary channels.

Basically, wide bandwidth operation in 802.11ac WLAN provides higher PHY data rates, achieving Gb/s throughput for individual users. However, transmissions using wider bandwidth are more likely to suffer from frequency selective fading, which causes signal-to-noise ratio (SNR) variations across the entire subcarriers. Additionally, fixed total transmission power and bandwidth heterogeneity with legacy devices cause potential hidden interference and frequency under-utilization problem, thus providing lower throughput. To solve these problems, decentralized bandwidth adaptation algorithms based on measurements are proposed in [16–18]. In [19–21], the authors propose centralized (primary) channel and bandwidth allocation methods to achieve higher throughput by reducing hidden interference.

Moreover, analytic frameworks to evaluate the performance of wide bandwidth operation are presented in [22–24]. The authors have verified various characteristics and problems of wide bandwidth operation in multiple basic service set (BSS) environment. Besides, several studies have focused on enhancing channel access mechanism or adjusting clear-channel-assessment (CCA) threshold [25–28], because sharing wide bandwidth increases contention level and reduces channel utilization.

However, none of the existing studies deals with the time-domain interference problem, where the receiver's baseband includes interference signal, the reception performance decreases even if the desired signal does not overlap with the interference on frequency domain.

1.2.3 Receive Architecture for WLAN Devices

Automatic Gain Control

There have been several studies on automatic gain control (AGC) circuit for WLAN receiver in the literature. In WLAN system, AGC needs to be settled within a few microseconds during the reception of preamble, some of the existing work enhances AGC performance to provide fast and stable gain control [29–31]. In [29], the authors deal with accuracy requirements for implementation of AGC and synchronization, providing a complete set of thresholds for the practical time and frequency synchronization subblocks. Singerl *et al.* propose an efficient method to obtain accurate and fast power estimates of the input signal [30]. In [31], the authors provides a new open-loop and multi-step AGC algorithm for OFDM system with CMOS circuit design. However, none of the existing studies deals with the time-domain interference problem, which causes both high quantization error in the I-Q plane, and clipping in analog-to-digital-converter (ADC) circuit.

Packet Synchronization

In WLAN system, packet detection and synchronization algorithm can vary depending on the implementation [32–35]. Schmidl and Cox algorithm uses auto-correlation of legacy short training field (L-STF) to detect and synchronize the incoming packet [32], and Chang *et al.* propose a joint algorithm which employs both auto-correlation and cross-correlation results of L-STF to accurately synchronize the incoming packet, since cross-correlation is well known to be robust to noise figure [33]. In [34, 35], the authors uses cross-correlation of legacy long training field (L-LTF) as well as auto-correlation of L-STF to synchronize the incoming packet, because L-LTF has a four times longer duration than L-STF's duration, which provides the better cross-correlation property. However, none of the existing work copes with wide bandwidth operation which uses up to 160 MHz bandwidth for packet transmission and reception.

Especially, since time-domain interference deteriorates synchronization performance, a new method to eliminate the impact of time-domain interference for packet detection and synchronization is required.

1.3 Main Contributions

The main objective of this dissertation is to provide robust and time-domain interference-resilient MAC/PHY layer strategies for IEEE 802.11 WLANs, to exploit the high achievable throughput of emerging aggregation technologies in time and frequency. Therefore, we propose compelling algorithms, *STRALE*, mobility-aware PHY rate and A-MPDU length adaptation method, and *RECONN*, receiver-driven operating channel width adaptation scheme. Moreover, we suggest a novel receive architecture, *REACTER*, to eliminate the impact of time-domain interference for packet detection and synchronization, in addition to provide real-time AGC level control during the A-MPDU reception.

1.3.1 Mobility-Aware PHY Rate and A-MPDU Length Adaptation

We first analyze the wireless channel dynamics considering mobility in IEEE 802.11 WLAN through extensive measurements. From this, we reveal the fundamental problem of existing frame aggregation schemes manifested over a wide range of mobility and IEEE 802.11n/ac PHY features. Moreover, we build a model that represents the impact of mobility with a noise (called *caudal noise*) in the I-Q plane, analyzing how the mobility affects the A-MPDU reception in WLAN environments. To cope with caudal loss problem, we develop *STRALE*, a ***st***andard-compliant and mobility-aware PHY ***ra***te and A-MPDU ***le***ngth adaptation scheme with ease of implementation. To verify the performance and feasibility, we implement the proposed *caudal noise* model and *STRALE* into 802.11ac model of network simulator 3 (ns-3) [36], and make a prototype using commercial 802.11n network interface card (NIC) by modifying the device

driver, *ath9k* [37,38]. *STRALE* simply requires device driver update only at one end of the wireless link (i.e., transmitter), thus allowing it to be applicable to any kind of platforms. Our extensive simulations and experiments with prototype under a wide range of scenarios show that *STRALE* achieves up to 2.9× higher throughput, compared to a fixed duration setting (i.e., the maximum frame duration according to IEEE 802.11n/ac standard).

1.3.2 Receiver-Driven Operating Channel Width Adaptation

We analyze the impact of time-domain interference in IEEE 802.11ac through extensive measurements using commercial off-the-shelf 802.11ac devices and software defined radio (SDR) platform. From this, we reveal that bandwidth adaptation without changing OCW causes packet detection and synchronization failure, undesirable receive locking problem, and AGC failure, when the baseband contains time-domain interference signal, not overlapping with the desired signal on frequency domain. To cope with time-domain interference problem, we develop *RECONN*, a standard-compliant and ***rec***eiver-driven ***o***perating cha***nn***el width adaptation scheme with ease of implementation. *RECONN* adaptively switches OCW using the frequency domain information obtained by receiver with very low overhead. *RECONN* fully complies with 802.11 MAC and does not require hardware modification. To verify the excellence and feasibility, we implement *RECONN* on the Linux-based open-source device driver, including *ath10k* and *mac80211*, and make a prototype using commercial 802.11ac NIC. Our extensive experiments under a wide range of scenarios show that *RECONN* enhances throughput performance up to 1.85× by completely eliminating time-domain interference.

1.3.3 Rx Architecture for Eliminating Time-Domain Interference

We first analyze the effect of digital low pass filter (DLPF), on packet detection and synchronization performance, depending on an incoming signal's bandwidth and the

signal strength of time-domain interference, through extensive link-level simulations. Moreover, we verify that time-domain interference not overlapping with the desired packet causes that 1) ADC operates in a range smaller than its optimal range, thus leading to high quantization error, and 2) the analog signal can exceed the dynamic range of ADC so that clipping can occur, resulting in signal distortions. In such scenarios, subframes can be successfully received by adapting AGC level in real-time, since the desired signal does not overlap on the frequency domain with time-domain interference, and A-MPDU subframes can be individually acknowledged by using block acknowledgement (BlockAck). Consequently, we develop *REACTER*, a ***re***ceive ***a******rc***hitecture for eliminating the impact of ***t***ime-domain int***er***ference, fully complying with the 802.11 specifications. *REACTER* improves packet detection and synchronization performance using DLPF, and conducts real-time AGC during A-MPDU reception to reduce quantization error and to prevent clipping at ADC. Regardless of the incoming signal's bandwidth, *REACTER* can be applied immediately upon the reception of the desired packets, without incurring any protocol overhead and latency. Our extensive simulation under a wide range of scenarios show that *REACTER* enhances the reception performance significantly by completely eliminating the impact of time-domain interference.

1.4 Organization of the Dissertation

The rest of the dissertation is organized as follows.

Chapter 2 presents *STRALE*, the standard-compliant and mobility-aware PHY rate and A-MPDU length adaptation scheme with *caudal noise* model. We evaluate the performance of *STRALE* based on prototype evaluation on the commercial 802.11n NIC and extensive simulation using ns-3.

In Chapter 3, we presents the impact of time-domain interference in IEEE 802.11ac WLAN networks, and then, propose *RECONN*, the receiver-driven OCW adaptation

scheme to eliminate time-domain interference. The performance of *RECONN* is heavily evaluated via prototype implementation on the commercial 802.11ac NIC.

Chapter 4 presents the proposed receive architecture, *REACTER*, which consists of 20 MHz DLPF and real-time AGC during A-MPDU reception. *REACTER* shows the ability to fundamentally enhance the reception performance against time-domain interference with very low cost and complexity.

Finally, Chapter 5 concludes this dissertation with the summary of contributions and discussion on the future work.

Chapter 2

STRALE: Mobility-Aware PHY Rate and A-MPDU Length Adaptation in IEEE 802.11 WLANs

2.1 Introduction

Designed primarily for indoor and nomadic environments, where the wireless channel does not dynamically change during a single frame reception, WLAN receiver conducts the channel estimation only once during the preamble reception (i.e., at the beginning of a frame). However, a significant growth of mobile data traffic volume, primarily generated by portable devices, has led to a change of WLAN communication environments; the wireless channel condition in WLAN system is no longer quasi-stationary over the duration of a single frame reception. Especially, frame aggregation, which lengthens frame duration significantly, causes the channel state information (CSI) obtained at the preamble can be no longer valid for successfully decoding the latter part of A-MPDUs, when the channel condition substantially changes during A-MPDU reception. In such cases, subframe error rate (SFER) significantly increases as the time gap between the preamble and subframe increases, which results in throughput degradation, even if an appropriate PHY rate is selected. This is referred to as *caudal loss* [2, 3].

The primary contribution of this dissertation is to precisely analyze the impact of caudal loss, and to propose a mobility-aware physical layer (PHY) rate and frame aggregation length adaptation algorithm designed to minimize caudal loss in a variety of scenarios. Our major contributions are summarized as follows.

- We first analyze the wireless channel dynamics considering mobility in IEEE 802.11 WLAN through extensive measurements. From this, we reveal the fundamental problem of existing frame aggregation schemes manifested over a wide range of mobility and IEEE 802.11n/ac PHY features.

- We build a model that represents the impact of mobility with a noise (called *caudal noise*) in the I-Q plane, analyzing how the mobility affects the A-MPDU reception in WLAN environments.

- We develop *STRALE*, a ***st***andard-compliant and mobility-aware PHY ***ra***te and A-MPDU ***le***ngth adaptation scheme with ease of implementation.

- We implement the proposed *caudal noise* model and *STRALE* into 802.11ac model of network simulator 3 (ns-3) [36], and make a prototype using commercial 802.11n network interface card (NIC) by modifying the device driver, *ath9k* [37,38]. *STRALE* simply requires device driver update only at one end of the wireless link (i.e., transmitter), thus allowing it to be applicable to any kind of platforms.

- Our extensive simulations and experiments with prototype under a wide range of scenarios show that *STRALE* achieves up to 2.9$\times$ higher throughput, compared to a fixed duration setting (i.e., the maximum frame duration according to IEEE 802.11n/ac standard).

To the best of our knowledge, this is the first work that dynamically adapts PHY rate and A-MPDU length robust against time-varying channels caused by mobility. We expect *STRALE* to contribute the performance enhancement of low error tolerance real-time applications such as online gaming and/or video streaming on a mobile device.

The rest of this chapter is organized as follows. Section 2.2 introduces the background of IEEE 802.11 systems, and Section 2.3 shows empirical study of the impact of mobility on IEEE 802.11 systems. In Section 2.4, we propose and verify *caudal noise* model. Detailed design of *STRALE* is presented in Section 2.5, and its implementation and simulation/experimental results are presented in Section 2.6. Finally, Section 2.7 summarizes this chapter.

2.2 Preliminaries

2.2.1 Channel Estimation and Compensation

Signal transmitted in wireless communication system is affected by pathloss, fading, shadowing, and noise. To compensate such distortions and decode orthogonal frequency division multiplexing (OFDM) data symbols, 802.11 receiver is required to obtain accurate CSI from the physical layer convergence protocol (PLCP) preamble at the beginning of a PHY layer protocol data unit (PPDU). Fig. 2.1 demonstrates IEEE 802.11n/ac mixed-mode PPDU frame format of A-MPDU. The legacy preamble identical to the fields used in IEEE 802.11a is composed of legacy short training field (L-STF) and legacy long training field (L-LTF), which are followed by a signal field (L-SIG). L-STF is used for signal detection, automatic gain control (AGC), timing synchronization, and coarse frequency offset estimation. L-LTF allows the receiver to obtain the CSI and fine frequency offset. On the other hand, (V)HT-STF included in the (V)HT preamble provides an enhanced AGC for multiple-input multiple-output (MIMO) system and (V)HT-LTFs are used to measure MIMO channel [1, 39].

Furthermore, the multi-path of the wireless channel and clock difference of the local oscillators between the transmitter and receiver induces symbol time offset (STO) and residual carrier frequency offset (CFO), which result in a phase rotation linearly proportional to the subcarrier index in frequency domain and linearly proportional to the OFDM symbol index in time domain, respectively [40]. Hence, evenly spread pi-

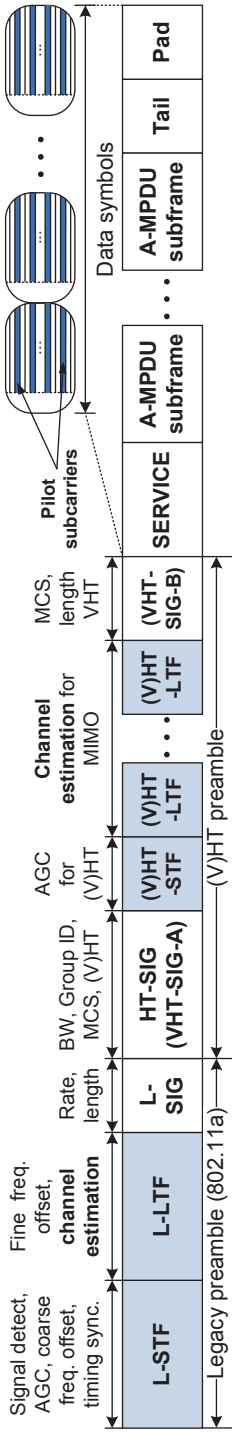

Figure 2.1: IEEE 802.11n/ac PPDU (mixed) frame format of A-MPDU. A receiver estimates the channel conditions to obtain CSI by using training symbols.

lot subcarriers are embedded in each OFDM data symbol to enable coherent detection during the frame reception, by linearly interpolating the measured phases. For example, the 802.11n/ac standard dedicates 4 out of 56 subcarriers to pilot subcarriers for 20 MHz bandwidth. Unfortunately, pilot subcarriers in WLAN system are insufficient to successfully compensate the CSI variations of each data subcarrier during the frame reception, since frequency spacing between pilot subcarriers ($4,375$ kHz) is too broad to cover delay spread in typical WLAN environments [41]. Accordingly, when the channel significantly changes due to user mobility, the CSI obtained at the preamble becomes insufficient to accurately decode OFDM data symbols at the latter part of a long frame.

2.2.2 Frame Aggregation

Frame aggregation is a core feature of IEEE 802.11n/ac to send multiple frames in a single transmission. Every data frame has a significant amount of overhead including PLCP preamble, MAC/PHY header, acknowledgement (ACK) transmission, and several Inter Frame Spaces (IFSs). These overheads often consume bandwidth comparable with the actual data payload, which results in much lower throughput compared with the underlying PHY data rate. To address this issue, the 802.11 standard defines aggregate MPDU (A-MPDU), which amortizes protocol overhead over multiple frames by aggregating multiple MPDUs into a single one as shown in Fig. 2.1 [1, 39].

A-MPDU considerably enhances MAC efficiency even in high error rate environment thanks to frame check sequence (FCS) in each subframe, because all individual subframes are positively/negatively acknowledged by the receiver using block acknowledgments (BlockAcks), and hence, can be individually retransmitted as shown in Fig. 2.2. Note that aggregating more subframes reduces protocol overhead, but long frame duration intensifies caudal loss in mobile environments, thus resulting in throughput degradation.

A-MPDU length is limited by both size and transmission time: 1) the maximum

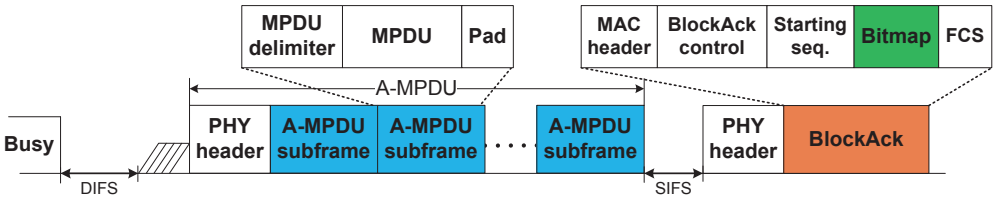

Figure 2.2: A-MPDU and BlockAck exchange. BlockAck can acknowledge up to 64 consecutive MPDUs with a fixed-size bitmap.

A-MPDU size is 65,535 bytes for the 802.11n and 1,048,575 bytes for the 802.11ac, and 2) the transmission time of an A-MPDU should be smaller than the maximum PPDU duration, *aPPDUMaxTime*, defined as 10 ms and 5.484 ms for the 802.11n and 802.11ac, respectively. Throughout this chapter, we refer to *A-MPDU length* as its transmission time, unless specifically stated otherwise.

2.2.3 Modulation and Coding Schemes

Modulation and coding schemes (MCSs) defined in IEEE 802.11 are used to denote the combination of modulation (i.e., binary phase shift keying (BPSK), quadrature PSK (QPSK), and m-ary quadrature amplitude modulation (QAM)), and code rate. Recent 802.11 standard supports 10 MCSs from MCS 0 (BPSK and 1/2-rate code) to MCS 9 (256-QAM and 5/6-rate code). PHY rate then is determined by the combination of MCS, bandwidth, and number of spatial streams.

2.2.4 MIMO, SM, STBC and channel bonding

IEEE 802.11n/ac provides multi-input-multi-output (MIMO) operation which utilizes multiple antennas at both transmitter and receiver. There are two transmission techniques which use multiple antennas, namely spatial multiplexing (SM) and space-time block coding (STBC). SM transmits multiple data streams through multiple antennas to enhance PHY rate. On the other hand, STBC transmits multiple coded copies of a data stream through multiple antennas to improve the reliability. To increase PHY

rate, the 802.11n/ac also supports channel bonding which aggregates multiple 20 MHz channels up to 40 MHz bandwidth for the 802.11n and 160 MHz bandwidth for the 802.11ac, respectively.

2.3 Case Study

In this section, we firstly present our experiment setting, and then we provide the analysis of the wireless channel dynamics and its impact of A-MPDU reception performance based on measurements.

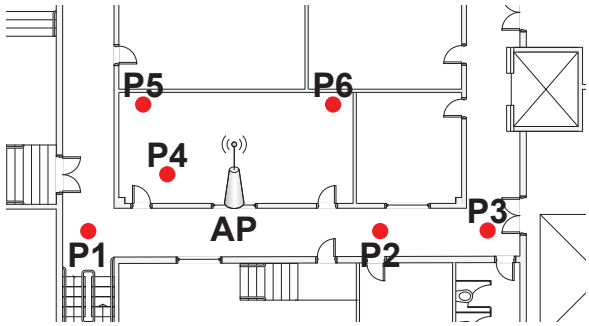

Figure 2.3: Floor plan (22 m $\times$ 14 m).

2.3.1 Experimental Setting

We have conducted our experiments in a controlled office environment, i.e., the basement of our building. Fig. 2.3 illustrates the floor plan used for our experiments, and points P1 to P6 represent different locations where stations are deployed. The operating channel is 44 with 5,220 MHz center frequency, where no external interference has been detected. We mainly use a programmable 802.11n device, Qualcomm Atheros AR9380 NIC, along with *hostAP* [42] to build an AP on a *Ubuntu* machine. Both AR9380 and IWL5300 (from Intel) NICs are utilized on the station side to evaluate the performance degradation on various WLAN devices [43]. We generate saturated UDP downlink traffic from the AP to stations using *Iperf* 2.0.5 with fixed MPDU length of

1,534 bytes including MAC header [44], and control A-MPDU length by modifying the device drivers *ath9k* and *iwlwifi* for AR9380 and IWL5300, respectively [37, 43]. For each set of experiment scenarios, we average the results of 5 runs, where each lasts for 120 s.

2.3.2 Temporal Selectivity

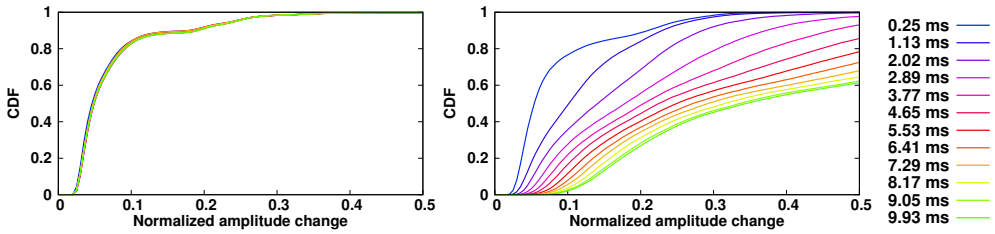

(a) Static case. (b) Mobile trace.

Figure 2.4: CDF of the normalized amplitude changes with varying time gap, τ.

To illustrate our findings, we first present the temporal selectivity of the wireless channel by using CSI statistics in static and mobile environments. For the mobile scenario, the station goes around between P1 and P2 at an average speed of 1 m/s. We collect CSI traces from IWL5300 NIC using the modified device driver at the receiver side [45]. Specifically, the NIC reports measured 40,000 CSIs from HT-LTFs for 30 subcarrier groups in the form of 1×3 matrix [39]. We enable one antenna at a sender and three antennas at a receiver. The sender broadcasts a NULL data frame with MCS 0 using 15 dBm transmit power every 250 μs.

We employ the following metric representing the normalized amplitude changes to evaluate the temporal selectivity [46]:

$$\frac{\|A(t) - A(t+\tau)\|_2}{\|A(t+\tau)\|_2}, \tag{2.1}$$

where the vector $A(t)$ represents all the subcarriers' amplitudes of the frame received at t, and τ is the time gap. $\|\cdot\|_2$ is the l^2-norm, and τ varies from 250 μs to 10 ms, which is *aPPDUMaxTime* for the 802.11n.

Fig. 2.4 shows the cumulative distribution function (CDF) of the normalized amplitude changes between CSI of two frames with varying τ. As shown in Fig. 2.4(a), the amplitude variation remains steady in the static scenario, resulting in the amplitude changes under 10%, for more than 85% of samples even for 10 ms of τ .

However, the amplitude variation increases with τ in the mobile scenario as shown in Fig. 2.4(b). When $\tau = 10$ ms, the amplitude varies by more than 10% between two consecutive frames for over 95% of samples. Furthermore, for over 55% of samples, the amplitude changes by more than 30%. Based on the result, it is trivial to expect that the error rate of the latter part of A-MPDU increases, because the channel estimation is performed only during the PLCP preamble reception as explained in Section 2.2.1.

To be more specific, we investigate the channel coherence time, which represents the time duration over which the wireless channel does not seem to be varying. Mathematically, it is defined as the time range over which the correlation coefficient of signal amplitudes is less than a threshold, i.e., 0.9, between two different signals [47] as follows:

$$\frac{\langle a_t a_{t+\tau}\rangle - \langle a_t\rangle\langle a_{t+\tau}\rangle}{\sqrt{\left[\langle {a_t}^2\rangle - \langle a_t\rangle^2\right]\left[\langle {a_{t+\tau}}^2\rangle - \langle a_{t+\tau}\rangle^2\right]}} \geq 0.9, \tag{2.2}$$

where a_t and $a_{t+\tau}$ represent the amplitudes of signals at time t and $t+\tau$, respectively, and $\langle x\rangle$ denotes the ensemble average of x. Using the obtained traces and (2.2), the measured coherence time for the scenario of 1 m/s average speed is about 3 ms, which is much shorter than *aPPDUMaxTime*, i.e., 10 ms and 5.484 ms for the 802.11n and 802.11ac, respectively.

2.3.3 Impact of Mobility

We now examine the A-MPDU reception performance, when mobility intensifies the time-varying nature of the wireless channel. As depicted in Section 2.3.1, we install a stationary AP equipped with AR9380, and use both AR9380 and IWL5300 on the station side. Saturated downlink traffic is sent from AP to a station which holds a

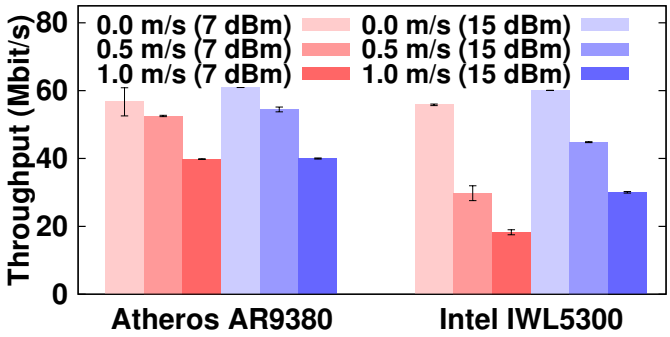

(a) Throughput results.

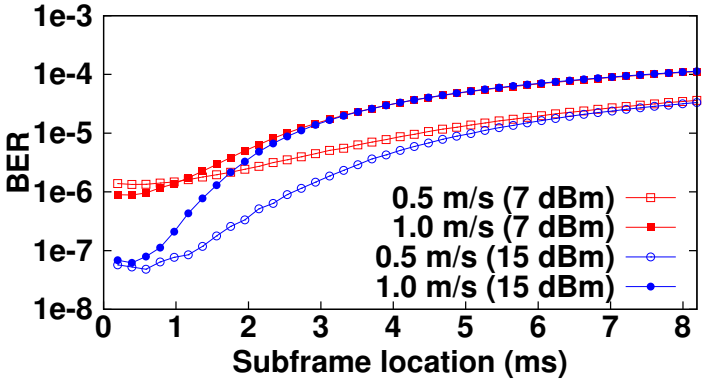

(b) BER of AR9380 NIC.

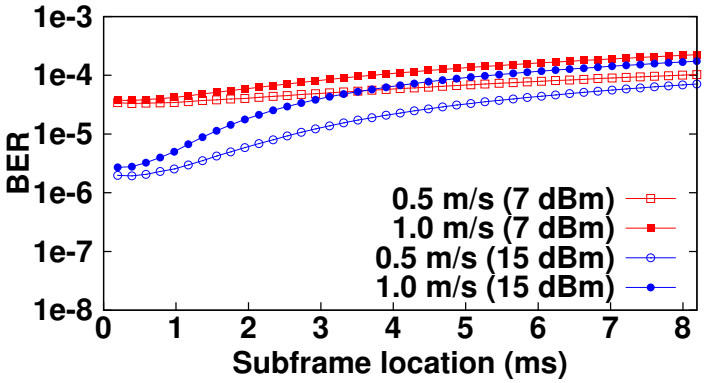

(c) BER of IWL5300 NIC.

Figure 2.5: Impact of mobility. We calculate BER using the fixed subframe length and SFER statistics obtained from the experiments.

position at P1 for the static scenario. For the mobile scenario, the station goes around between P1 and P2 at an average speed of 0.5 or 1 m/s. The size of each subframe is set to 1,538 bytes including MPDU delimiter and padding bits, and hence, an A-MPDU contains at most 42 subframes (due to byte-size limitation), which is transmitted by the fixed MCS 7 (65 Mb/s). Therefore, the actual transmission duration of a single A-MPDU becomes 8 ms.

Fig. 2.5(a) shows the received throughput of AR9380 and IWL5300 NICs. No matter how strong the transmission power is, throughput decreases as the user mobility increases for both cases, and the throughput losses become as high as one third and two thirds for AR9380 and IWL5300, respectively. Interestingly, within the range of the station's movement, signal-to-noise-ratio (SNR) remains very high, since the static station deployed at P1, i.e., the farthest position from AP, obtains the maximum throughput achieved by using MCS 7.

To investigate this further, we analyze the bit error rate (BER) performance. Fig. 2.5(b) shows the BER measured by AR9380 NIC on a logarithmic scale according to the subframe location, which stands for the transmission starting instant of the corresponding subframe relative to the beginning of the PPDU over the air. We observe that subframes in the latter part of A-MPDU experience higher BER, and the gradient of BER curves becomes higher as the user mobility increases. Additionally, BER curves converge depending on the mobility for both transmit powers (7 dBm and 15 dBm) regardless of the BER at the beginning of A-MPDU, since the mobility becomes the main cause of MPDU losses in the latter part of A-MPDU. In other word, even if the appropriate PHY rate is selected for transmission, this undesirable phenomenon, i.e. *caudal loss*, can occur, leading to throughput degradation. As shown in Fig. 2.5(c), the result of IWL5300 shows a similar tendency even if RF circuit structure, antenna gain, and receiver sensitivity of these two NICs are different.

In order to delve into the characteristics of caudal loss, we conduct additional experiments by changing MCS, bandwidth, and the number of spatial streams. For

the remaining experiments, we use only AR9380 NIC since AR9380 has shown more stable performance and also is easier to play with.

Table 2.1: MCS information.

	MCS 0	MCS 2	MCS 4	MCS 7
Modulation	BPSK	QPSK	16-QAM	64-QAM
Code rate	1/2	3/4	3/4	5/6
Data rate (Mbit/s)	6.5	19.5	39	65

2.3.4 Impact of MCSs

MCS is a critical factor determining the receiving performance as described in Section 2.2.3. Although the higher order MCS achieves the higher PHY rate, it is vulnerable not only to the channel degradation but also to mobility, since constellation points are closer from each other and coding gain is generally smaller. To verify this, we conduct experiments by changing MCSs for a given mobility. Table 2.1 summarizes the detailed information of MCSs used in this measurement.

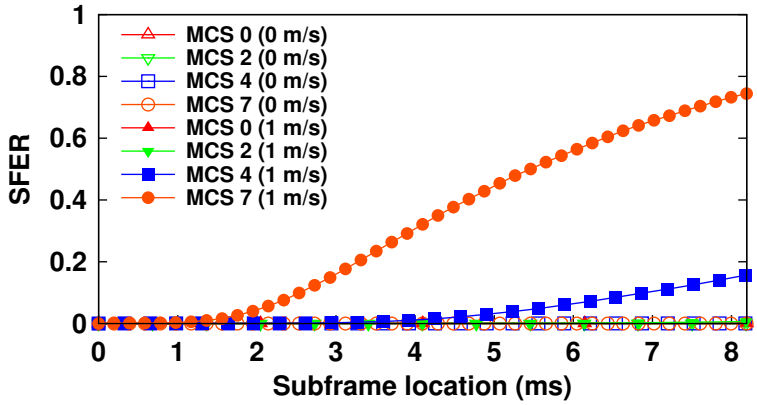

Figure 2.6: SFER according to subframe location.

Fig. 2.6 shows SFER depending on the subframe location. Unlike the evaluation

of previous sections, we plot SFER instead of BER for better intuition. When a station holds its position at P1, SFER remains almost zero in all subframe locations regardless of the employed MCS, because the channel quality between AP and the station, i.e., SNR, is considerably high. However, when the station moves at an average speed of 1 m/s, MCS 4 and MCS 7 employing both *amplitude* and phase modulation (i.e., 16-QAM and 64-QAM, respectively) show higher SFER in the latter part of A-MPDU, while MCS 0 and MCS 2 which use only phase modulation (i.e., BPSK and QPSK, respectively) achieve stable SFER across the entire subframe locations. That is, MCSs which use amplitude modulation are highly susceptible to mobility. Therefore, both A-MPDU length and MCS index should be considered jointly.

2.3.5 IEEE 802.11n/ac Features

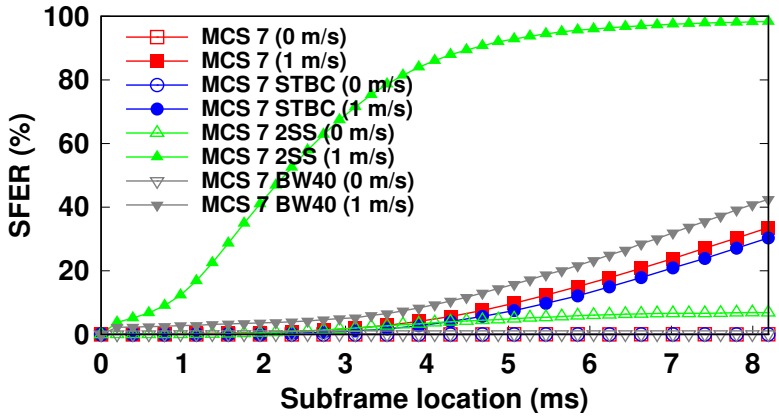

Figure 2.7: SFER of various 802.11n/ac features.

We investigate the impact of IEEE 802.11n/ac features, such as STBC, SM, and channel bonding, in order to verify whether these features alleviate or aggravate caudal loss. Fig 2.7 shows SFER of various 802.11n features, according to subframe location. We basically use the results of MCS 7 as a reference for the performance comparison. First, STBC is well known for offering diversity gain, but we observe that SFER is only slightly decreased by STBC. That is, STBC cannot suppress the SFER increase

in the latter part of A-MPDU.

With SM, which is denoted as *MCS 7 2SS* (using two spatial streams with 64-QAM and 5/6-rate code), SFER is further deteriorated. Even if the station does not move, SFER grows as subframe location increases, since MIMO requires more accurate channel compensation to eliminate the spatial interference. When the station moves, only a few subframes in the beginning part of A-MPDU can be successfully transmitted. The result of 40 MHz bandwidth shows slightly higher SFER than that of 20 MHz bandwidth. That is because not only the power per bandwidth is decreased but also the channel compensation is more difficult than 20 MHz bandwidth due to frequency selectivity.

In all the above cases, the 802.11n/ac features do not solve caudal loss problem; SM and 40 MHz channel bonding are more severely affected by mobility. Moreover, STBC does not alleviate the performance degradation induced by mobility either.

Table 2.2: Throughput and SFER using *Minstrel*

Length (μs)	0	1,024	2,048	4,096	6,144	10,240
Throughput (Mbit/s)	37.54	73.12	79.83	66.38	53.64	44.24
SFER (%)	5.13	11.92	19.42	37.77	50.87	58.33

2.3.6 Rate Adaptation: *Minstrel*

Rate adaptation algorithm (RA) selects the most suitable MCS (or PHY rate) for a given channel condition. Every 802.11 device implements a RA to maximize the performance (e.g., to maximize the throughput) while these algorithms are implementation dependent. We use a measurement to investigate the impact of mobility when a RA runs. *Minstrel* is employed in this experiment, since it is well known for achieving good performance in practical environments [48] and Linux wireless tool adopts it as the default embedded RA [49]. *Minstrel* is a window-based RA, which collects the

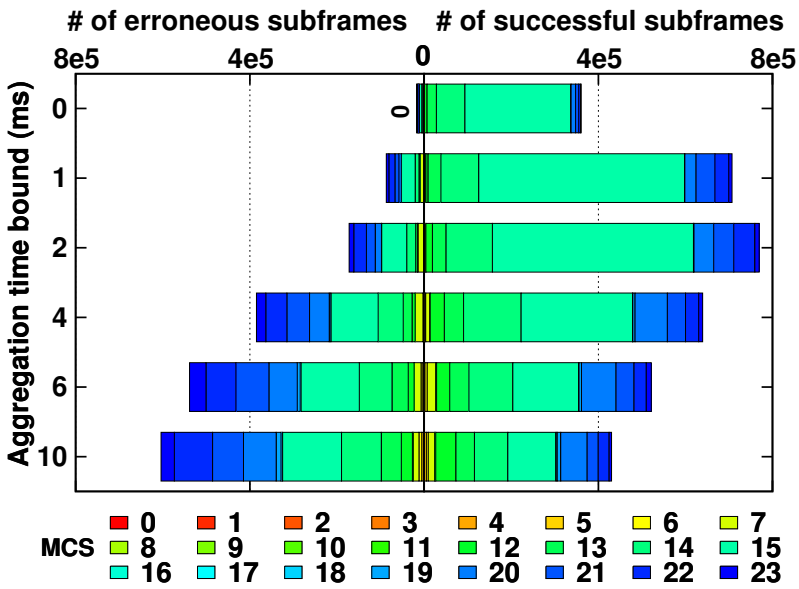

Figure 2.8: Rate distribution on *Minstrel*. Because we use the 802.11n NIC, MCS notation, in this figure, follows the definition from IEEE 802.11n standard: for exmaple, MCS 15 matches to 64-QAM with 5/6-code rate using two spatial streams.

wireless channel statistics by transmitting probing frames, i.e., data frames transmitted with a randomly selected PHY rate. The ratio of probing frames is generally 10% of the total traffic. Based on that, *Minstrel* calculates the best throughput rate within a time window, and adopts it as a basic rate for the next window.

Fig. 2.8 illustrates the MCS distribution measured for a mobility scenario with varying aggregation time bound (i.e., fixed A-MPDU length). Each stacked bar represents the number of subframes transmitted with a specific MCS, where left-side and right-side correspond to the numbers of erroneous and successful subframes, respectively. Probing frames are not counted in the statistics since they are not aggregated into A-MPDU. When A-MPDU is not used (aggregation bound of 0 ms), there are few frame errors. However, as A-MPDU length increases, SFER also increases, especially, it rises steeply between 2 ms and 4 ms. In this experiment, the highest throughput can be achieved by using 2 ms A-MPDU length, using mostly MCS 15 (two spatial streams

and 64-QAM with 5/6-code rate).

We observe that *Minstrel* tries to use higher order MCSs over MCS 15 more often, when A-MPDU length is set to be larger than 2 ms. The reason of this malfunction is mainly caused by the fact that SFER of the currently selected MCS increases due to caudal loss, thus resulting in rate transition to which is expected to support the higher throughput. Note that probing frame does not experience caudal loss, since it are sent to the air without aggregation. Therefore, the estimated throughput using the higher MCS index might be larger than the throughput of the current MCS. As a result, the PHY rate is updated to one of the probed rates, which additionally induces unnecessary and frequent PHY rate variation. Consequently, throughput is further deteriorated when the RA runs in mobile environments. More detailed information is summarized in Table 2.2. As expected, the maximum throughput is achieved by 2 ms A-MPDU length.

2.4 Caudal Noise Model

In IEEE 802.11 WLAN, caudal loss is caused by the fact that the CSI obtained at the PLCP preamble is not accurate to successfully decode OFDM data symbols belonging to the latter part of the A-MPDU. Such an inaccurate channel estimation increases error vector magnitude (EVM), representing the amount of error in the I-Q plane between the ideal transmit symbol and the received symbol [10]. Accordingly, SNR decreases at the latter part of the A-MPDU, thus resulting in A-MPDU performance degradation in mobile environments. To fully understand the caudal loss problem, and then, to develop an appropriate solution, we build a caudal loss model, which represents the impact of mobility with a noise (called *caudal noise*) in the I-Q plane. Based on the model, we can demonstrate the performance degradation caused by mobility through simulations and precisely evaluate the performance of *STRALE* designed to minimize caudal loss in a variety of scenarios.

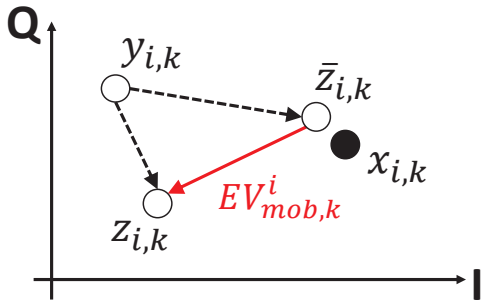

Figure 2.9: Error vector caused by mobility in the I-Q plane.

2.4.1 Caudal Noise Modeling for $n \times n$ MIMO Channel

The received symbol at time τ (i.e., after time τ elapsed from the preamble over $n \times n$ MIMO channel can be represented by

$$Y_k(\tau) = H_k(\tau)X_k(\tau) + N_k(\tau), \tag{2.3}$$

where $H_k(\tau) \in \mathbb{C}^{n\times n}$ is the channel matrix of subcarrier k, and $X_k(\tau)$, $Y_k(\tau)$, $N_k(\tau) \in \mathbb{C}^n$ denote the transmitted symbol, received symbol, and Gaussian noise at time τ, respectively. Assuming that a minimum mean square error (MMSE) receiver is used, the MMSE coefficient matrix $W_k(\tau) \in \mathbb{C}^{n\times n}$ is given by

$$W_k(\tau) = (H_k^H(\tau)H_k(\tau) + N_oI)^{-1}H_k^H(\tau), \tag{2.4}$$

where A^H and A^{-1} indicate the Hermitian and inverse of matrix A, respectively, and $I \in \mathbb{C}^{n\times n}$ is an identity matrix of size n [50]. In WLAN system, $\hat{W}_k(= W_k(0))$ is used for the entire frame reception, since the channel estimation is conducted only at the preamble. Therefore, the decoded symbol $Z_k(\tau)$ can be obtained by multiplying (2.3) and $\hat{W}_k$:

$$Z_k(\tau) = \hat{W}_kH_k(\tau)X_k(\tau) + \hat{W}_kN_k(\tau). \tag{2.5}$$

Let $\bar{Z}_k(\tau)$ be the ideally decoded symbol with an assumption of the perfect CSIs for all OFDM data symbols: $\bar{Z}_k(\tau) = W_k(\tau)Y_k(\tau)$, i.e., (2.4) instead of $\hat{W}_k$ is used for the reception. Then, error vector caused by mobility, i.e., $EV^i_{mob,k}$, which represents

the difference in the I-Q plane between $Z_k(\tau)$ and $\bar{Z}_k(\tau)$ for the i-th spatial stream can be defined as

$$\begin{aligned} EV^i_{mob,k}(\tau) &= z_{i,k} - \bar{z}_{i,k} \\ &= \sum_{j=1}^{n} \left(\frac{\hat{w}^T_{i,k} h_{j,k}}{w^T_{i,k} h_{j,k}} - 1 \right) w^T_{i,k} h_{j,k} x_{j,k} \\ &+ \hat{w}^T_{i,k} n_{i,k} - w^T_{i,k} n_{i,k}, \end{aligned} \tag{2.6}$$

where A^T indicates the transpose of matrix A, and $z_{i,k}$, $\bar{z}_{i,k}$, and $x_{i,k}$ are the i-th element of $Z_k(\tau)$, $\bar{Z}_k(\tau)$, and $X_k(\tau)$, respectively. In addition, $\hat{w}_{i,k}$, $w_{i,k}$, $h_{i,k}$, and $n_{i,k}$ denote the i-th column vector of matrix $\hat{W}^T_k$, $W^T_k(\tau)$, $H_k(\tau)$, and $N_k(\tau)$, respectively. Note that $EV^i_{mob,k}(\tau)$ negatively affects the decoding performance in the I-Q plane as shown in Fig. 2.9, and especially, its magnitude exactly corresponds to an additional noise caused by mobility at time τ, which we refer to as *caudal noise*. Then, the variance of *caudal noise* of the i-th spatial stream, $N^i_{caudal,k}(\tau)$, can be represented by

$$N^i_{caudal,k}(\tau) = \mathbb{E}\left[\sum_{j=1}^{n} \left| \frac{\hat{w}^T_{i,k} h_{j,k}}{w^T_{i,k} h_{j,k}} - 1 \right|^2 \left| w^T_{i,k} h_{j,k} \right|^2 \right], \tag{2.7}$$

where $\mathbb{E}[\cdot]$ denotes ensemble average and $|\cdot|$ is l^2-norm. Consequently, signal-to-interference-plus-noise-ratio (SINR) at time τ for the i-th spatial stream at subcarrier k can be calculated by

$$SINR^i_k(\tau) = \frac{P^i_{rx,k}(\tau) \left| w^T_{i,k} h_{i,k} \right|^2}{P^i_{rx,k}(\tau) \sum_{j \neq i} \left| w^T_{i,k} h_{j,k} \right|^2 + |w_{i,k}|^2 N_o + N^i_{caudal,k}(\tau) \times P^i_{rx,k}(\tau)}, \tag{2.8}$$

where $P^i_{rx,k}(\tau)$ is the received power at subcarrier k for the i-th spatial stream.

For frequency selective fading channel, multipath causes each subcarrier to have different SINR. In order to provide the same error performance on a narrowband channel in selective fading channel, Halperin *et al.* have adopted *effective* SINR, which is a representative SINR value determined by averaging the subcarrier bit error rates

(BERs) and then finding the corresponding SNR [51]. Therefore, we can obtain *effective* SINR for the i-th spatial stream averaged across all the subcarriers N as follows:

$$SINR_{eff}^{i}(\tau) = BER^{-1}\left(\frac{1}{N}\sum_{k} BER\left(SINR_{k}^{i}(\tau)\right)\right), \tag{2.9}$$

where $BER(\cdot)$ is a mapping function from SINR to BER and $BER^{-1}(\cdot)$ is an inverse mapping. Finally, *effective* SINR for $n \times n$ MIMO channel, $SINR_{eff}^{n}(\tau)$, can be calculated by

$$SINR_{eff}^{n}(\tau) = BER^{-1}\left(\frac{1}{n}\sum_{i} BER\left(SINR_{eff}^{i}(\tau)\right)\right). \tag{2.10}$$

2.4.2 Impact of Caudal Noise

We have conducted simulations using WINNER channel model II for a typical indoor environment, where the maximum delay spread of the channel is set to about 230 ns [52]. We collect $50,400$ CSIs sampled at a constant time interval (200 μs) for each subcarrier and spatial stream during about 10 s, assuming that a transmission time of a subframe is about 200 μs and each A-MPDU consists of 40 subframes. Applying the CSIs to (2.6)–(2.10), we have obtained SINR distribution over the duration of A-MDPU, and averaged across approximately 1,200 A-MPDU transmissions.

Fig. 2.10 shows SINR results according to subframe location, where user mobility and SNR at the preamble is fixed to 0.3, 0.6, 0.9 m/s and 40, 30, 25 dB, respectively. We observe that SINR decreases as subframe location (i.e., τ) increases; the channel obtained from LTFs becomes increasingly different from the channel which OFDM data symbols actually go through. Moreover, SINR curves decrease faster when user mobility becomes higher, and converge at the latter part of A-MPDU depending on user mobility, since *caudal noise* becomes a dominant cause of MPDU losses. This trend is more strongly observed in 2×2 MIMO case, which requires more precise channel compensation to eliminate the spatial interference.

Furthermore, in order to verify the accuracy of the *caudal noise* model, we compared simulation results with the measurement results shown in Fig. 2.5. For the fair

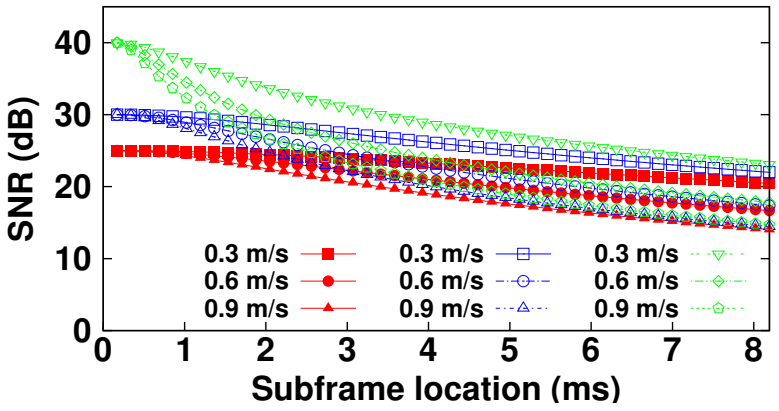

(a) SNR for SISO case.

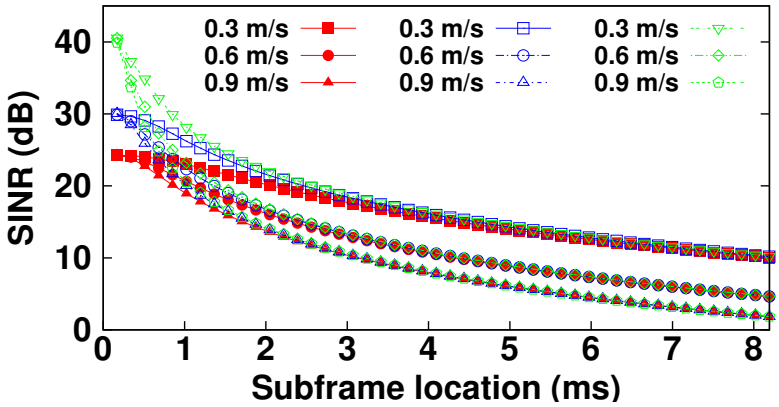

(b) SNR for 2×2 MIMO case.

Figure 2.10: WINNER channel model II simulation results according to user mobility (different marks) and SNR at the PLCP preamble (different colors)

.

comparison, we set up the same simulation environment as the measurement topology, using CSIs obtained from WINNER II channel model in the same way as above.

We have observed that BER increases gradually as the subframe location increases; SINR decreases gradually towards the end of A-MPDU, thus degrading BER over time in mobile environment. Moreover, the slope of the curves becomes higher as the average speed of the station increases. It is worth noting that the amount of caudal

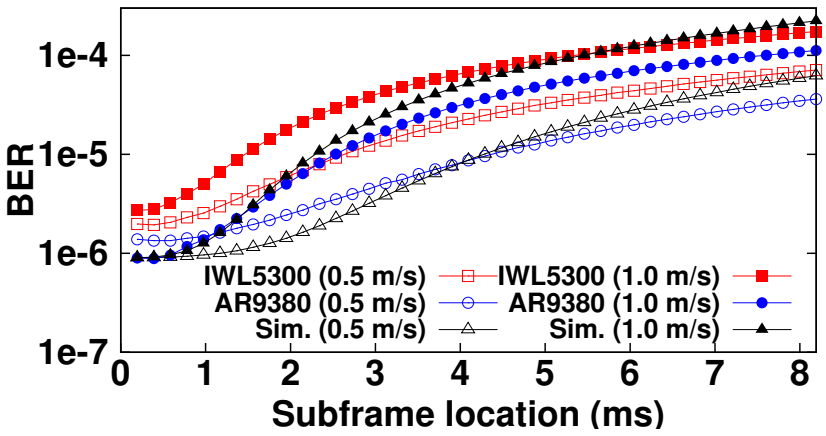

Figure 2.11: BER comparison between simulation and measurement results from Atheros AR9380 and Intel IWL5300 NICs.

loss obviously depends on surrounding environments such as the degree of multipath scattering and the receiver's hardware such as RF circuit structure, antenna gain, and receive sensitivity. Nonetheless, the trends of BER curves obtained from experiments and simulations show the same characteristics, which appropriately guarantees that the proposed model properly reflects the actual performance degradation caused by caudal loss, thus providing better understanding of the impact of mobility. Therefore, by employing the model for simulations, we can properly evaluate the caudal loss problem under a wide range of scenarios.

2.5 *STRALE*: Proposed Algorithm

In this section, we discuss how to solve the caudal loss problem, considering practical features of WLAN. We then propose *STRALE*, a standard-compliant and mobility-aware PHY rate and A-MPDU length adaptation algorithm, designed to minimize caudal loss. It fully complies with the 802.11 MAC and requires no PHY modification such that it can be applicable to the existing hardware by simply updating the device driver only at the transmitter.

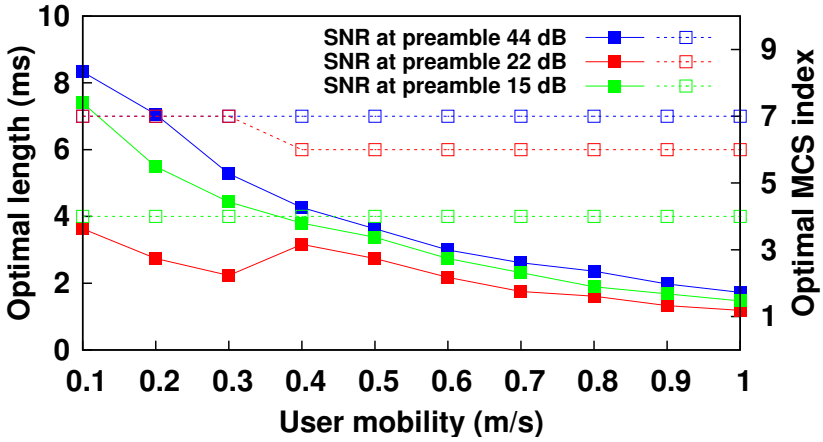

Figure 2.12: The optimal PHY rate (dotted line) and A-MPDU length (line) for the given user mobility and CSIs.

2.5.1 Possible Solutions for Caudal Loss Problem

One of the simplest ways to overcome caudal loss is to adapt A-MPDU length depending on the degree of mobility; as user mobility increases, A-MPDU length is decreased appropriately. For example, One of our previous work proposes a mobility-aware frame length adaptation algorithm, which dynamically controls A-MPDU length by observing the increase of SFER in the latter part of A-MPDU [2].

Additional way to cope with caudal loss is to decrease PHY rate. Note that *caudal noise* causes to decrease SINR as explained in Section 2.4, and the higher SINR at the preamble is, the larger decline in SINR at the latter part of the A-MPDU. Therefore, MCSs which employ both amplitude and phase modulation such as 16-QAM and 64-QAM are much vulnerable to caudal loss as well as the channel degradation, compared to MCSs which use only phase modulation such as BPSK and QPSK as discuss in Section 2.3.4. To be more specific, we perform simulations using the proposed model to numerically find a combination of the optimal MCS and A-MPDU length simultaneously, which provides the best throughput performance for the given user mobility and channel. Fig. 2.12 shows the optimal MCS index (dotted line) and

A-MPDU length (line), as user mobility varies from 0.1 m/s to 1.0 m/s. When SNR at the preamble is fixed to 44 dB, the optimal MCS index becomes MCS 7 and only the optimal A-MPDU length decreases as user mobility increases. On the other hand, when SNR is set to 22 dB, the optimal MCS index changes from MCS 7 to MCS 6, while the optimal A-MPDU length slightly increases at the moment when user mobility changes from 0.3 m/s to 0.4 m/s. This result provides an interesting insight that PHY rate adaptation (i.e., decreasing MCS index) can result in significant caudal loss reduction.

Consequently, we design *STRALE*, which jointly adapts PHY rate and A-MPDU length without additional hardware modifications of WLAN module. Additionally, computational complexity of *STRALE* is almost negligible compared to other normal operations of WLAN modules.

2.5.2 Operation of *STRALE*

How to respond to caudal loss

STRALE statistically estimates the degree of mobility by investigating whether A-MPDU length decrease is expected to provide higher throughput. Based on that, when the degree of mobility increases/decreases, *STRALE* decreases/increases A-MPDU length or MCS index for the next transmission.

After receiving a BlockAck, *STRALE* calculates the optimal A-MPDU length, t^*_{lim}, which could achieve the highest throughput for the previous A-MPDU transmission:

$$\begin{aligned} t^*_{lim} &= \sum_{i=1}^{m^*} l_i/r + T_{PHY}, \\ \text{s.t. } m^* &= \underset{k \le m}{\operatorname{argmax}} \left(\frac{\sum_{i=1}^{k} l_i \cdot s_i}{\sum_{i=1}^{k} l_i/r + T_{PHY} + T_{MAC}} \right), \end{aligned} \tag{2.11}$$

where r is PHY rate, and l_i denotes the i-th subframe's length including MAC header, A-MPDU delimiter, and padding bits. T_{PHY} denotes the transmission time of PLCP preamble and header, T_{MAC} represents MAC protocol overhead including distributed

coordinate function (DCF) IFS (DIFS), backoff, short IFS (SIFS), and BlockAck transmission time, and s_i means the transmission result of the i-th subframe, where it is equal to 1 or 0 depending on whether the corresponding subframe succeeded or failed, respectively. In addition, m is the number of subframes within the A-MPDU, and m^* is the number of subframes smaller than or equal to m that could provide the highest throughput for the previous transmission.

After determining t^*_{lim}, *STRALE* statistically obtains A-MPDU length for the next transmission, t'_{lim}, based on exponentially weighted moving average (EWMA).

$$t'_{lim} = (1-\alpha)t_{lim} + \alpha t^*_{lim}, \tag{2.12}$$

where t_{lim} denotes the previous A-MPDU length, and $\alpha = \min\left(\frac{t_{lim}-t^*_{lim}}{t^*_{lim}}, 1\right)$. We set EWMA weighting factor α to a ratio of $(t_{lim} - t^*_{lim})$ and t^*_{lim}. Accordingly, as the degree of mobility increases, α carries large weight to t^*_{lim} in the estimation, since t^*_{lim} is likely to be much shorter than t_{lim}. By doing so, *STRALE* is able to quickly adapt to a sudden increase in the degree of mobility.

In this regard, t'_{lim} can be used as a key clue to estimate the degree of mobility statistically. Note that longer A-MPDU improves channel efficiency, while becoming increasingly vulnerable to caudal loss. Therefore, if the degree of mobility increases, t'_{lim} obtained by (2.12) becomes much shorter than t_{lim}, otherwise t'_{lim} becomes almost close to t_{lim}, since t^*_{lim} is always shorter than or equal to t_{lim}, i.e., $t^*_{lim} \leq t_{lim}$. Based on this aspect, *STRALE* compares $t_{lim} - t'_{lim}$ with a decision threshold T_d, and then makes a decision on how to adapt A-MPDU length and PHY rate.

$$t_{lim} - t'_{lim} \gtrless T_d. \tag{2.13}$$

In this section, we adopt T_d as the average transmission time of a single MPDU, i.e., $T_{mpdu} = \sum_{i=1}^{m} l_i/(m \cdot r) + T_{PHY}$, to rapidly respond to caudal loss. In other words, if reducing even a single MPDU transmission time is likely to increase throughput by curtailing the impact of *caudal noise*, *STRALE* decreases A-MPDU length to minimize SFER conservatively.

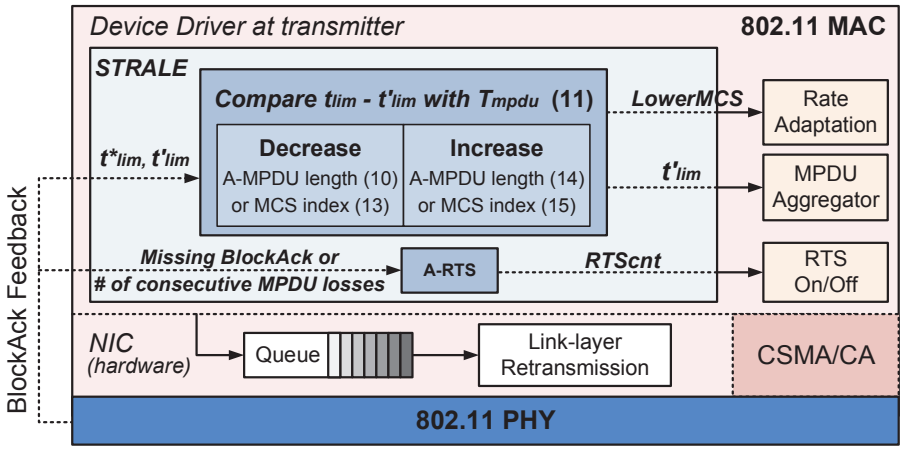

Figure 2.13: Detailed operation of *STRALE*.

PHY rate and A-MPDU length adaptation

The most important module of *STRALE* is to adapt the length of A-MPDU and/or PHY rate in real-time. The detailed operation of *STRALE* is best explained with a blueprint in Fig. 2.13. Based on (2.13), *STRALE* statistically decides to decrease or increase A-MPDU length/PHY rate.

A-MPDU length/PHY rate decrease: When $t_{lim} - t'_{lim} > T_{mpdu}$, that is, the impact of *caudal noise* is getting worse, *STRALE* either decreases A-MPDU length or lowers MCS index. Since the latter without deliberation might unnecessarily degrade transmission efficiency of A-MPDU, we need to verify whether using lower MCS index provides better performance compared to reducing A-MPDU length. Let r_- be PHY rate using one-level lower MCS index compared to r. Assuming that r_- guarantees successful transmissions for t_{lim},[1] the estimated throughput using r_- without decreasing A-MPDU length, defined as $TP(r_-, t_{lim})$, can be calculated by

$$TP(r_-, t_{lim}) = \frac{(t_{lim} - T_{PHY})r_-}{t_{lim} + T_{MAC}}. \tag{2.14}$$

Intuitively, when $TP(r_-, t_{lim})$ is larger than or equal to the estimated throughput using

[1] If the rate adaptation algorithm and *STRALE* are consistently well executed, r_- provides more robust transmissions to both the channel error and caudal loss.

r and t'_{lim}, i.e.,

$$TP(r_-, t_{lim}) \geq TP(r, t'_{lim}), \tag{2.15}$$

lowering MCS index by one is a better choice to achieve higher throughput than decreasing A-MPDU length. Specifically, when (2.15) holds, *STRALE* decides to lower MCS index by one, while maintaining A-MPDU length at t_{lim} for the next transmission instead of t'_{lim}. Otherwise, if (2.15) is not satisfied, A-MPDU length is set to t'_{lim} without decreasing MCS index.

To control PHY rate, *STRALE* needs to inform the built-in rate adaptation (RA) of its decision whether MCS index is required to be decreased or not for the next transmission. Therefore, *STRALE* shares a flag, named $LowerMCS$, with the RA. In detail, when MCS index needs to be decreased, *STRALE* simply sets $LowerMCS$ flag to $TRUE$. As long as $LowerMCS$ flag remains $TRUE$, *STRALE* only adapts A-MPDU length, and the RA uses one-level lower MCS index than that selected by its own decision. In this way, *STRALE* helps the RA be robust to caudal loss and not be misled by the errors caused by mobility.

A-MPDU length/PHY rate increase: On the other hand, if $t_{lim} - t'_{lim} \leq T_{mpdu}$, the current channel is predicted to be ready to support a longer A-MPDU. Under this condition, *STRALE* increases the next A-MPDU length, t'_{lim}, or recovers MCS index by setting $LowerMCS$ flag to $FALSE$ if $LowerMCS$ flag is currently $TRUE$.

Specifically, in case that $LowerMCS$ flag is currently $FALSE$, *STRALE* recalculates t'_{lim} as follows:

$$t'_{lim} := \min\left(\max\left(t_{lim} + T_{mpdu}, \left(1 + \frac{t_{lim}}{t_{max}}\right) t_{lim}\right), t_{max}\right), \tag{2.16}$$

where t_{max} is the maximum PPDU duration defined in the standard. Note that the amount of increase in A-MPDU length depends on the ratio of t_{lim} and t_{max}. That is, t_{lim} relatively smaller than t_{max} means that the degree of mobility is still high. Therefore, *STRALE* increases A-MPDU length in small portion to prevent excessive length fluctuation and to reduce undesirable probing overhead in such a situation.

Otherwise, when $LowerMCS$ flag is $TRUE$, *STRALE* has a chance to recover MCS index instead of increasing A-MPDU length by setting $LowerMCS$ flag back to $FALSE$.[2] In this case, t'_{lim} should be carefully decided, because the higher (recovered) PHY rate might be severely affected by caudal loss. Accordingly, *STRALE* decreases A-MPDU length to the amount of time that provides the same expected throughput achieved by using the previous PHY rate r and t'_{lim} obtained by (2.16). Specifically, let PHY rate calculated by using recovered MCS index be r_+, then t'_{lim} is recalculated as follows:

$$t'_{lim} := \frac{T_{PHY}(t'_{lim} + T_{MAC})r + T_{MAC}(t'_{lim} - T_{PHY})r}{(t_{lim} + T_{MAC})r - (t'_{lim} - T_{PHY})r}. \tag{2.17}$$

As a result, the length of the next A-MPDU is decreased, and *STRALE* recovers MCS index by setting $LowerMCS$ flag back to $FALSE$.

Enhanced adaptive use of RTS/CTS

The performance of the 802.11 is significantly deteriorated in the presence of hidden interference [2]. Specifically, some error patterns induced by the hidden collision is not apparently differentiated from the error caused by mobility, which leads to an ill behavior of *STRALE*. In this section, we improve the concept of *adaptive RTS* (A-RTS) *filter* proposed in [2], which selectively turns on RTS transmission per data frame by adapting to the dynamic collision level incurred by hidden stations. Different from the A-RTS proposed in [2], which uses only SFER threshold to detect a hidden interference, we adopt a hidden detection tool proposed in [53]. Anwar *et al.* demonstrate that hidden collision induces the complete A-MPDU loss and/or burst MPDU losses [53]. Therefore, we activate RTS/CTS handshake when BlockAck is missing or subframes are consecutively lost.

[2] In order to prevent MCS index fluctuation, t_{lim} should be larger than the A-MPDU length at the moment when $LowerMCS$ flag was set to be $TRUE$. Otherwise, *STRALE* simply increases A-MPDU length based on (2.16).

Fairness issue

The DCF of IEEE 802.11 basically provides an equal opportunity for the channel access to all the contending stations, thus resulting in throughput-fairness. However, providing throughput-fairness is not necessarily desirable, since throughput is bounded by the minimum among them [54]. On the other hand, IEEE 802.11e defines transmission opportunity (TXOP), where a station can transmit multiple frames back-to-back without additional contention during each TXOP duration bounded by *TXOPLimit* [39]. TXOP operation can equate actual transmission time among the contending stations, thus providing temporal-fairness [55]. Likewise, if all contending stations have the same A-MPDU length, A-MPDU operation then closely achieves temporal-fairness. However, since *STRALE* controls A-MPDU length according to the degree of the mobility, some stations might experience throughput starvation due to short A-MPDU length [2]. In order to mitigate this problem, we utilize *STRALE* with TXOP simultaneously. Therefore, when a mobile station wins the contention, it transmits *multiple A-MPDUs* back-to-back without the additional channel access during *TXOPLimit*. All contending stations thus can closely achieve temporal-fairness as long as *TXOPLimit* is set to sufficiently large value compared to A-MPDU length.

2.6 Performance Evaluation

In this section, we comparatively evaluate the performance of *STRALE* under a wide range of scenarios. To verify the excellence and feasibility, we have implemented *STRALE* on both ns-3 and commercial 802.11 NIC [36, 37].

2.6.1 Methodology

Simulation: We have implemented *IEEE 802.11ac* MAC and PHY features along with *caudal noise* model and all features of *STRALE* on ns-3. We assume a frequency flat fading, where all subcarriers have the same CSI at a given time, and adopt the pathloss

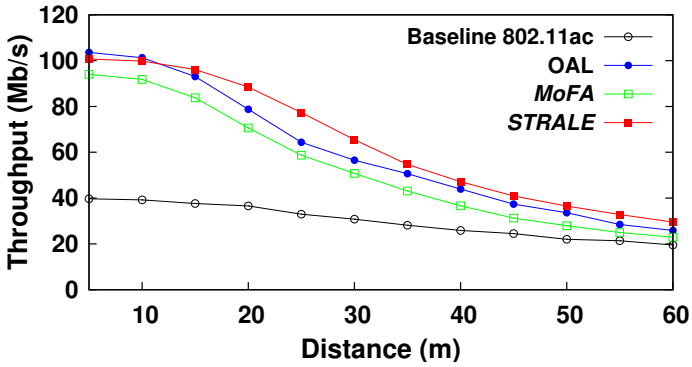

(a) Throughput according to the distance.

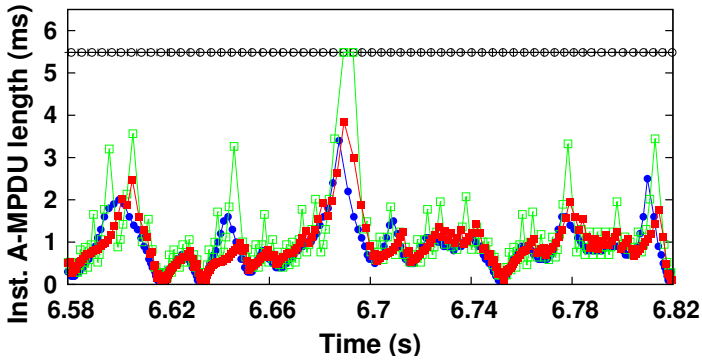

(b) Snapshot of instantaneous A-MPDU length.

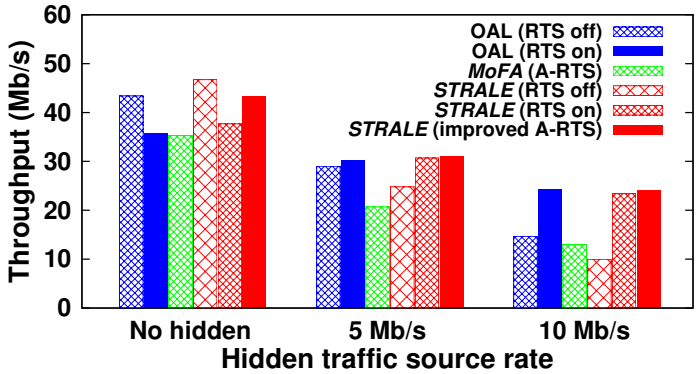

(c) Throughput in presence of hidden terminal.

Figure 2.14: Simulation results for one-to-one scenario: *STRALE* shows the best throughput performance under any circumstances, when user moves 0.8 m/s.

model with pathloss exponent of 3.5 for typical indoor environments. All simulation results are averaged over 100 runs, where each run lasts for 10 s.

Measurement: We have conducted experiments in a controlled office environment, i.e., the basement of our building. Fig. 2.3 illustrates the floor plan for our experiments, where each point from P1 to P6 represents a location as described in Section 2.3.1. Contrary to the 802.11ac simulation environment, we have used the 802.11n NIC, since *ath10k*, which is an open-source device driver for 802.11ac NIC, does not support per A-MPDU length adaptation structurally.

2.6.2 Simulation Results

We compare *STRALE* with baseline 802.11ac (i.e., 5.484 ms fixed A-MPDU length), the optimal A-MPDU length scheme (OAL), and *MoFA* [2]. OAL allows a transmitter to acquire CSIs in advance and numerically calculate highest throughput-providing A-MPDU length before sending the A-MPDU.

One-to-one scenario: Initially, we deploy an AP and a station where the distance varies from 1 m to 60 m. We employ *Minstrel* as a baseline RA [49]. *Minstrel* and *STRALE* independently run except that they share $LowerMCS$ flag. We modify *Minstrel* to use one-level lower MCS index if $LowerMCS$ is set to $TRUE$.

Fig. 2.14(a) shows throughput when user mobility is fixed to 0.8 m/s. Since *caudal noise* negatively affects the reception performance, baseline 802.11ac shows the worst throughput performance. OAL achieves the highest throughput when the distance is under 10 m, because PHY rate adaptation of *STRALE* does not achieve the benefit due to very high SINR as shown in Fig. 2.12. Fig. 2.14(b) demonstrates a time snapshot of instantaneous A-MPDU length when the distance is 10 m. Both *MoFA* and *STRALE* track the optimal A-MPDU length during run time well. While *MoFA* exponentially increases A-MPDU length, *STRALE* carefully increases A-MPDU length to prevent excessive length fluctuation as explained in Section 2.5.2. This conservative adaptation provides slightly higher throughput than that obtained by *MoFA* by reducing SFER.

As the distance becomes over 10 m, *STRALE* shows the best throughput of up to 26.5% higher than the throughput obtained by OAL. This gain comes from the fact that (a) *STRALE* provides stable A-MPDU length adaptation, and (b) using one-level lower MCS index contributes to minimizing caudal loss. In addition, lowering MCS index helps quickly adapt to the channel dynamics such as deep fading.

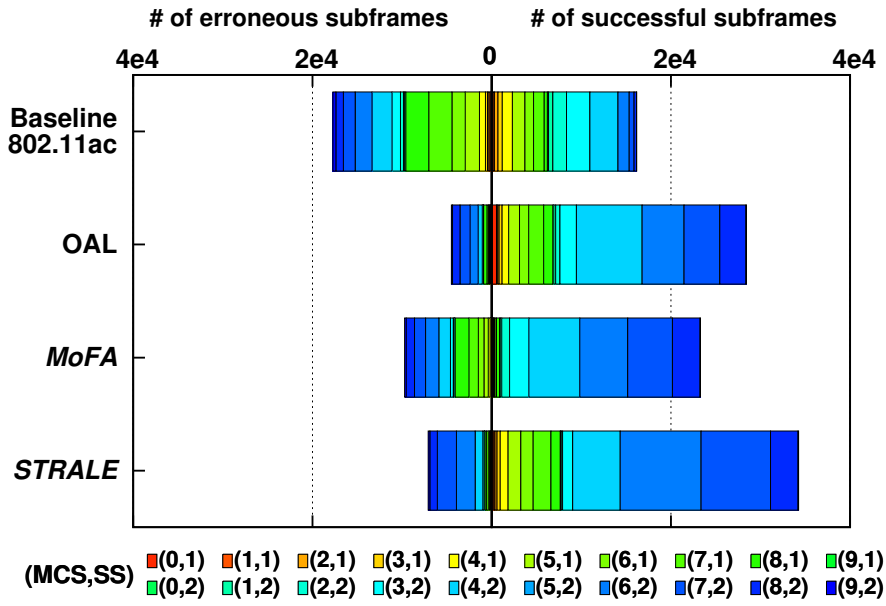

Figure 2.15: MCS and spatial stream (SS) distribution used at 30 m distance.

To be more concrete, Fig. 2.15 illustrates PHY rate distribution when the distance is 30 m. Each stacked bar represents the number of subframes transmitted with a specified MCS, where left-side and right-side correspond to the numbers of erroneous and successful subframes, respectively. The horizontal height of right-side stack exactly matches the obtained throughput, and hence, *STRALE* shows the highest throughput, dominantly using MCS 6 and MCS 7 with double streams, which are one or two level lower MCS indexes compared to the MCS distribution of OAL.

Interestingly, throughput gain of *STRALE* compared to baseline 802.11ac decreases as the distance between the AP and the station increases. That is caused by the fact that

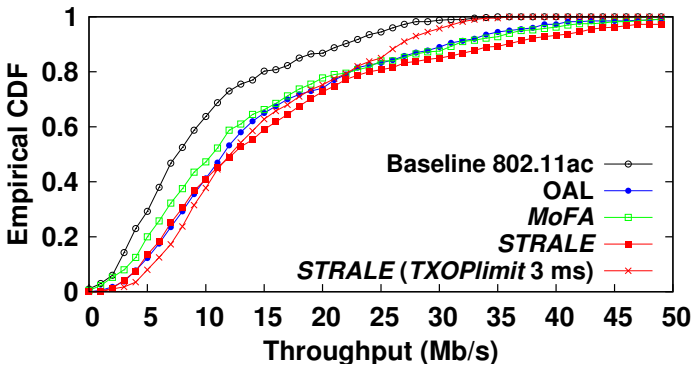

(a) Empirical CDF of throughput.

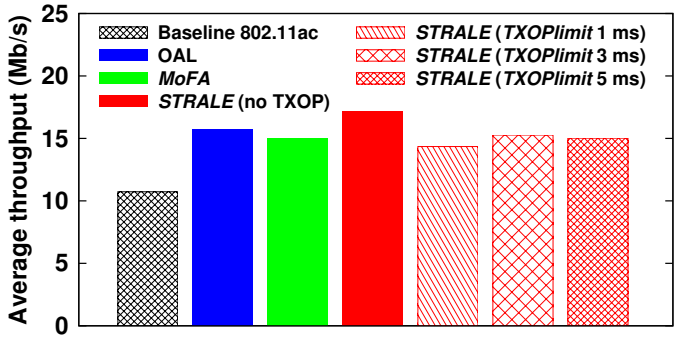

(b) Average per-station throughput.

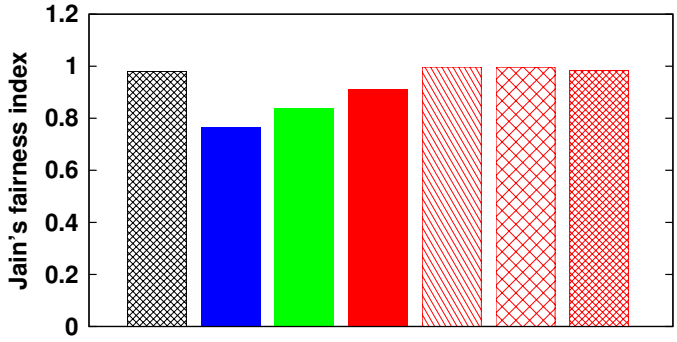

(c) Jain's fairness index of consumed airtime.

Figure 2.16: Simulation results of multiple station scenario: *STRALE* provides 59.9% and 14.3% higher throughput than those of baseline 802.11ac and *MoFA*.

Minstrel is likely to use low order of modulations such as QPSK and BPSK as the distance increases. In other words, *caudal noise* does not severely affect the reception performance of A-MPDU at a long distance. In such cases, *STRALE* does not need to decrease A-MPDU length and/or MCS index, since SFER at the latter part of A-MPDU will not be much increased.

We further investigate how effective the improved A-RTS in *STRALE* is in the presence of hidden terminals. We intentionally create a topology where a transmitter cannot sense transmissions from the hidden terminal, while a receiver is affected by the hidden interference. Fig. 2.14(c) shows throughput according to the hidden traffic source rate. Here, 'RTS on/off' means the transmitter always activates/deactivates RTS/CTS exchange before sending an A-MPDU. Therefore, when *STRALE* (RTS on) and OAL (RTS on) are used, the receiver is rarely affected by the hidden interference. However, throughput decreases by 19.4% and 18.8%, respectively, in the absence of hidden interference, since the use of RTS/CTS exchange incurs waste of the wireless resource. When the hidden traffic source rate becomes 5 Mb/s or 10 Mb/s, using the improved A-RTS on *STRALE* provides the best throughput (even better than 'RTS on') by intelligently enabling RTS/CTS exchange. Without hidden interference, the amount of throughput degradation compared with 'RTS off' is only 7.5%.

Multiple station scenario: We also evaluate the performance of *STRALE* by deploying an AP and five stations where the distance between the AP and each station is randomly selected within a radius of 30 m. All stations have packets to transmit to the AP all the time, and user mobility for each station is uniformly distributed between 0.1 m/s and 0.8 m/s. Fig. 2.16(a) shows the empirical cumulative distribution function (CDF) of throughput. As expected, baseline 802.11ac shows the worst performance. In addition, since *MoFA* aggressively adapts A-MPDU length, it achieves relatively low throughput for highly mobile stations, showing that 20% of the stations obtain throughput below 5 Mb/s. On the other hand, *STRALE* achieves the highest throughput under all circumstances. Fig. 2.16(b) demonstrates the average per-

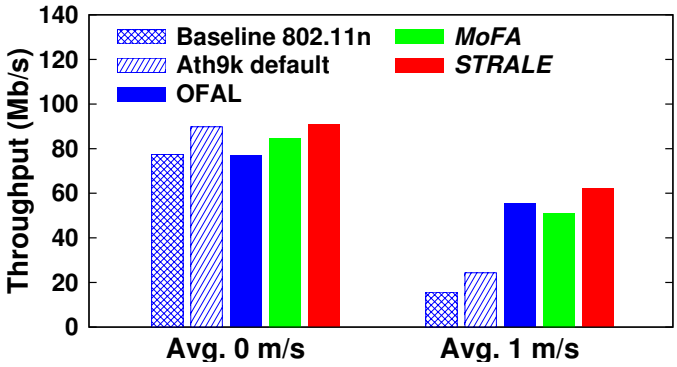

(a) Throughput for one-to-one scenario.

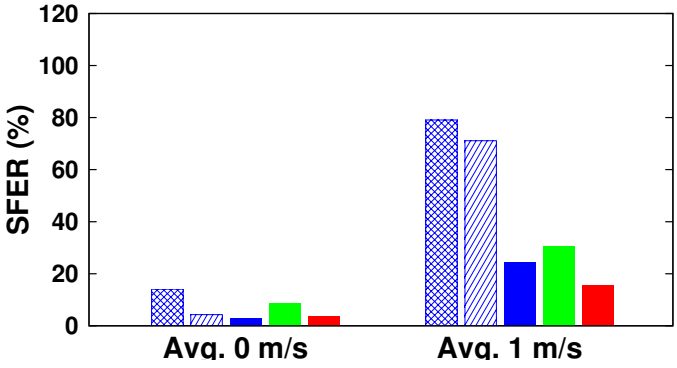

(b) SFER for one-to-one scenario.

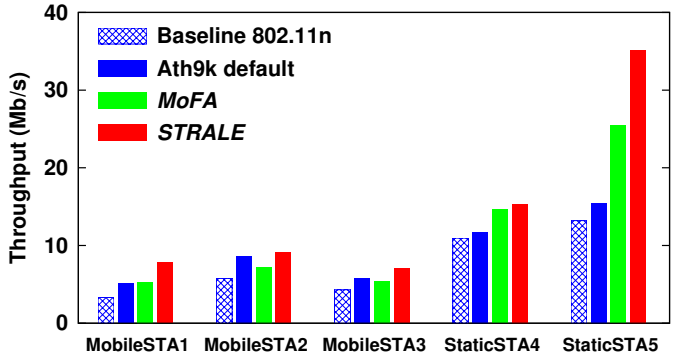

(c) Downlink throughput of each station.

Figure 2.17: Experiment results: *STRALE* shows the best performance by jointly adapting PHY rate and A-MPDU length according to the degree of user mobility.

station throughput. *STRALE* provides 59.9%, 9.1%, and 14.3% higher throughput than those of baseline 802.11ac, OAL, and *MoFA*, respectively. Meanwhile, as explained in Section 2.5.2, OAL, *MoFA*, and *STRALE* harm the temporal-fairness by decreasing A-MPDU length. We enable TXOP in order to alleviate the fairness problem. Using TXOP guarantees the temporal-fairness, but the network throughput can be degraded. Therefore, *STRALE* shows 12.2% lower throughput by enabling TXOP with $TXOPlimit = 3$ ms. On the other hand, Fig. 2.16(c) illustrates Jain's fairness index of the consumed airtime by each station, averaged over all iterations. OAL obtains the worst fairness index as expected, while *STRALE* using TXOP achieves fairness index close to 1. This observation can be also found in Fig. 2.16(a), where *STRALE* (*TXOPlimit* 3 ms) shows a steeper slope.

2.6.3 Prototype Implementation

We have implemented *STRALE* on an off-the-shelf 802.11n NIC with Qualcomm Atheros AR9380 by modifying the open-source *ath9k* device driver, and have opened the source code to the public [38]. We employ *Minstrel* as a baseline RA for all scenarios, and modify its code in *mac80211* to use one-level lower MCS index if *LowerMCS* flag is set to *TRUE*. For a fair comparison, we investigate the performance of baseline 802.11n (10 ms fixed), ath9k default setting (4 ms fixed), the optimal fixed A-MPDU length scheme (OFAL),[3] and *MoFA*.

One-to-one scenario: When the station does not move, *STRALE* achieves the best throughput by suitably maintaining A-MPDU length and PHY rate as shown in Fig. 2.17(a). Ath9k default setting shows almost the same performance with *STRALE*, while baseline 802.11n provides the worst performance. Interestingly, A-MPDU length of 10 ms is too long to support 2×2 spatial stream even in the static scenario, so that the average SFER becomes relatively high as demonstrated in Fig. 2.17(b). OFAL also shows bad

[3]We exhaustively find the fixed A-MPDU length, 0.9 ms, which provides the best throughput for a given topology at the average speed of 1 m/s.

performance, since too short A-MPDU length of 0.9 ms increases protocol overheads, even if it achieves the lowest SFER.

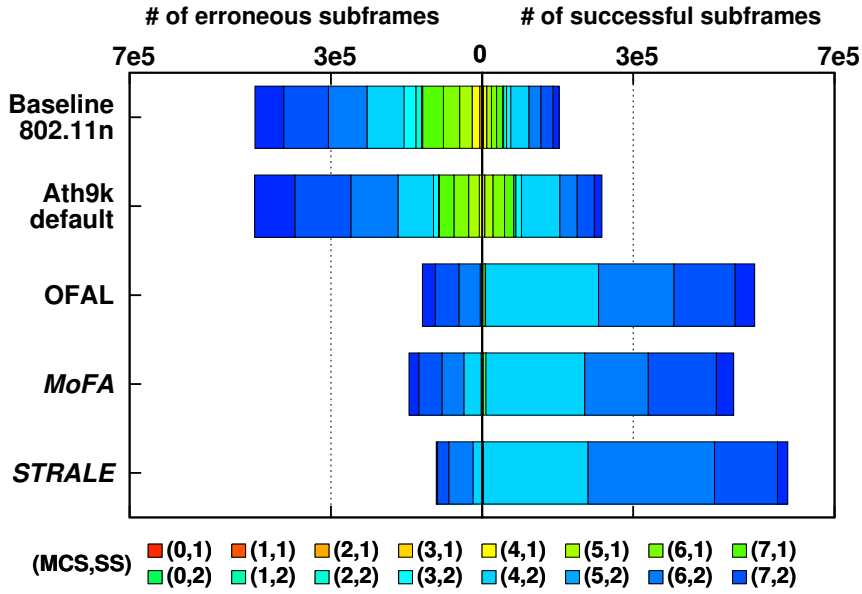

Figure 2.18: PHY rate distribution measured between P1 and P2.

For the mobile scenario, we carry the station equipped with the 802.11n NIC using a cart between P1 and P2 repeatedly. Thanks to the intelligent A-MPDU length and PHY rate adaptation, *STRALE* also shows the best performance, achieving up to 2.9× higher throughput compared to baseline 802.11n. Fig. 2.18 demonstrates PHY rate distribution measured between P1 and P2. *STRALE* dominantly uses one level lower MCS index (i.e., MCS 5 with double streams), compared to the distribution of OFAL. Using lower MCS index guarantees more robust A-MPDU transmissions to *caudal noise* as well as the channel dynamics, thus resulting in the highest throughput by reducing SFER. Furthermore, we also calculate standard deviation of the instantaneous throughput, obtained by measuring 200 ms interval during run time. The lower standard deviation is observed, the more stable performance is guaranteed, since it means throughput does not fluctuate during the measurement. *STRALE* obtains 0.136, which

shows the most stable performance during run time, while baseline 802.11n, ath9k default, OFAL, and *MoFA* achieve 0.524, 0.444, 0.178, and 0.238, respectively.

Multiple station scenario: We finally evaluate the performance of *STRALE* in a multiple station environment. Five stations and one AP are deployed with the floor plan as illustrated in Fig. 2.3. The AP sends fully saturated downlink traffic to each station simultaneously. Three mobile stations (i.e., STA1, STA2, and STA3) move repeatedly between P1 and P2, P5 and P6, P2 and P3, respectively. Two static stations (i.e., STA4 and STA5) hold their positions at P3 and P4.

Fig. 2.17(c) shows the downlink throughput obtained by each station. Ath9k default setting shows the higher throughput than that of baseline 802.11n for STA1, STA2, and STA3 by reducing SFER. *MoFA* also reduces SFER for the mobile stations, but it suffers from the fairness problem as explained in Section 2.5.2. Therefore, the mobile stations achieve relatively lower throughput, while the static stations obtain high throughput gain, dominantly utilizing the additionally obtained wireless resources. For example, static STA5 which is closely located to the AP achieves the biggest gain. *STRALE* shows the similar tendency with *MoFA*, but it provides the highest throughput for all stations. Enabling TXOP can solve this unfairness as explained in Section 2.5.2, but our prototype does not support TXOP implementation due to hardware limitation. Consequently, the network throughput gains of *STRALE* are 98.7%, 59.4%, and 28.2% compared to baseline 802.11n, ath9k default setting, and *MoFA*, respectively.

2.7 Summary

We first analyze the wireless channel dynamics considering mobility in IEEE 802.11 WLAN through extensive measurements. From this, we reveal the fundamental problem of existing frame aggregation schemes manifested over a wide range of mobility and IEEE 802.11n/ac PHY features. We then build a *caudal noise* model and identi-

fied the cause of caudal loss. Based on our observation, we develop *STRALE*, a novel ***st***andard-compliant algorithm, which dynamically adapts the PHY ***ra***te and A-MPDU ***le***ngth simultaneously during run time. Our extensive simulation and prototype-based measurement results demonstrate that *STRALE* achieves up to 2.9× higher throughput compared to the default setting of 802.11 in mobile environments by minimizing caudal loss.

The significant growth of mobile WLAN devices will lead to the increase of the degree of mobility and hidden interferences, and hence, *STRALE* will highly benefit the future large-scale WLANs. We also envision *STRALE* to be applicable to any commercial 802.11 devices and to enhance the performances of high bandwidth-requiring applications such as file transfer and video streaming/conference on mobile devices.

Chapter 3

RECONN: Receiver-Driven Operating Channel Width Adaptation in IEEE 802.11ac WLANs

3.1 Introduction

As a key feature to enhance throughput performance, IEEE 802.11ac defines wide bandwidth operation, which enables aggregating multiple 20 MHz channels. Specifically, IEEE 802.11ac supports bandwidth of 20, 40, and 80 MHz as a mandatory feature, and optionally supports 160 MHz bandwidth. To transmit and receive packets using such wide bandwidth, 802.11ac devices need to increase the size of fast Fourier transform (FFT), equivalently, twice the baseband bandwidth, referred to as *operating channel width* (OCW). Understandingly, it is possible to transmit and receive a packet using the bandwidth less than or equal to OCW. Given that, once OCW is set, it is hardly changed.

The use of wide channel bandwidth has greatly contributed to throughput performance improvement, but there are still many operational issues to be taken care of, such as frequency under-utilization, secondary channel hidden interference problem [21,27], and coexistence with other technologies such as LTE-LAA [6]. Therefore, there have been many researches that propose new channel access schemes, chan-

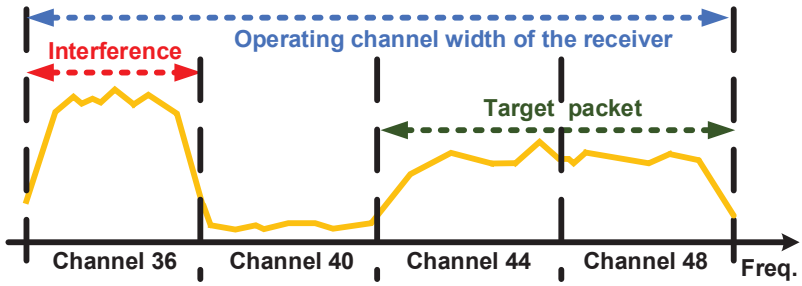

Figure 3.1: Spectrum example in which the time-domain interference degrades reception performance. Time-domain interference can be eliminated by reducing OCW to 40 MHz.

nel allocation algorithms, and/or bandwidth adaptation methods [16–20, 22–26, 28]. Moreover, recent 802.11ac chipsets such as Broadcom BCM43602 and Qualcomm QCA9980 provide an internal bandwidth adaptation implemented in the firmware, where the detailed operations are unknown.

However, none of these studies and methods deal with *time-domain interference* when the baseband includes not only the desired signal, but also interference signal that does not overlap with the desired signal on frequency domain. In this chapter, our experiment results have revealed strong evidence that using the bandwidth less than OCW causes *time-domain interference problem* such as 1) *packet detection and synchronization failure*, 2) *undesirable receive locking problem*, and 3) *automatic gain control (AGC) failure*, thus leading to poor throughput performance. For example, when the baseband of 802.11ac receiver includes interference signal generated by other WLAN devices or LTE-LAA devices at channel 36 in 5 GHz band, reception performance decreases even if the desired signal transmitted in channels 44 and 48 does not overlap with the interference on frequency domain as shown in Fig. 3.1. More seriously, changing the baseband bandwidth for every packet is impossible in WLAN system, since the switching delay is known to be several tens of microseconds due to

the reconfiguration delay of hardware such as RF front end [4]. This problem might become severer in coexistence with other emerging technologies such as IEEE 802.11ax (e.g., OFDMA structure and non-contiguous channel bonding) or LTE-LAA, as well as due to bandwidth heterogeneity of the existing WLAN devices [5, 6].

The main purpose of this chapter is to empirically analyze the impact of time-domain interference in 802.11ac WLAN, and to propose a receiver-driven OCW adaptation algorithm with very low overhead, which is amiable to IEEE 802.11ac, to enhance throughput performance. Our major contributions are summarized as follows.

- We first analyze the impact of time-domain interference in IEEE 802.11ac through extensive measurements using commercial off-the-shelf 802.11ac devices and a software defined radio (SDR) platform. From this, we reveal that bandwidth adaptation without changing OCW causes packet detection and synchronization failure, undesirable receive locking problem, and AGC failure, when the baseband contains time-domain interference signal, not overlapping with the desired signal on frequency domain.

- We develop *RECONN*, a standard-compliant and ***rec***eiver-driven ***o***perating cha***nn***el width adaptation scheme with ease of implementation. *RECONN* adaptively switches OCW using the frequency domain information obtained by receiver with very low overhead. *RECONN* fully complies with 802.11 medium access control (MAC) and does not require hardware modification.

- We implement *RECONN* on the Linux-based open-source device driver, including *ath10k* and *mac80211*, and make a prototype using commercial 802.11ac NIC.

- Our extensive experiments with prototype under a wide range of scenarios show that *RECONN* enhances throughput performance up to 1.85$\times$ by completely eliminating time-domain interference.

To the best of our knowledge, this is the first work that reports time-domain interference problem and develops the OCW adaptation algorithm to handle the time-domain

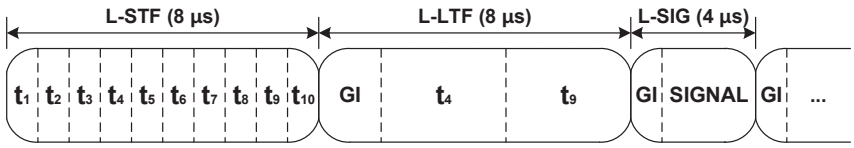

Figure 3.2: Structure of the legacy preamble identical to 802.11a preamble.

interference problem in 802.11ac WLAN.

The rest of the chapter is organized as follows. Section 3.2 provides the background of IEEE 802.11ac wide bandwidth operation. In Section 3.3, we empirically study the impact of time-domain interference. The detailed design of *RECONN* is presented in Section 3.4, and its implementation and experimental evaluations are presented in Section 3.5. Finally, Section 3.6 summarizes this chapter.

3.2 Preliminaries

3.2.1 Packet Detection and Initial Synchronization

IEEE 802.11 receiver detects the incoming packet by receiving legacy short training field (L-STF) at the beginning of a PHY protocol data unit (PPDU). Fig. 3.2 shows the legacy preamble structure, identical to 802.11a preamble.[1] L-STF is composed of 10 short repeated symbols from t_1 to t_{10}. Each symbol uses 12 out of 52 subcarriers based on 64-point inverse FFT (IFFT), thus resulting in 0.8 μs periodicity. Because of the repetitive nature of L-STF sequence, the received signal is correlated with a delayed version of itself periodically. Therefore, receiver uses time-domain samples for packet detection in general, i.e., time-domain auto-correlation value exceeding a threshold indicates a detected packet [32]. Thanks to good correlation property of L-STF sequence, incoming packets can be recognized accurately even after signal distortion induced by wireless channel and/or analog RF front end.

[1] For backward compatibility, IEEE 802.11n/ac PPDU also contains legacy preamble at the beginning, which is duplicated over each 20 MHz channel.

Moreover, auto-correlation peaks obtained by time-domain samples can be also used to set AGC parameters and to acquire symbol timing offset (STO). Additionally, receiver calculates initial carrier frequency offset (CFO) by using the difference in phase between two consecutive time-domain samples of L-STF, separated by 0.8 μs.

3.2.2 Wide Bandwidth Operation

Channelization and contention mechanism

IEEE 802.11ac supports the bandwidth of 20, 40, and 80 MHz as a mandatory feature, and optionally provides 160 MHz channel including non-contiguous 80+80 MHz. The wide bandwidth including 40, 80, and 160 MHz can be divided by the primary 20 MHz channel and one or more secondary channels. Basically, only the primary 20 MHz channel follows IEEE 802.11 distributed coordination function (DCF) contention mechanism, where the channel needs to be idle until an interval of DCF inter frame space (DIFS) plus the backoff counter reaches zero to access the wireless medium. On the other hand, all secondary channels need to be idle for point coordination function (PCF) inter frame space (PIFS) immediately preceding the expiration of primary channel's backoff counter. Specifically, when the backoff counter of primary channel becomes zero, if one or more secondary channels are busy, a station then proceeds either to restart the contention process by randomly selecting a new backoff counter without increasing backoff window (static channel access), or to transmit a packet using the bandwidth including primary 20 MHz channel plus adjacent PIFS-idle secondary 20, 40, or 80 MHz channel (dynamic channel access) [27].

Operating channel width (OCW)

OCW denotes twice the baseband bandwidth supported by 802.11ac system, or equivalently analog-to-digital-converter (ADC) sampling rate, which can be 20, 40, 80, or 160 MHz corresponding to 64-point, 128-point, 256-point, and 512-point (I)FFT, respectively. Specifically, OCW determines the amount of the maximum bandwidth ac-

tually used for packet within basic service set (BSS), where the AP and its associated station should use the bandwidth less than or equal to the minimum value of OCW among them. When a station transmits and receives packets using the bandwidth less than OCW, it does not need to change the baseband bandwidth by adjusting ADC sampling rate, because the station can disregard the unused subcarriers. In this chapter, however, we verify that using bandwidth less than OCW might lead to poor reception performance due to time-domain interference not overlapping with the incoming desired signal on frequency domain.

Note that a station can change its OCW without disassociation, using operating mode notification process [1]. However, since it incurs excessive delay due to hardware reconfiguration and protocol overhead, which is known to be several tens of microseconds [4], OCW is rarely changed during run-time.

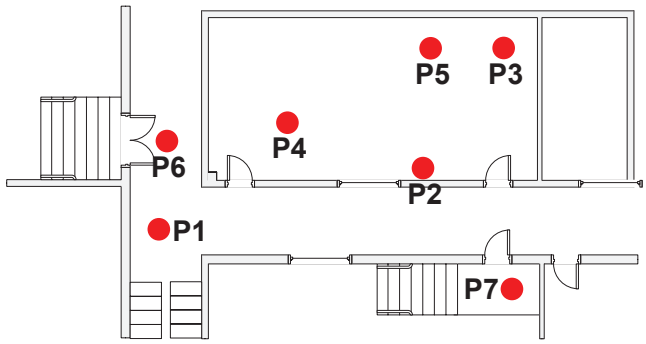

Figure 3.3: Floor plan of our experiments (22 m $\times$ 12 m). Each point represents locations where devices are deployed.

3.3 Cast Study

In this section, we present extensive experiment results to verify the cause and effect of the time-domain interference problem, occurring when interference signal is not overlapping with the desired signal on frequency domain. We use two 802.11ac commercial

APs, TP-link Archer AC3200 (AC3200) equipped with Broadcom BCM43602 chipset and Archer AC2600 (AC2600) equipped with Qualcomm QCA9980 chipset. Additionally, for in-depth analysis, we also employ SDR platform, i.e., NI USRP equipped with Xilinx Kintex-7 FPGA, using LabVIEW Communication System Design Suite (CSDS) and 802.11 Application Framework (AF), which is compliant to IEEE 802.11 specification [56].

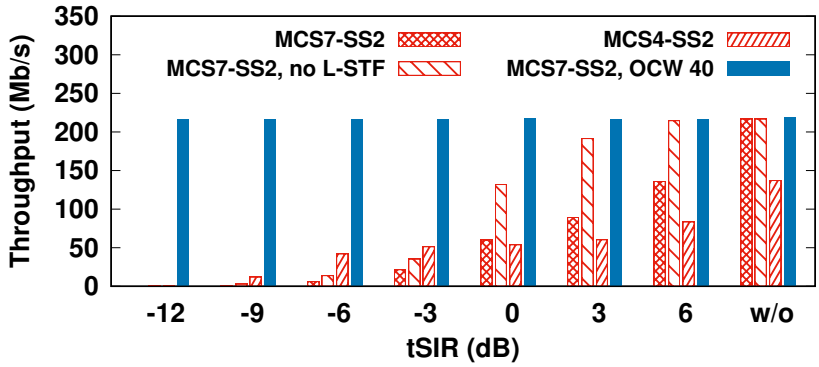

(a) Throughput using AC3200.

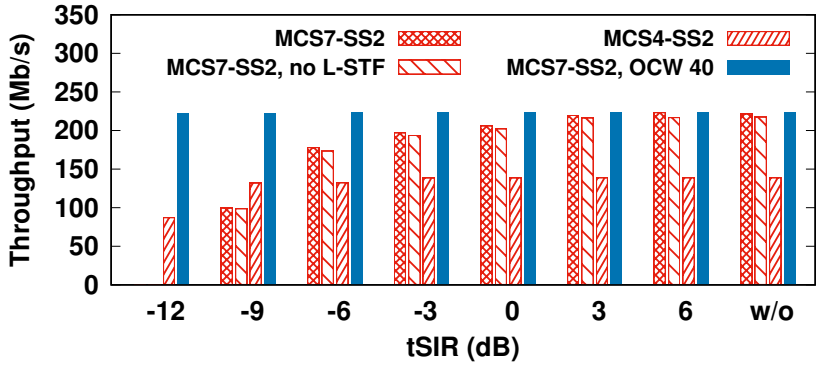

(b) Throughput using AC2600.

Figure 3.4: Uplink throughput obtained by AC3200 and AC2600 according to tSIR. The interference is generated by NI USRP with 802.11 AF, where no frequency overlapping exists.

3.3.1 Motivation

We initially conduct an experiment using commercial devices in a controlled office environment, i.e., the basement of our building without neighboring WLAN. Fig. 3.3 illustrates our floor plan, where circles from P1 to P7 represent different locations where access points (APs) and stations are deployed.

Either AC3200 or AC2600 is installed at P1, and its associated 802.11n station, generating 40 MHz uplink traffic on channel 44 and 48, is placed at P5. For better control of the experiment, we adopt an 802.11n station, which has the baseband of 40 MHz, thus making sure of no contention with the interferer. Interference traffic is generated at P4, using NI USRP, which sends 802.11a packets (occupying 20 MHz) over channel 36. Therefore, transmitters do not share the wireless medium, i.e., no frequency-domain overlapping occurs. Note that the setting corresponds to Fig. 3.1.

Because there is no transmit signal overlapping on frequency-domain between two transmitters, we cannot adopt conventional signal-to-interference-and-noise ratio (SINR). Therefore, we newly define *time-domain signal-to-interference ratio (tSIR)* as a power ratio of desired and interference signal, both contained in time-domain samples (i.e.,twice baseband of the receiver), but non-overlapping with each other on frequency domain. The interference packets generated by NI USRP have the size of 1,460 B, being transmitted using modulation and coding scheme (MCS) index 0. Note that MCS in IEEE 802.11 denotes a combination of modulation and code rate, where higher MCS index means higher PHY rate. The airtime of interference signal then becomes 2 ms with inter frame space (IFS) of 108 μs.[2] Fig. 3.4 shows uplink throughput obtained by AC3200 and AC2600 according to tSIR. The 802.11n station uses MCS 7 with double spatial stream over 40 MHz channel width, and OCW of the 802.11ac AP is initially set to 80 MHz (*MCS7-SS2*). We compare throughput by modifying L-STF

[2]802.11 AF supports a fixed backoff value rather than the random backoff feature. We set IFS to 12 slots, i.e., 108 μs, which is an approximation of DIFS plus average backoff duration with initial contention window.

sequence of interference signal to all zeros (*MCS7-SS2, no L-STF*) using NI USRP, and then we change MCS of the 802.11n station to MCS 4 (*MCS4-SS2*). Finally, OCW of the 802.11ac AP is set to 40 MHz (*MCS7-SS2, OCW 40*).

Throughput result obtained by AC3200 is shown in Fig. 3.4(a). Without interference, the obtained throughput reaches 219 Mb/s or 137 Mb/s, depending on used MCS. However, when OCW of AC3200 is set to 80 MHz, throughput is severely deteriorated as tSIR decreases. Interestingly, when interference signal does not include L-STF signal (*MCS7-SS2, no L-STF*), AC3200 achieves higher throughput compared to *MCS7-SS2*. Moreover, when the 802.11n station uses MCS 4, which is more robust to distortion (*MCS4-SS2*), the performance becomes slightly tolerant to time-domain interference. On the other hand, when OCW of AC3200 is set to 40 MHz, throughput does not fluctuate depending on tSIR. In the meantime, AC2600 shows more stable throughput results compared to AC3200 as shown in Fig. 3.4(b). AC2600 is not affected by the preamble of interference signal, and throughput of *MCS4-SS2* does not decrease until tSIR reaches -12 dB. Additionally, as expected, throughput does not fluctuate when OCW of AC2600 is set to 40 MHz.

As a result, we observe that throughput decreases depending on tSIR even though interference signal is not overlapping on frequency domain, as long as the receiver's OCW contains the interference. This throughput degradation is not caused by the contention between two transmitters, because the 802.11n station cannot carrier-sense interference signal generated by NI USRP. Moreover, the adjacent channel interference is not the reason either, because throughput of *MCS7-SS2, OCW 40* does not fluctuate according to tSIR.

It is worth noting that receiver processes time-domain samples of the identically repeated L-STF signal as explained in Section 3.2.1 in WLAN system. In this regard, we have verify that throughput degradation is mainly caused by 1) packet detection and synchronization failure, 2) undesirable receive locking to the interference signal, and 3) AGC failure. The detailed analysis is presented in the following.

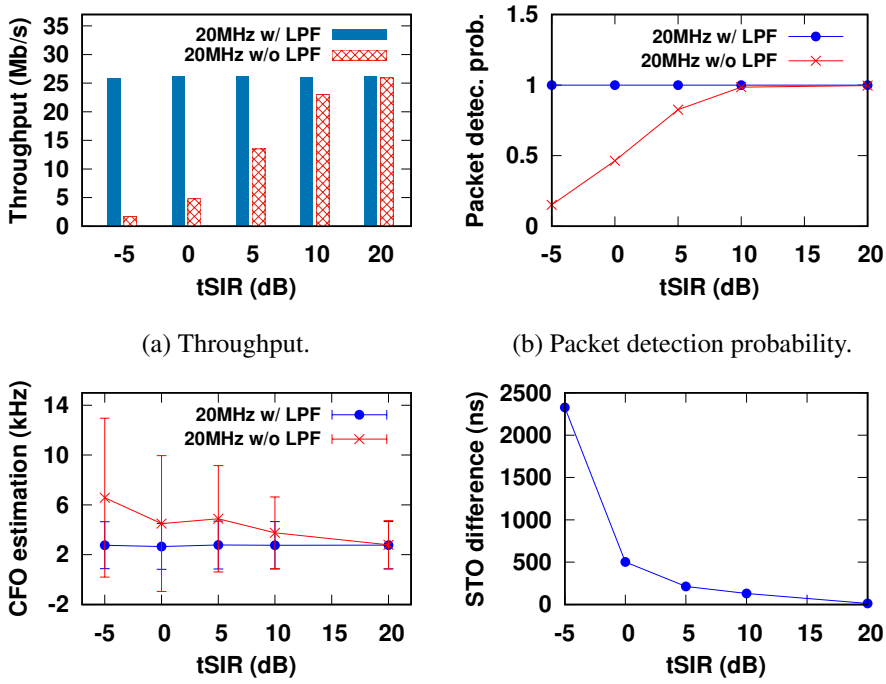

(a) Throughput.

(b) Packet detection probability.

(c) Estimated CFO.

(d) STO difference.

Figure 3.5: Average packet detection and time/frequency synchronization measurement results obtained by NI USRP based on Schmidl and Cox algorithm.

3.3.2 Packet Detection and Synchronization Failure

For detailed analysis, we have verified the impact of time-domain interference on the reception performance empirically. We employ 802.11 AF on the top of NI USRP, which provides a ready-to-run, modifiable real-time PHY and MAC reference design [56]. Total three NI USRPs are deployed in proximity as a transmitter, a receiver, and an interferer, respectively. OCW of the receiver is set to 80 MHz based on 256-point FFT, while only 20 MHz bandwidth is used for packet transmission and reception. The transmitter sends packets on channel 48 and the interferer uses channel 40 such that no frequency-domain overlapping exists. In order to change tSIR, we change the transmit power of the interferer from -10 dBm to 15 dBm.

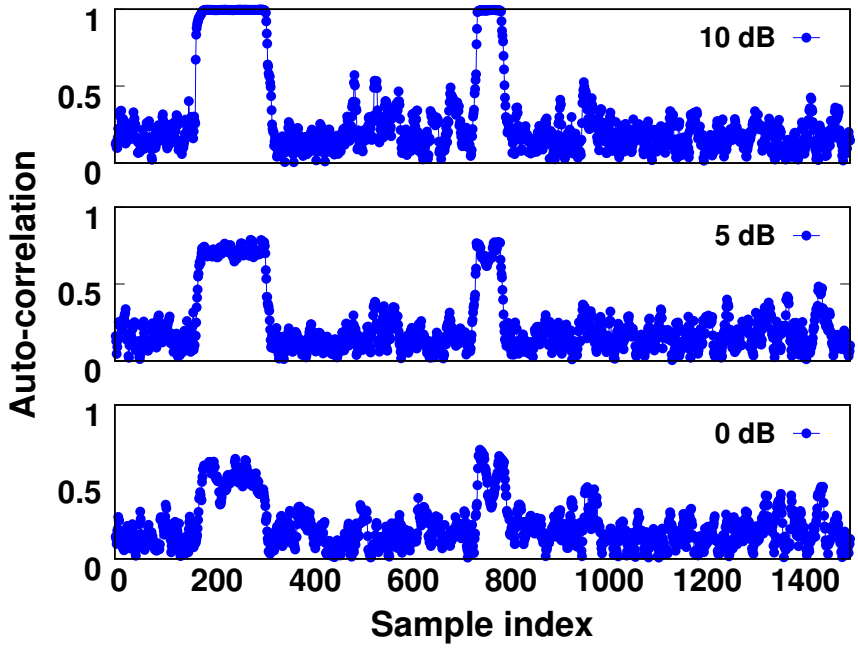

Figure 3.6: Normalized auto-correlation magnitude according to time sample index measured by NI USRP.

Fig. 3.5 shows average packet detection probability, throughput, CFO, and STO results. Specifically, using 802.11 AF, receiver detects packets, finds STO index, and estimates CFO based on Schmidl and Cox algorithm (SC) [32]. Moreover, 802.11 AF provides digital low pass filter (DLPF), to extract the primary 20 MHz signal within the entire baseband of 80 MHz, only for the packet detection and synchronization. Accordingly, when DLPF is utilized, time-domain interference signal can be filtered out, thus providing much better packet detection and synchronization performance.[3] Therefore, using DLPF prior to executing SC, throughput is not affected by tSIR as shown in Fig. 3.5(a), while throughput decreases gradually without using DLPF, as tSIR decreases. This throughput degradation is caused by low packet detection probability as demonstrated in Fig. 3.5(b). To be more specific, Fig. 3.6 shows a snapshot

[3]Based on the results in Fig. 3.4, we believe that DLPF is not used for synchronization in commercial off-the-shelf devices. More detailed discussion is presented in Section 3.4.1.

of the normalized auto-correlation magnitude according to time sample index at the receiver for a given tSIR, without employing DLPF. Note that NI USRP calculates the normalized auto-correlation magnitude based on moving window of 64 samples. Due to the repeated nature of L-STF sequence, the normalized auto-correlation magnitude is maintained at a value of one during L-STF reception as shown in the case of 10 dB tSIR.[4] However, as tSIR decreases, the normalized peak auto-correlation magnitude decreases. What is worse, when tSIR becomes 0 dB, the peak goes even under 0.5. It is worth noting that although the specific packet detection and synchronization algorithm can vary depending on the implementation, i.e., type of chipset, peak fluctuation negatively affects packet detection and synchronization performance eventually.

Additionally, CFO estimation performance is also deteriorated due to time-domain interference. In this setup, CFO should remain around 3 kHz because of the clock difference between the transmitter and the receiver. However, CFO error rapidly increases and widely fluctuates without using DLPF as shown in Fig. 3.5(c). Fig. 3.5(d) shows the difference in STO index with and without using DLPF. Note that even a small STO error significantly affects reception performance [57]. Especially, when tSIR is -5 dB, STO error becomes greater than 2 μs, much larger than the guard interval (i.e., 800 ns) used in 802.11 system.

3.3.3 Receive Locking to Interference Signal

Going back to Fig. 3.4(a), when interference signal uses zero sequence instead of the original L-STF sequence, the throughput does not decrease when tSIR is larger than 3 dB. This phenomenon is observed by only using AC3200 equipped with BCM43602 chipset. Here, we further investigate the impact of L-STF by changing the interference pattern. Along with the airtime of interference packet set to 2 ms with IFS of 108 μs as in Section 3.3.1, we additionally consider the airtime of interference packet set to

[4] Since the transmitter sends packets in the format of 802.11ac, correlation peak can be observed twice in L-STF and very high throughput (VHT) STF.

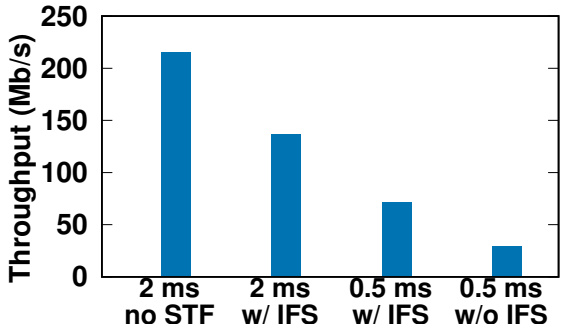

(a) Throughput results.

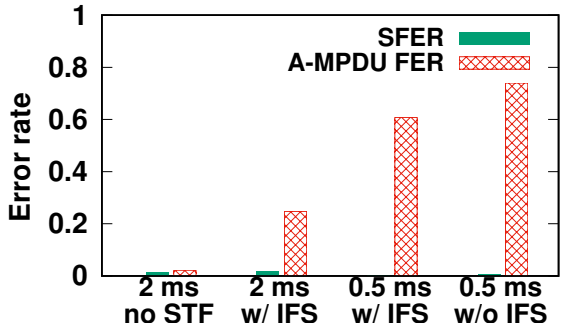

(b) Error rate results.

Figure 3.7: Uplink throughput and two types of error rate according to the different interference patterns when tSIR is 6 dB.

0.5 ms with and without IFS for additional comparison.

Fig. 3.7 shows the throughput of AC3200 and two types of error rate, when tSIR is 6 dB. Aggregate MPDU (A-MPDU) frame error rate (FER) stands for a ratio that the entire A-MPDU is broken such that block acknowledgement (BlockAck) missing event occurs. On the other hand, subframe error rate (SFER) means a subframe error ratio determined by receiving BlockAck. Without L-STF, throughput does not decrease and both A-MPDU FER and SFER remain under 2%. However, if the interference contains L-STF sequence, throughput becomes down to 136 Mb/s with A-MPDU FER of 25%, when the airtime of interference signal is set to 2 ms. Additionally, if L-STF of the interference is transmitted more frequently, throughput decreases even further, and

A-MPDU FER also increases rapidly. Interestingly, SFER is not increased for all cases, which means that as long as an A-MPDU is successfully detected, all subframes can be also successfully received. This is not packet detection and synchronization issues dealt with in Section 3.3.2, because there is *no performance degradation when interference signal does not include L-STF*. From this experiment, we conclude that some chipsets might receive the preamble of packets not occupying the primary 20 MHz channel, which is undesirable behavior that violates 802.11ac specification. We refer to this phenomenon as *undesirable receive locking*, which results in detection failure of desired packets incoming through the primary channel.

3.3.4 AGC Failure

In this section, we verify that AGC failure also deteriorates reception performance when interference signal not overlapping with the desired signal on frequency domain is contained in the receiver's baseband.

In general, AGC is conducted to provide controlled signal amplitude of the output signal, despite variation of the amplitude in the input signal [58]. WLAN receiver performs AGC using the power measured at L-STF as illustrated in Fig. 3.2. Unlike packet detection/synchronization failure and undesirable receive locking, AGC failure can occur when an interference packet arrives while the receiver is receiving a desired packet. To be more specific, we have conducted an additional experiment to verify whether AGC failure actually degrades reception performance. The experiment setting is described in Section 3.3.1, while we change interference pattern generated by NI USRP, where the airtime of interference packet becomes 248 μs with and without IFS of around 1.8 ms long. Therefore, interference packet comes in the middle of desired packet reception. In this experiment, we use AC2600 as a receiver, because of undesirable receive locking problem observed only in AC3200.

Fig. 3.8 shows measurement results for three different tSIR values. When tSIR is 6 dB, time-domain interference does not influence reception performance of AC2600

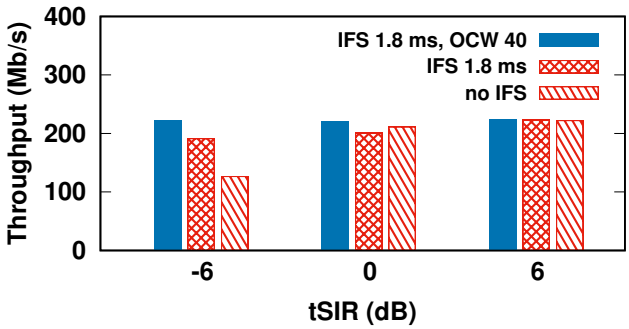

(a) Throughput results.

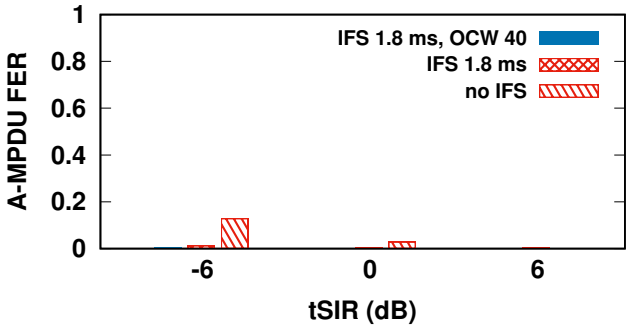

(b) A-MPDU FER.

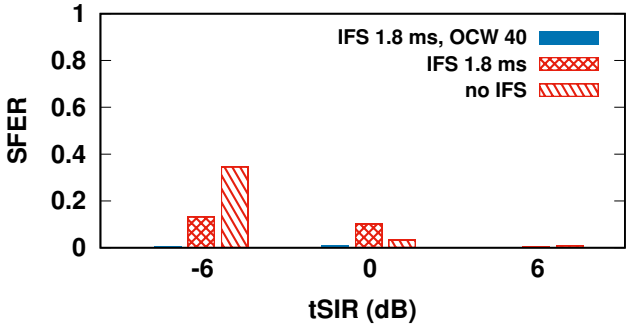

(c) SFER.

Figure 3.8: Uplink throughput and two types of error rate measured by using AC2600, according to three different interference patterns.

for all cases. In case of -6 dB tSIR, when interference packets are continuously transmitted without IFS (*no IFS*), throughput of 126.9 Mb/s with 34.5% SFER and 12.8%

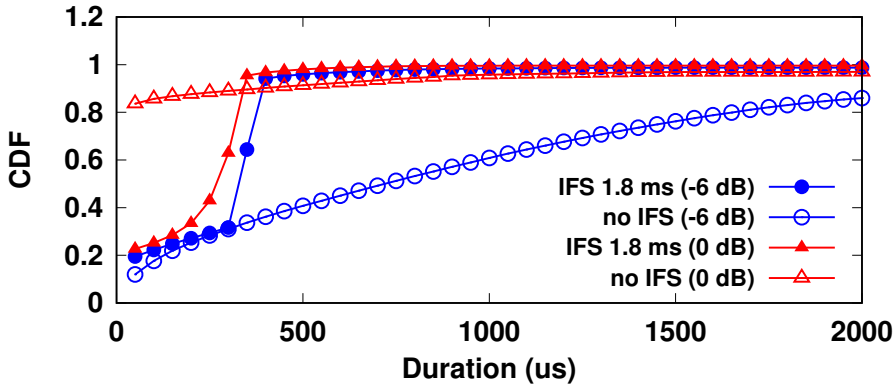

Figure 3.9: CDF of duration in which subframe errors occur within an A-MPDU.

A-MPDU FER is achieved due to packet detection and synchronization failure. However, when interference packets are transmitted intermittently with IFS of 1.8 ms (*IFS 1.8 ms*), throughput of 191.7 Mb/s, 51% higher than *no IFS* result, is achieved because only 10% of the wireless medium is occupied by interference signal. AC2600 is not affected by the interference, as expected, when OCW is set to 40 MHz (*IFS 1.8 ms, OCW 40*).

Interestingly, when tSIR is 0 dB, *IFS 1.8 ms* shows the worst performance, obtaining 10.5 Mb/s lower throughput with 6.9% higher SFER, compared with *no IFS* results. This reduction comes from AGC failure, observing consecutive subframe errors within an A-MPDU. To be more specific,

Fig. 3.9 shows cumulative distribution function (CDF) of duration in which subframe errors occur within an A-MPDU. Note that 802.11n station associated with AC2600 transmits A-MPDUs with airtime of 2 ms each, thus making the maximum duration (x-axis) around 2,000 μs.[5] In case that interference packets are transmitted continuously without IFS, subframe errors within an A-MPDU closely follow a uniform distribution. However, when interference packet comes in the middle of A-MPDU reception, i.e., after AGC processing, corresponding time-domain samples are clipped

[5]Using MCS 7 with double spatial stream and 40 MHz, the total airtime of an A-MPDU is around 2 ms fixed, due to the size limitation of 65,535 B for a single A-MPDU.

off, thus resulting in signal distortion [59], even though interference signal does not overlap with the desired A-MPDU on frequency domain. Therefore, subframe errors occur consecutively during the interval of interference packet, thus leading to sudden increase in statistical probability near the duration of $350\ \mu$s. This phenomenon can be more strictly observed when the interference power increases.

3.4 *RECONN*: Proposed Algorithm

Motivated by the observation presented above in Section 3.3, we first discuss how to overcome time-domain interference. We then propose *RECONN*, a novel receiver-driven OCW adaptation algorithm, designed to eliminate time-domain interference with very low overhead. *RECONN* enables receiver to intelligently adapt OCW based on the frequency-domain information.

3.4.1 Possible Solutions

When the interference does not occupy the primary 20 MHz channel of receiver, DLPF can eliminate time-domain interference by filtering out the interference components in time-domain samples as shown in Section 3.3.2. Note that L-STF is duplicated over each of 20 MHz channels such that the receiver is able to recognize the incoming packet and acquire synchronization, not affected by the interference by using DLPF to extract signal at the primary 20 MHz channel. However, employing DLPF requires a new hardware feature, and causes an additional delay, thus making them costly and impractical for large-scale adoption by commercial products. Moreover, packet detection and synchronization performance might be degraded when the receiver uses L-STF sent over only the primary 20 MHz channel due to frequency selectivity. Additionally, AGC failure still deteriorates the reception performance even with employing DLPF. Further analysis of DLPF will be discussed in Chapter 4.

Another way to overcome time-domain interference is to reduce MCS index to be

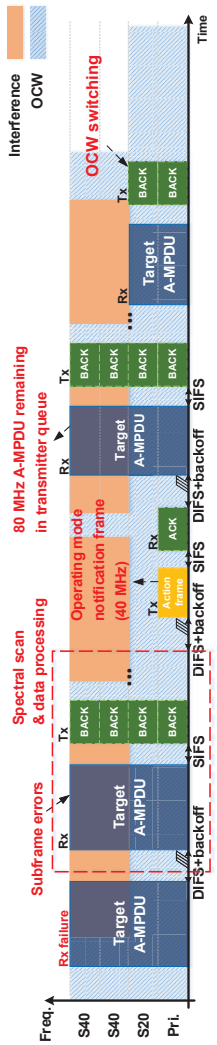

Figure 3.10: Example of decreasing OCW due to time-domain interference: A-MPDU loss triggers spectral scan, while A-MPDU reception continues. If the receiver detects the interference, in this case, at the secondary 40 MHz channel, it sends an operating mode notification frame to the transmitter prior to reducing OCW to 40 MHz. After receiving 40 MHz A-MPDU, the receiver finally reduces OCW in order to receive A-MPDUs scheduled to be transmitted over 80 MHz channels.

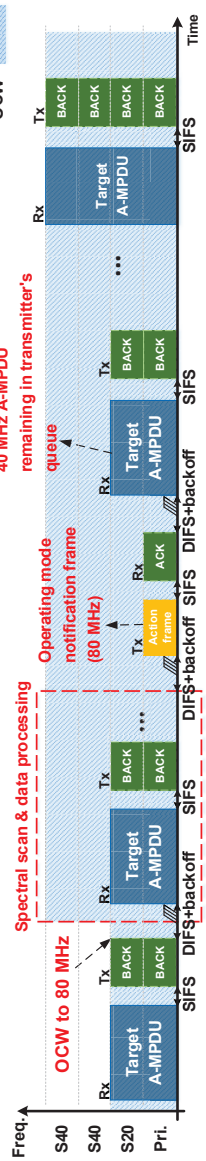

Figure 3.11: Example of increasing OCW: Expiration of N_{wnd} triggers probing, where the receiver increases OCW to 80 MHz, and conducts spectral scan. Because time-domain interference does not exist, the receiver decides to remain on 80 MHz OCW, and hence, sends a operating mode notification frame to the transmitter.

more robust to signal distortion as shown in Section 3.3.1. However, since lower MCS provides lower throughput, it cannot be generally a desirable solution.

We develop *RECONN*, a standard-compliant and receiver-driven OCW adaptation scheme, designed to eliminate time-domain interference with very low overhead. *RECONN* fully complies with 802.11 MAC and requires no hardware modification such that it can be applicable to the existing hardware.

3.4.2 *RECONN*

OCW adaptation

When a packet error event occurs, or n subframes are consecutively lost at a receiver, *RECONN* needs to scan frequency spectrum because the loss might have been due to time-domain interference. We refer to this spectrum scanning as *spectral scan*.[6] Spectral scan reports FFT output, i.e., 4 μs long spectral snapshots, and the bandwidth that can be scanned through spectral scan is equal to the current OCW. Moreover, since spectral scan is conducted during idle state by reusing hardware block, its output can be used to detect the interference, not overlapping on the primary 20 MHz channel, i.e., time-domain interference, without incurring an additional overhead.

Assuming that current OCW is set to 80 MHz, received signal strength (RSS) of secondary 20 MHz and 40 MHz channels, obtained by processing the spectral scan results, are denoted by P_{s20} and P_{s40}, both in dBm, respectively. *RECONN* then compares RSS of the most recent successfully received A-MPDU, denoted as P_{ampdu} (dBm), with P_{s20} and P_{s40} in sequence. In case that $P_{ampdu} - P_{s20} \leq \alpha_{dB}$, receiver reduces OCW to 20 MHz, to eliminate time-domain interference. If the above condition is not satisfied, but $P_{ampdu} - P_{s40} \leq \alpha_{dB}$, receiver changes OCW to 40 MHz. On the other hand, if current OCW is 40 MHz, receiver obtains only P_{s20}, and changes OCW to 20 MHz if $P_{ampdu} - P_{s20} \leq \alpha_{dB}$.

[6] Linux-based open-source device driver, *ath9k* or *ath10k*, provides *spectral scan* operation. Note that scanning the frequency-domain in idle state can be easily supported by any kinds of chipsets.

Note that α_{dB} denotes tSIR threshold to determine whether the interference degrades reception performance or not. An appropriate α_{dB} value varies depending on chipset type, channel condition, interference pattern, and OCW. To reflect this flexibly, *RECONN* initially sets α_{dB} to 0 dB, and intelligently adapts α_{dB} during run-time. Specifically, *RECONN* compares PHY data rate used before and after OCW switching, and then adjusts α_{dB} in the direction of increasing PHY data rate. For instance, if reducing OCW results in decreasing (increasing) PHY data rate, α_{dB} is also decreased (increased) by 1 dB such that OCW reduction becomes more difficult (easier). In this manner, *RECONN* tries to find the optimum OCW consistently according to the pattern and magnitude of time-domain interference to improve the throughput performance.

In the meantime, if the current OCW is 20 MHz or 40 MHz, receiver needs to verify whether time-domain interference still deteriorates reception performance in order to check the possibility to widen OCW. Accordingly, receiver periodically performs probing, i.e., spectral scan on the entire 80 MHz. Specifically, *RECONN* employs probing window, N_{wnd}, i.e., the number of A-MPDUs required to trigger probing. Therefore, if the number of received A-MPDUs reaches N_{wnd}, receiver performs spectral scan on the entire 80 MHz channel after increasing OCW to 80 MHz. If time-domain interference is still expected to negatively affect reception performance, that is, $P_{ampdu} - P_{s20} \leq \alpha_{dB}$ or $P_{ampdu} - P_{s40} \leq \alpha_{dB}$, *RECONN* then reduces OCW back to 20 MHz or 40 MHz and doubles N_{wnd}. On the other hand, if none of the above two conditions is satisfied, receiver remains on OCW of 80 MHz, because it is expected that time-domain interference does not exist anymore.

Notification of the change

OCW switching is triggered by receiver, which is actually interfered. Therefore, whenever OCW is newly selected, receiver should notify transmitter of the changed OCW in order to be able to update the available bandwidth.[7]

[7]The increase in OCW to 80 MHz for probing does not need to be notified.

When a station changes its OCW, it needs to transmit an *operating mode notification frame* to its AP. Operating mode notification frame is an action frame used to notify other stations of changing OCW or the maximum number of spatial streams [1]. On the other hand, when AP changes OCW, it should announce the changed width to all associated stations. AP can notify associated stations of the change, using individually addressed operating mode notification frames, but it takes too much overhead in practice. Instead, the AP is able to broadcast *channel switch announcement action frame* without performing a backoff after PIFS-long idle time.

Discussion

As mentioned in Section 3.2.2, switching OCW incurs delay which is known to be several tens of microseconds such that OCW cannot be changed for each packet in the current 802.11ac system. Indeed, depending on the random backoff value selected by transmitter, receiver might not be able to receive A-MPDU during switching period, thus resulting in frame loss. Therefore, when receiver cannot tolerate frame loss, it can utilize *power management operation* alternatively, as if it enters power saving mode during switching period. After completing OCW switching, receiver then sends a frame to AP to indicate that it has exited power saving mode. However, since an exchange of power management frame causes an additional overhead, a careful consideration is required to effectively use the power saving feature with OCW adaptation, which will be included in our future work. Instead, *RECONN* sets the initial value of N_{wnd} to 1,000 A-MPDUs, and exponentially increases N_{wnd} up to 16,000 A-MPDUs, to prevent excessive OCW changes, and hence, the overhead incurred by changing OCW can be effectively reduced.

One thing to note is that the notification of OCW change should occur prior to a decrease and following an increase in OCW [1]. The transmission bandwidth of a packet is determined when the packet is enqueued in transmitter's queue, and it cannot be changed once the packet is enqueued. Accordingly, if receiver suddenly reduces its

OCW, it will not be able to receive packets, which are scheduled to be transmitted over wider bandwidth. Therefore, receiver should give enough time to transmitter to update the bandwidth. On the other hand, when OCW increases, receiver has no problem to receive packets transmitted by using smaller bandwidth. Accordingly, receiver informs transmitter of its change, after completing OCW switching. Figs. 3.10 and 3.11 show examples of switching OCW with notification using action frames, where the y-axis denotes channel including the primary 20 MHz (*Pri.*) and secondary channels (*S20* and *S40*). Note that BlockAck (*BACK*) is transmitted after Short IFS (SIFS) from the end of A-MDPU reception, which is duplicated in each 20 MHz channel.

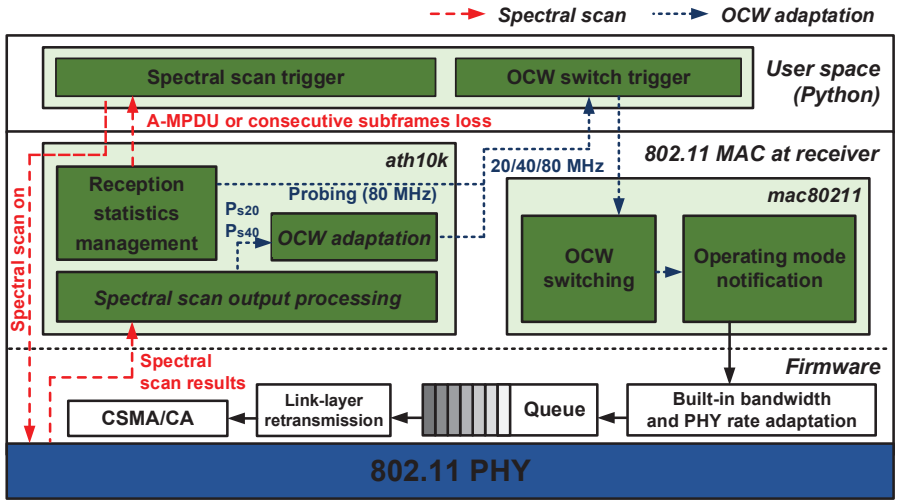

Figure 3.12: Implementation structure of *RECONN*.

3.5 Performance Evaluation

To verify the feasibility and excellence, we implement *RECONN* on the Linux-based open-source device driver, *ath10k* and *mac80211*, and make a prototype using commercial 802.11ac NIC with QCA9880.[8] Detailed implementation of *RECONN* is best

[8]Because QCA9880 does not suffer from undesirable receive locking problem, performance of *RECONN* might be underestimated using QCA9880. Nevertheless, we implement *RECONN* on *ath10k* and

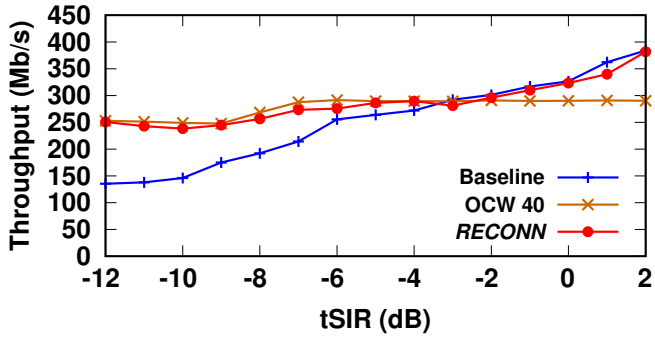

(a) Throughput according to tSIR.

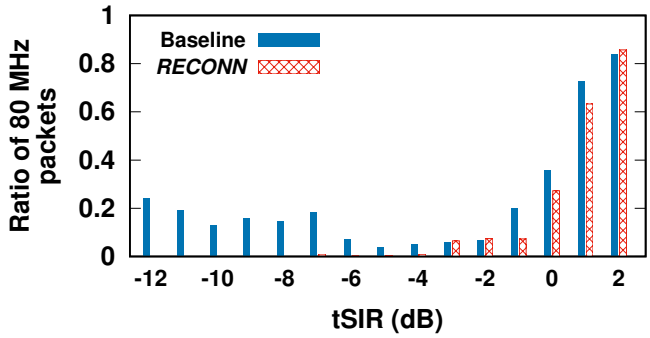

(b) Ratio of 80 MHz subframes.

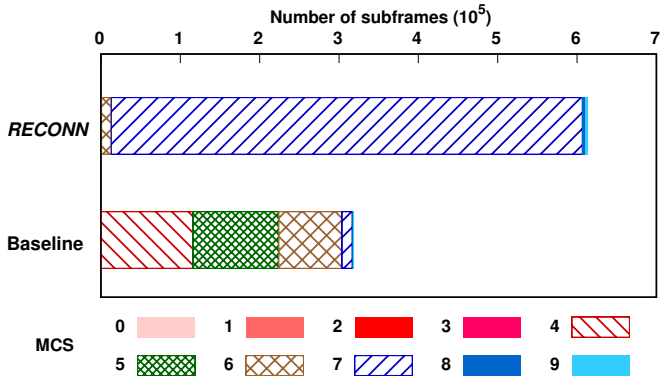

(c) MCS distribution with tSIR $= -12$ dB.

Figure 3.13: Measurement results obtained by the receiver according to tSIR. The transmitter is AC2600 and the interference is generated by NI USRP.

mac80211, due to accessibility and ease of playing with the open-source device driver.

explained with a blueprint in Fig. 3.12. *RECONN* is composed of 1) spectral scan module implemented in *ath10k*, 2) OCW switching and notification module managed by *mac80211*, and 3) triggering module in python-based user space program. Specifically, the need for spectral scan is determined in *ath10k* by detecting A-MPDU or three consecutive subframe losses [53], and the actual triggering is conducted via a python-based triggering program, not disturbing on-going packet reception. An appropriate OCW is then calculated in *ath10k* by processing the spectral scan results. Finally, OCW switching and notification are triggered in user space, and then, actually performed in *mac80211*.

3.5.1 One-to-One Scenario

We firstly conduct an experiment of an one-to-one scenario in the same topology shown in Fig. 3.3, where AC2600 sends saturated downlink traffic at P1 to an associated 802.11ac station located at P3, using channel 48 as the primary 20 MHz channel. Interference is generated by NI USRP at P5, using channel 36 and 20 MHz bandwidth. All measurement results are averaged over five runs, where each run lasts for 20 s.

Fig. 3.13(a) shows throughput obtained by 802.11ac station according to tSIR. We compare performance of *RECONN* with baseline 802.11ac (*baseline*), which uses 80 MHz fixed OCW. For a comparison, we also consider the case of receiver's OCW equal to 40 MHz (*OCW 40 MHz*). When tSIR is higher than -3 dB, *Baseline* achieves the highest throughput, because the interference does not significantly influence on the reception performance of 802.11ac station. However, when tSIR is lower than -3 dB, *OCW 40 MHz* shows the best performance. As expected, *RECONN* adapts OCW depending on the degree of interference to effectively eliminate time-domain interference, thus following the upper most curves and achieving $1.85\times$ higher throughput than that of *Baseline* when tSIR is -12 dB.

Furthermore, Fig. 3.13(b) shows a ratio of successfully received 80 MHz subframes. Since *RECONN* uses 40 MHz OCW when tSIR is lower than -3 dB, no

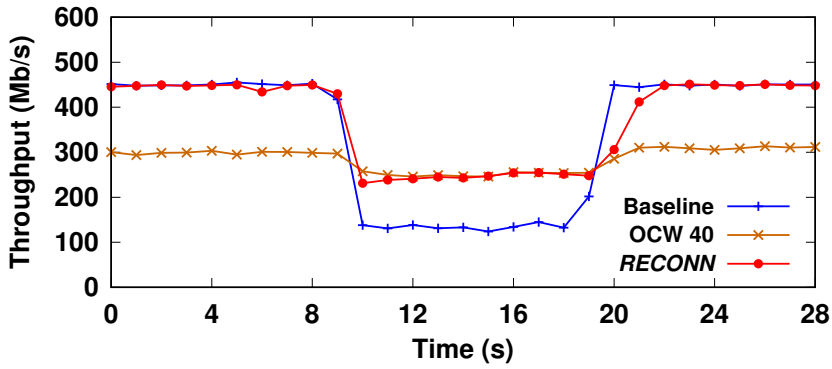

Figure 3.14: Snapshot of instantaneous throughput when tSIR is -12 dB. Interference is turned on at 9 s and turned off between 18 s and 19 s.

80 MHz subframe is observed. Interestingly, even though *Baseline* employs autonomous bandwidth adaptation implemented in AC2600 firmware, we have observed that more than 10% of subframes are received by sharing the wireless medium with the interferer, when tSIR is lower than -6 dB, thus resulting in low channel utilization [23, 27]. Furthermore, more than 80% of subframes are received at 40 MHz bandwidth, by lowering MCS index unnecessarily due to time-domain interference. In particular, as shown in Fig. 3.13(c), *Baseline* uses MCS 3, 4, and 5, while *RECONN* dominantly uses MCS 7 when tSIR is -12 dB.

In order to check the adaptability of *RECONN*, we obtain instantaneous downlink throughput results as shown in Fig. 3.14. Interference traffic making -12 dB tSIR begins at 9 s and disappears between 18 s and 19 s. As soon as interference traffic is generated, *RECONN* reduces OCW to 40 MHz, by immediately detecting time-domain interference. On the other hand, after interference traffic is turned off, *RECONN* waits until probing window expires, and then increases OCW to 80 MHz.

3.5.2 Multi-station Scenario

We deploy three stations at P5 (STA1), P6 (STA2), and P7 (STA3), where AC2600 transmits saturated downlink traffic to each station. Different from other experiments, interference traffic is generated by commercial 802.11n devices equipped with Qualcomm AR9380, where an 802.11n AP located at P3 sends saturated downlink traffic to its associated 802.11n station deployed at P2. Accordingly, only STA1 at P5 is severely interfered by the interferer at P3.

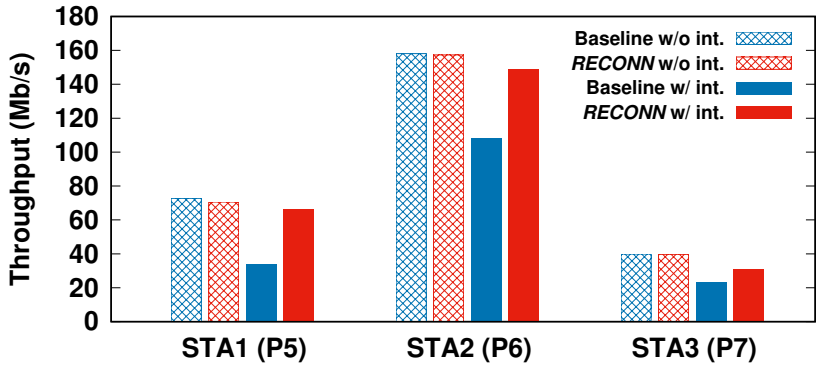

Figure 3.15: Multi-station environment. *RECONN* achieves 1.49× higher network throughput than that of *Baseline*, when the interference exists.

Fig. 3.15 shows downlink throughput obtained by three stations. When the interference does not exist (*w/o int.*), *Baseline* and *RECONN* provide almost the same throughput, using 80 MHz bandwidth. On the other hand, when the interference is generated (*w/ int.*), *Baseline* achieves throughput of 33.6 Mb/s, 108 Mb/s, and 23 Mb/s for STA1, STA2, and STA3, respectively. Even though only STA1 is intensively affected by the interference with tSIR $= -10$ dB, both STA2 and STA3 also suffer from throughput degradation, due to the airtime waste and heavy retransmission attempts to STA1. However, *RECONN* reduces STA1's OCW to 40 MHz, and hence, it is not affected by time-domain interference, thus resulting in 96.5% throughput enhancement. Interestingly, although packets to STA1 consume longer airtime due to

the reduced bandwidth, network throughput of *RECONN w/ int.* is slightly decreased (only 8% reduction) compared to *RECONN w/o int.* because 1) STA2 and STA3 are independent from the interference, and 2) STA1 obtains higher power spectral density thanks to fixed transmit power and less impact of frequency selectivity. Finally, we find that *RECONN w/ int.* achieves 48.9% higher aggregate throughput, compared to *Baseline w/ int.*.

3.6 Summary

In this chapter, we have verified that using bandwidth less than OCW might cause packet detection and synchronization failure, undesirable receive locking problem, and AGC failure due to time-domain interference not overlapping with the incoming desired signal on frequency domain. To solve this problem, we develop *RECONN*, which intelligently adapts OCW using the frequency-domain information at receiver side. *RECONN* fully complies with 802.11 MAC and requires no hardware modification. Our prototype implementation in commercial 802.11ac devices demonstrates that *RECONN* achieves up to 1.85$\times$ higher throughput compared to baseline 802.11ac, by completely eliminating time-domain interference. We expect that *RECONN* will highly benefit the future large-scale and heterogeneous 5 GHz network, where the time-domain interference problem might be severer in the future.

Chapter 4

REACTER: Receive Architecture for Eliminating Time-Domain Interference

4.1 Introduction

IEEE 802.11ac WLAN supports wide bandwidth operation, often referred to as channel bonding, which aggregates multiple 20 MHz channels up to 160 MHz bandwidth, to enhance throughput performance.

In order to transmit and receive packets through the wide bandwidth channel, a station needs to increase the size of fast Fourier transform (FFT), for example, 128-FFT and 256-FFT for 40 MHz and 80 MHz bandwidth, respectively, without changing the position and spacing of subcarriers. Understandingly, the station does not need to change FFT size during run-time, once it is set to 256-FFT, because the unused subcarriers can be disregarded.

However, in Chapter 3, we have shown that using bandwidth less than the receiver's operating channel width (OCW), i.e., twice the baseband bandwidth, leads to poor reception performance, due to *time-domain interference*.[1] Specifically, in case the

[1] We refer to *time-domain interference* as the interference not overlapping with the desired signal in frequency-domain, but contained in the receiver's baseband bandwidth. Therefore, time-domain samples include both the interference and desired signals.

time-domain interference signal arrives first, preceding to the reception of the desired signal, the station might not receive the desired packet by unnecessarily attempting to decode the interference signal. Moreover, packet detection and synchronization performance might also be severely deteriorated, because the station detects a packet and makes a synchronization, using time-domain samples of the preamble. On the other hand, if the strong interference signal comes in the middle of the desired packet reception, time-domain samples including both the interference and desired signals can be clipped off at analog-to-digital-converter (ADC) circuit, thus leading to signal distortion as explained in Section 3.3.1.

To cope with time-domain interference problem, *RECONN* proposed in Chapter 3 dynamically switches OCW depending on the frequency domain information at receiver. *RECONN* provides a practical solution for the existing 802.11ac devices to eliminate time-domain interference in analog circuit without hardware modification, thus simply requiring the device driver update only at the receiver. However, it takes time to collect frequency-domain information and incurs the additional latencies such as RF front end reconfiguration time up to several tens of microseconds [4], and the protocol overhead for exchanging notification action frames.

The main purpose of this chapter is to propose *REACTER*, a receiver architecture to eliminate the impact of time-domain interference, complying with the 802.11 specifications. Our major contributions are summarized as follows.

- We first analyze the effect of digital low pass filter (DLPF) on packet detection and synchronization performance, depending on the incoming signal's bandwidth and the signal strength of time-domain interference, through extensive link-level simulations. Based on the results, we propose a suitable DLPF application plan.

- We verify that time-domain interference overlapping with the desired packet causes that 1) ADC operates in a range smaller than its optimal range, thus leading to high quantization error and 2) the analog signal can exceed the dynamic range of ADC so taht clipping can occur, resulting in signal distortion. In such scenarios, A-MPDU

subframes can be successfully received by adapting AGC level in real-time since 1) the desired signal does not overlap on the frequency domain with time-domain interference, and 2) subframes can be individually acknowledged by using block acknowledgement (BlockAck).

- We develop *REACTER*, a ***re***ceive ***ar***chitecture for eliminating the impact of ***t***ime-domain int***er***ference, fully complying with the 802.11 specifications. *REACTER* improves packet detection and synchronization performance using 20 MHz DLPF,[2] and conducts real-time AGC during A-MPDU reception to prevent clipping and high quantization error at ADC. Regardless of the transmit bandwidth, *REACTER* can be applied immediately upon the reception of the desired packets, without incurring any protocol overhead and latency.

- Our extensive simulations under a wide range of scenarios show that *REACTER* enhances the reception performance significantly by completely eliminating the impact of time-domain interference.

The rest of the chapter is organized as follows. Section 4.2 provides the preliminaries of wide bandwidth operation, packet detection and synchronization, and AGC method in IEEE 802.11 WLANs. The detailed design of *REACTER* is presented in Section 4.3, and its evaluation results are presented in Section 4.4. Finally, Section 4.5 summarizes this chapter.

4.2 Preliminaries

4.2.1 Packet Detection and Synchronization

An 802.11 receiver detects and synchronizes the incoming packet using a physical layer convergence protocol (PLCP) preamble at the beginning of PHY protocol data

[2]The cut-off frequency of DLPF is set to 16 MHz, since it is possible to minimize the inter-channel interference (ICI) caused by the non-ideality of the filter, by filtering the approximately 16 MHz bandwidth excluding the guard band.

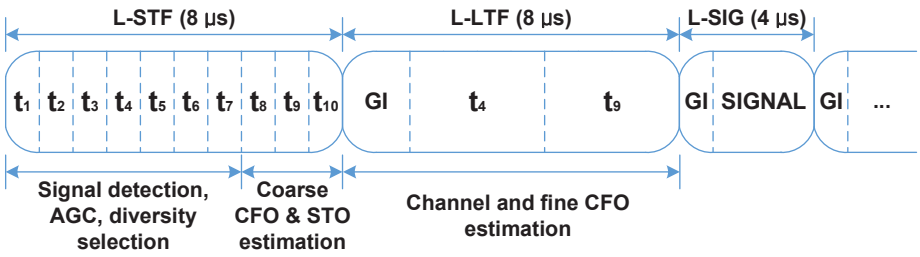

Figure 4.1: Structure of the legacy preamble identical to 802.11a preamble.

unit (PPDU), where the PLCP preamble contains the legacy preamble identical to IEEE 802.11a preamble as shown in Fig. 4.1.

The legacy preamble includes legacy short training field (L-STF) and legacy long training field (L-LTF), which are followed by a signal field (L-SIG). The L-STF is used for packet detection, AGC, coarse carrier frequency offset (CFO) and symbol timing offset (STO) estimation, and the L-LTF allows receiver to acquire channel state information (CSI) and fine synchronization.

Specifically, the L-STF consists of 10 short repeated symbols, which use 12 out of 52 subcarriers based on 64-point inverse FFT (IFFT) for 20 MHz bandwidth, thus resulting in $0.8\ \mu$s periodicity. Thanks to the repetitive nature of L-STF with a good correlation property, receiver is able to detect an incoming packet using auto-correlation, a_n, of the time-domain samples with the delayed version of themselves:

$$a_n = \frac{\left|\sum_{i=0}^{L-1} r_{n+i} \cdot (r_{n+i-L})^*\right|^2}{\sqrt{\sum_{i=0}^{L-1} |r_{n+i}|^2}\sqrt{\sum_{i=0}^{L-1} |r_{n+i-L}|^2}}, \tag{4.1}$$

where r_n denotes the n-th time domain sample and L is the length of auto-correlation window, and a_n exceeding a threshold indicates a packet detection. Moreover, peak and phase values of a_n can also be used to find AGC and makes synchronization to estimate CFO and STO [32].

For wide bandwidth transmission such as 40 MHz and 80 MHz, a transmitter duplicates the legacy preamble over each of 20 MHz channel for backward compatibility.

Therefore, extracting the preamble of the primary 20 MHz or 40 MHz bandwidth signal using DLPF also allows receiver to find accurate detection and synchronization, even though incoming packet is transmitted through 80 MHz bandwidth. More details about synchronization using DLPF is presented in Section 4.3.2.

4.2.2 Automatic Gain Control in IEEE 802.11 WLAN

AGC provides a controlled signal amplitude of the output signal, or equivalently, the amplitude of ADC input signal, despite variation of the input signal amplitude [58]. Note that, in case AGC level is set too high, the analog signal can exceed the dynamic range of ADC so that clipping can occur, resulting in signal distortion. On the other hand, if AGC level is set very low, it operates in a range smaller than the optimal range of ADC, thus leading to high quantization error at ADC.

Using L-STF, WLAN receiver conducts AGC in analog circuit within a few microseconds as shown in Fig. 4.1 [29–31]. The model used for AGC, in this chapter, is based on the amplitude clipping feedback from ADC, with a target settling time of approximately 4 μs, i.e., five L-STF symbols [34].

4.3 *REACTER*: Proposed Architecture

4.3.1 Simulation Methodology

In this section, we introduce IEEE 802.11ac link-level simulator based on IT++, which is an open-source C++ library of mathematical, signal processing, and communication classes and functions [60]. The simulator provides all features of the 802.11ac specifications, and both transmitter and receiver support 80 MHz bandwidth based on 256-FFT, i.e., the OCW is set to 80 MHz. We adopt TGac channel model to generate the wireless channel [61]. The primary 20 MHz channel is set to channel 40 with 5,200 MHz center frequency, and time-domain interference is generated on channel 48 with 5,240 MHz center frequency (i.e., one of the 20 MHz channels in the secondary

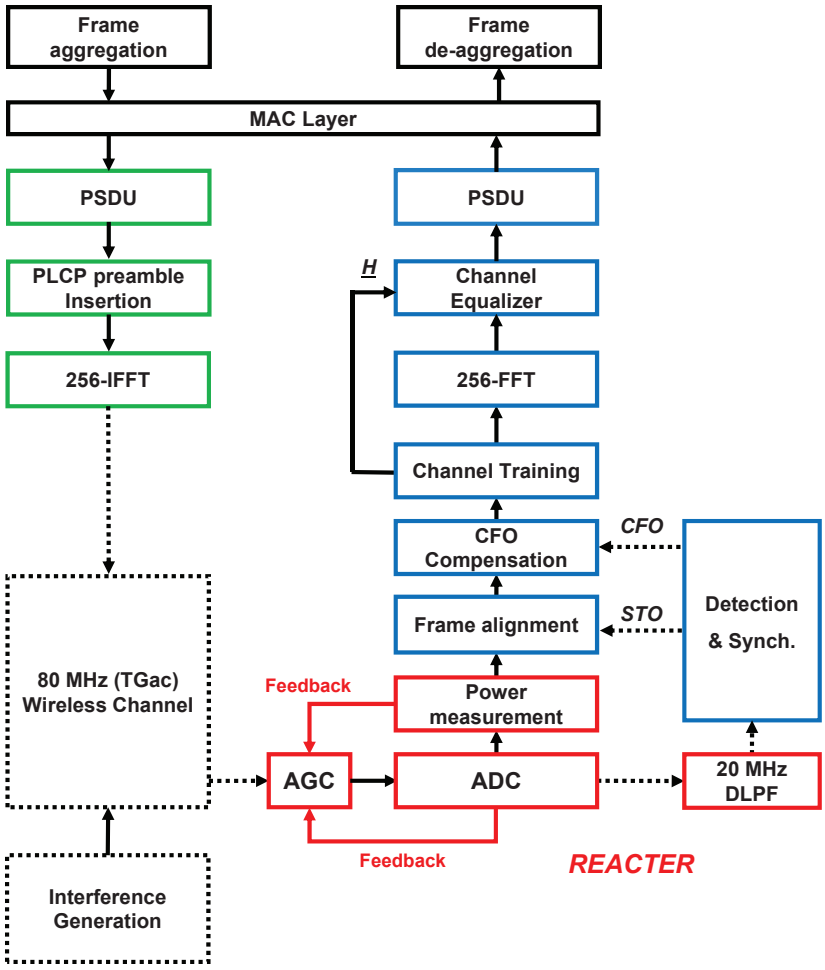

Figure 4.2: Structure of IT++ based IEEE 802.11ac link-level simulator.

40 MHz channel), as illustrated in Fig. 4.3. The time-domain interference signal is also WLAN OFDM symbol without synchronization with the desired signal.

For packet detection and synchronization, we adopt Chang's algorithm which employs both auto-correlation and cross-correlation results of L-STF to accurately synchronize the incoming packet [33], because it is practically well designed and easy to implement.

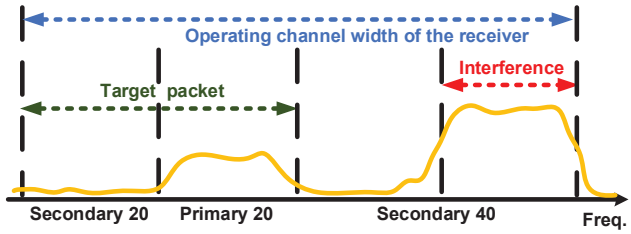

(a) Transmit bandwidth of 20 MHz on the primary channel.

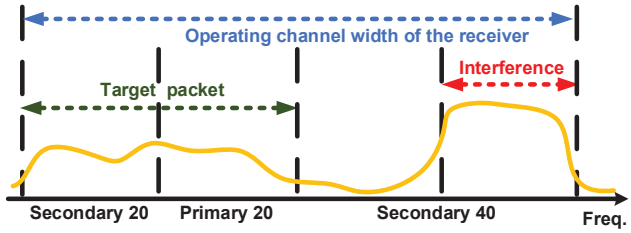

(b) Transmit bandwidth of 40 MHz including the primary and secondary 20 MHz channels.

Figure 4.3: Spectrum usage for our simulation. The 20 MHz time-domain interference signal is generated on channel 48 (i.e., on the 20 MHz channel within the secondary 40 MHz channels).

4.3.2 Digital Low Pass Filter (DLPF)

In this section, we present a suitable DLPF application plan, based on the extensive simulation of DLPF performance on packet detection and synchronization. To extract the primary channel and secondary channel, we adopt raised cosine filter (RCF) with roll-off factor of 0.25, which is frequently used for pulse-shaping in digital domain because of its ability to minimize inter-symbol interference (ISI) [62].

Without Time-domain Interferences

Figs. 4.4 and 4.5 show the normalized auto-correlation peak (NAP) of L-STF, STO error, and frame error rate (FER) according to signal-to-noise (SNR). For a given SNR,

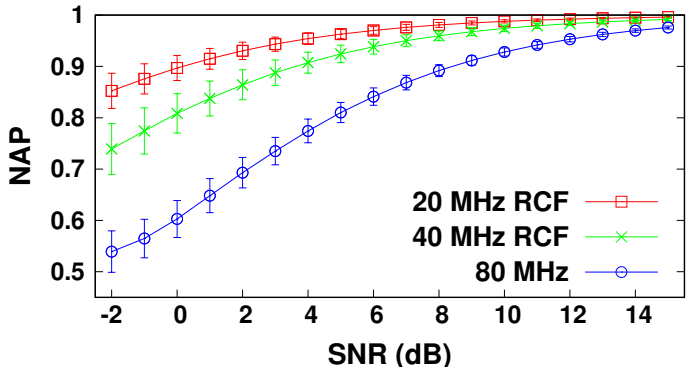

(a) NAP results.

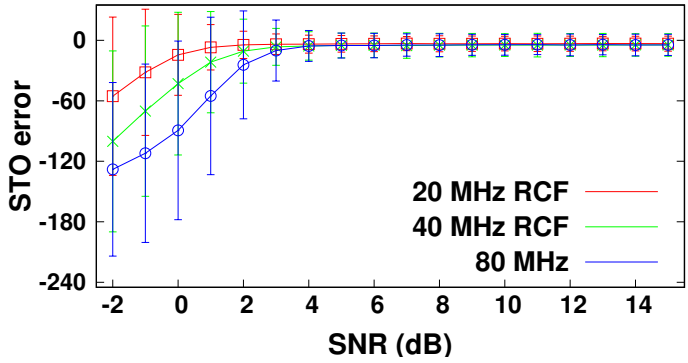

(b) STO error in sample index.

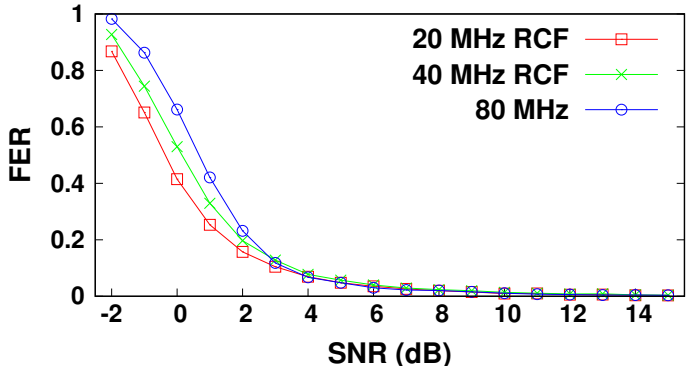

(c) FER results.

Figure 4.4: Packet detection and synchronization performance according to SNR, when the transmission bandwidth is 20 MHz.

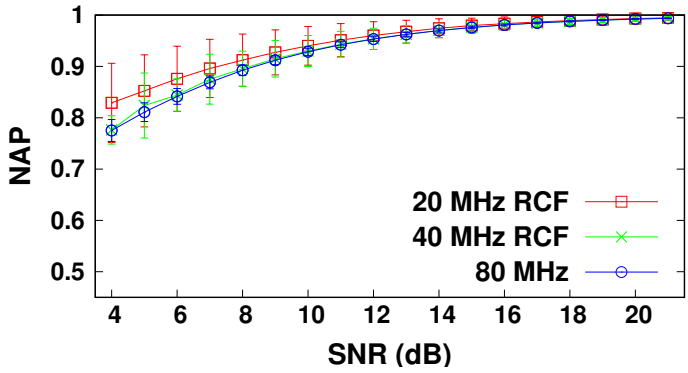

(a) NAP results.

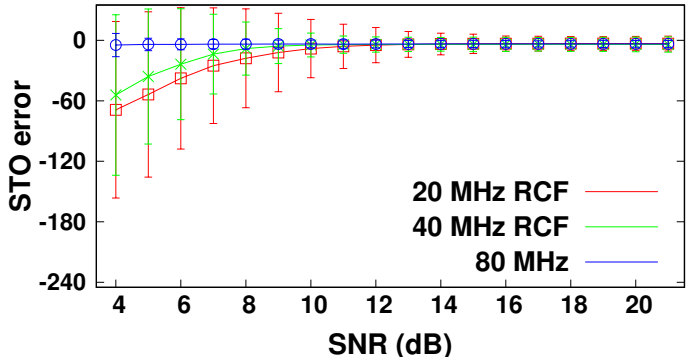

(b) STO error in sample index.

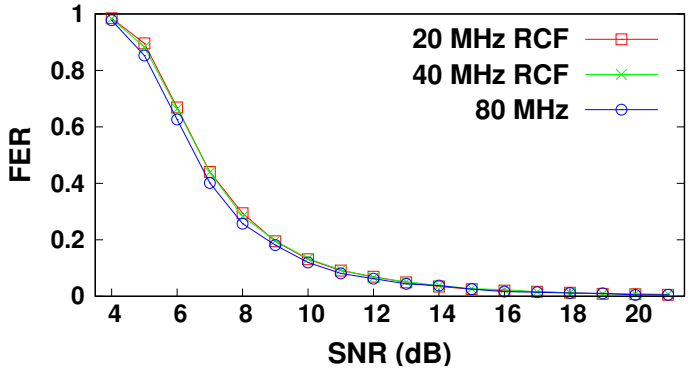

(c) FER results.

Figure 4.5: Packet detection and synchronization performance according to SNR, when the transmission bandwidth is 80 MHz.

$10,000$ frames in total are transmitted. Each frame is 100 B long without aggregation, and transmitted with PHY rate of 6.5 Mb/s (i.e., MCS 0). The bandwidth used for packet transmission within the OCW is 20 MHz or 80 MHz for Fig. 4.4 or Fig. 4.5, respectively. Packet detection and synchronization are conducted using the preamble extracted by the *20 MHz RCF*, *40 MHz RCF*, or without filtering (*80 MHz*), assuming that the transmission bandwidth is unknown to the receiver.

When the transmission bandwidth is 20 MHz, *20 MHz RCF* shows the highest NAP and the minimum STO error as shown in Figs. 4.4(a) and 4.4(b). Because the preamble is carried only on the primary 20 MHz channel, time-domain samples obtained through *40 MHz RCF* and *80 MHz* contain the more noise component from the unused bandwidth. Therefore, using the 20 MHz filtered signal achieves the minimum FER for all SNR region as presented in Fig. 4.4(c).

On the other hand, if the transmission bandwidth is set to 80 MHz, that is, the duplicated preamble is also carried on all the secondary channels, *80 MHz* shows the best performance, i.e., the lowest STO error and FER as shown in Figs. 4.5(a)–4.5(c). Although the average SNR of each subcarrier is exactly same for all the cases, *80 MHz* achieves the highest diversity gain against multi-path fading. However, regardless of the cut-off frequency, *all cases show very similar detection and synchronization performance in the meaningful SNR region providing lower than 10% FER.*

Note that *20 MHz RCF* always achieves the highest NAP,[3] because the band-limited white noise has a non-zero correlation between time-domain samples. Specifically, as the size of bandwidth decreases, the auto-correlation of two time-domain noise samples increases gradually. Therefore, using 20 MHz filtered signal for synchronization increases the magnitude of non-zero offset in NAP results.

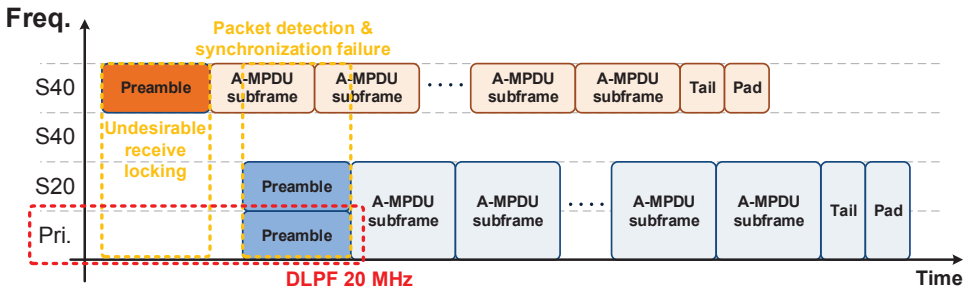

Figure 4.6: Time-domain interference causes undesirable packet detection and synchronization failure, when time-domain interference arrives first. In this scenario, extracting the primary channel using 20 MHz DLPF can effectively eliminate the impact of time-domain interference.

Existence of Time-domain Interferences

When the time-domain interference signal not overlapping with the desired signal exists during the entire A-MPDU reception, the packet detection and synchronization performance can be severely deteriorated as shown in Fig. 4.6.

To verify the impact of time-domain interference, we conduct simulations using IEEE 802.11ac link-level simulator. We adopt *time-domain signal-to-interference ratio (tSIR)* as a power ratio of desired and interference signal, both contained in time-domain samples (i.e.,twice the baseband of the receiver), but not overlapping with each other on frequency domain, defined in Section 3.3.1. For a given tSIR, totally $3,000$ fully aggregated A-MPDUs are transmitted. Each A-MPDU subframe is 300 B long, and transmitted with PHY rate of 65 Mb/s (i.e., MCS 7). The transmission bandwidth is set to 40 MHz at the transmitter. The time-domain interference signal is generated on channel 48 as illustrated in Fig. 4.3, which fully overlaps with the desired signal only on the time-domain from the beginning of A-MPDU reception. More details about simulation environment is presented in Section 4.3.1.

Fig.4.7 shows NAP, STO error, and SFER performance according to tSIR. Specif-

[3]The highest NAP does not guarantee the best performance, which corresponds to the lowest FER.

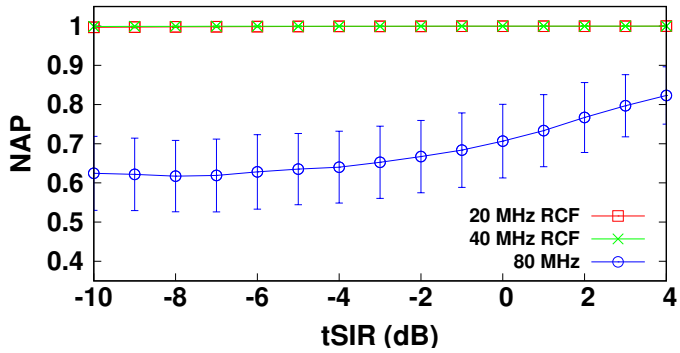

(a) NAP results.

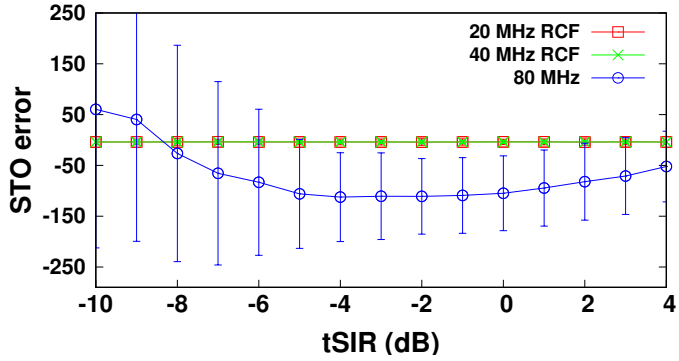

(b) STO error in sample index.

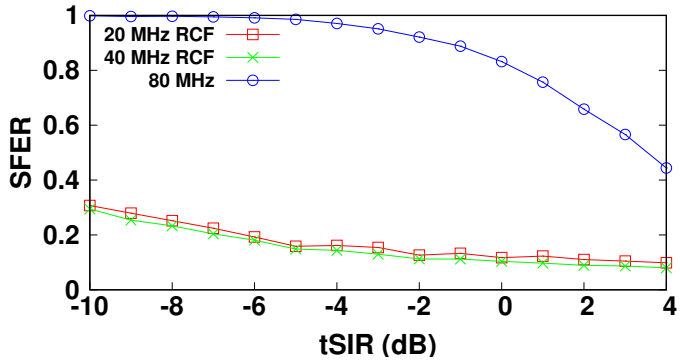

(c) FER results.

Figure 4.7: Packet detection and synchronization performance according to tSIR.

ically, *80 MHz*, which uses the whole 80 MHz signal for detection and synchronization without filtering, obtains NAP even below 0.6, which causes packet detection

failures [32–34]. Moreover, STO errors exceed the number of guard interval (i.e., cyclic prefix of 64 samples in 80 MHz bandwidth), resulting in severe inter-symbol-interference (ISI). As a results, *80 MHz* shows very high SFER close to 1 when tSIR is below -3 dB shown in Fig. 4.7(c).

On the other hand, both *20 MHz RCF* and *40 MHz RCF* always provide NAP close to 1 without STO error for all tSIR variations. In other words, *using DLPF, packet detection and synchronization is not affected by time-domain interference at all, effectively extracting the preamble not including time-domain interference* as shown in Fig. 4.6. Nevertheless, we can observe slight SFER increase with decrease of tSIR. This is because 1) non-ideality of the filter, 2) the increase in the amount of quantization error due to the low AGC level as explained in Section 4.2.2, and 3) the increase in inter-carrier-interference (ICI) from time-domain interference. Specifically, even though time-domain interference is not overlapping with the desired signal in frequency domain, its sidelobe affects the decoding performance, since both are not synchronized, that is, the orthogonality does not hold.

Discussion

Through the extensive simulations, we have verified that using bandwidth equal to the transmission bandwidth provides the optimal packet detection and synchronization performance, because it contains relatively lower amount of noise component and fully achieves diversity gain. However, considering the performance similarities in the meaningful SNR region providing lower than 10% FER, and the impact of time-domain interference shown in Section 3.3.2, we insist that *using the 20 MHz filtered signals for packet detection and synchronization* 1) ensures practically good performance over 2 dB SNR, 2) provides packet detection and synchronization results that are not affected by time-domain interference, and 3) troubleshoots undesirable receive locking problem, because it allows the receiver to use the preamble which always comes in the primary channel. Moreover, using the 20 MHz filtered signal guarantees

low complexity through decimation of time-domain samples, and enables reusing the existing synchronization hardware block.

Meanwhile, using digital filters for data symbols (i.e., time-domain samples of OFDM data symbols) significantly degrades the decoding performance, due to non-ideality of DLPF such as phase distortion, gain fluctuation, and inter-symbol interference (ISI). On the other hand, packet detection and synchronization can be conducted using the digitally filtered signals, because it only utilizes the repeatability and similarity of successive signals in time-domain.

4.3.3 Real-Time AGC

In WLAN system, AGC is conducted in analog circuit, to provide controlled amplitude of the input signal to ADC. AGC level is determined during the preamble reception, especially, within several L-STF symbols. Therefore, AGC level does not change while receiving the data symbols, assuming that the input power level is constant. However, when the strong time-domain interference signal comes in the middle of frame reception, the analog signal can exceed the dynamic range of ADC, thus leading to clipping as illustrated in Fig. 4.8. On the other hand, when time-domain interference arrives first, preceding to a reception of the desired packet, receiver needs to set AGC level low to prevent clipping while receiving data symbols. Especially, when the time-domain interference signal disappears during A-MPDU reception, AGC operates in a range smaller than the optimal range of ADC, thus leading to high quantization error at ADC unnecessarily.

To verify the impact of clipping and quantization error, we conduct simulations, assuming that AGC circuit has a settling time of approximately $4\ \mu$s i.e., five L-STF symbols, as described in Section 4.2.2. We use a cost-effective 10-bit ADC model which is commonly used in commercial equipment, with full-scale power level of -10 dBm. Considering thermal and quantization noise, SNR of the ADC model is given by 61.96 dB [63]. Additionally, we also take ADC jitter noise, differential and integral

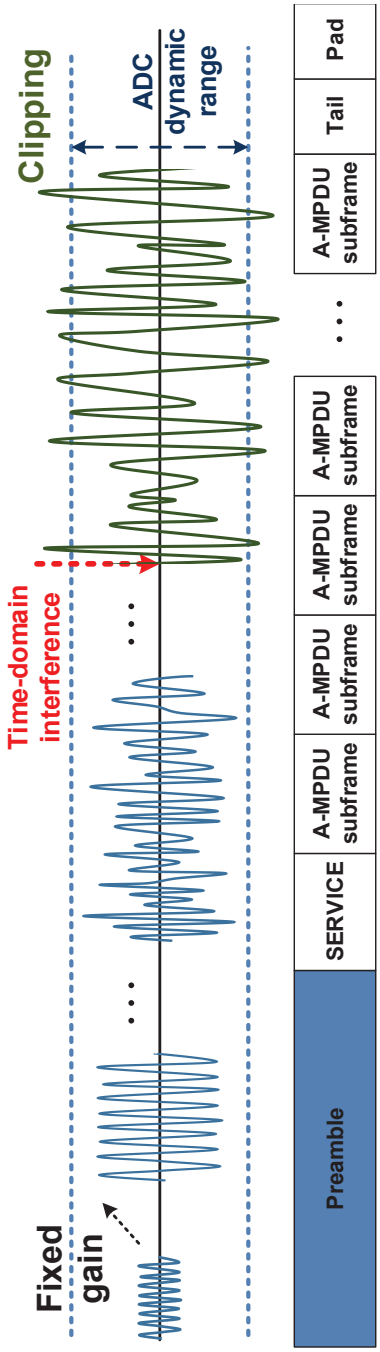

Figure 4.8: Time-domain interference causes clipping, exceeding ADC dynamic range.

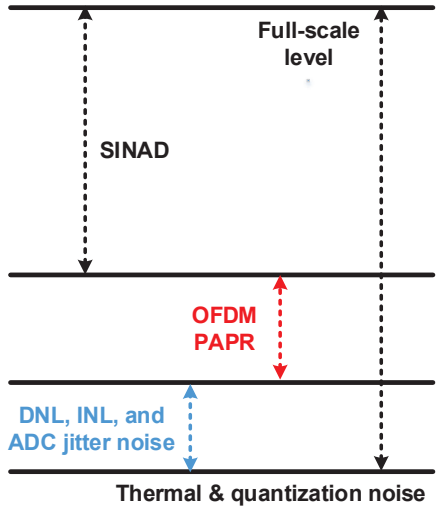

Figure 4.9: ADC noise contributions.

non-linearity into account, which are given by totally 3 dB [64, 65]. Finally, as shown in Fig. 4.9, signal-to-noise and distortion ratio (SINAD) then becomes 46.96 dB, because OFDM has high peak-to-average power ratio (PAPR) of between approximately 8 dB to 12 dB [66].

Fig. 4.10 shows the average SFER and an average number of observed clipping in a single A-MPDU. For a given tSIR, totally $3,000$ fully aggregated A-MPDUs are transmitted, where each subframe is transmitted with MCS 7 with 300 B length. The transmission bandwidth is set to 40 MHz, and detection and synchronization are conducted using 20 MHz RCF-filtered signal as discussed in Section 4.3.2. Time-domain interference overlaps with 1) the front-positioned (first half) A-MDPU subframes (*front*), 2) the end-positioned (second half) A-MPDU subframes (*end*), or 3) the entire A-MPDU subframes over all (*whole*) on the time-domain. More details about simulation environment is presented in Section 4.3.1.

As demonstrated in Fig. 4.10(a), when tSIR is lower than -4 dB, *end* obtains the highest SFER, because AGC level is determined without the impact of time-domain

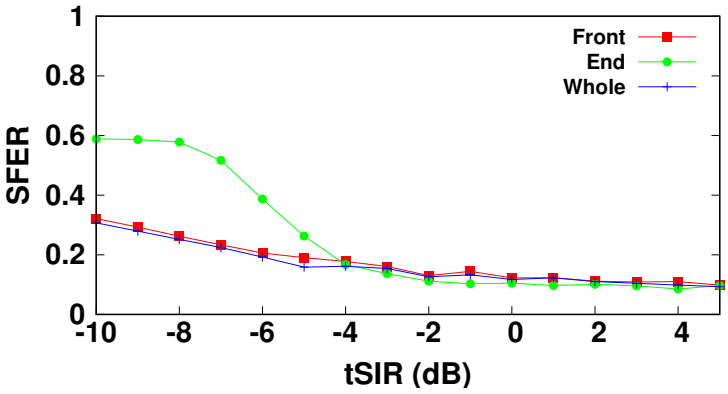

(a) SFER results.

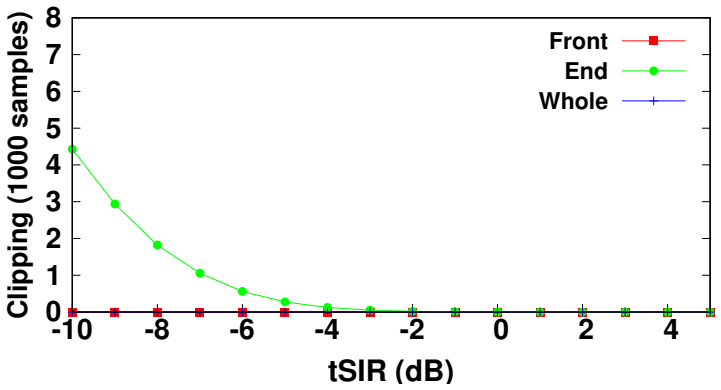

(b) Number of clipping during reception of an A-MPDU.

Figure 4.10: SFER and the number of clipping results according to tSIR, when time-domain interference overlaps with the desired A-MPDU reception.

interference, while receiving several L-STF symbols. Specifically, *front* and *whole* do not suffer clipping shown in Fig. 4.10(b), but SFER increases as tSIR decreases due to high quantization error. Specifically, Fig. 4.11 presents the average SFER according to subframe index.[4] In case of *end*, the front-positioned subframes shows under 10% SFER for all tSIR, but subframes overlapping with time-domain interference present the very high SFER caused by clipping. In case of *front* and *whole*, AGC level is well

[4]A single A-MPDU consists of totally 64 subframes, due to the size constraints of the bitmap contained in BlockAck.

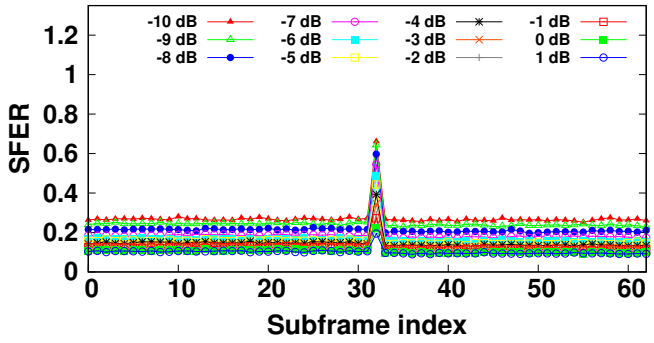

(a) Average SFER of *front*.

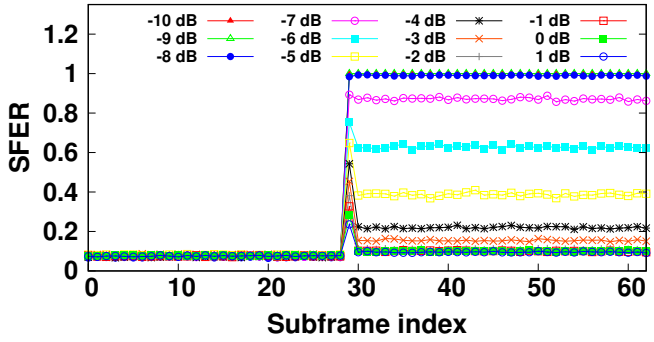

(b) Average SFER of *end*.

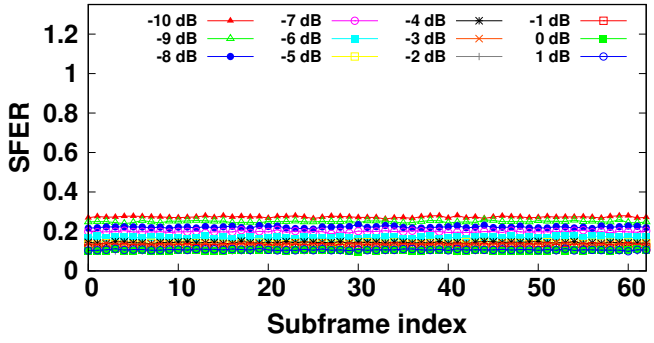

(c) Average SFER of *whole*.

Figure 4.11: Average SFER according to subframe index, when time-domain interference entirely or partly overlaps with the desired A-MPDU.

determined to be able to avoid clipping. However, the average SFER increases over all subframe index, because quantization error increases, that is, the desired signal amplitude becomes relatively small. As a result, when tSIR is -10 dB, the overall SFER stays at 25%. Note that even though the time-domain interference signal disappears in the middle of A-MPDU (i.e., at the 32-th subframe) for the *front* case, SFER is not decreased, because of the fixed AGC level settled at the preamble.

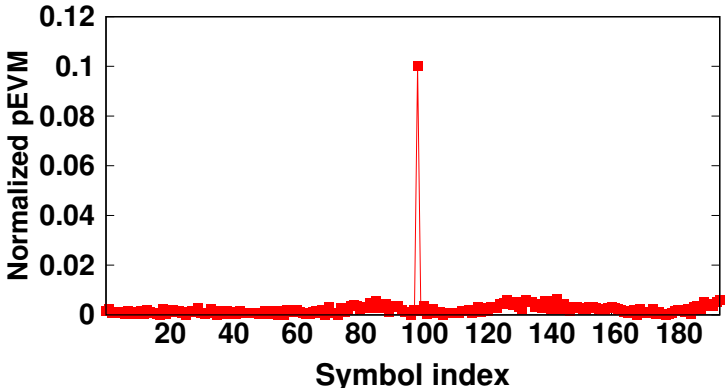

(a) Normalized pEVM.

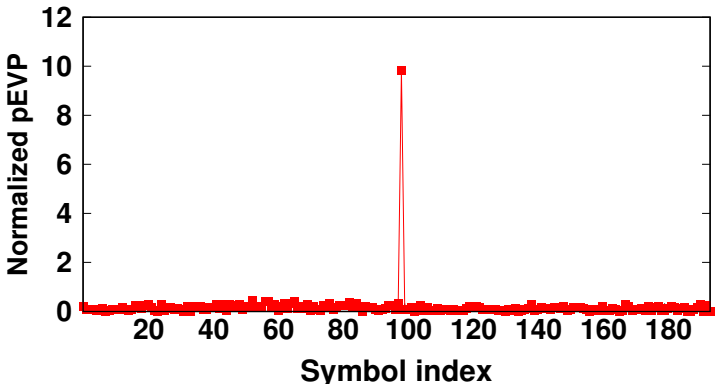

(b) Average normalized pEVP (in degree).

Figure 4.12: Normalized pEVM and pEVP according to OFDM symbol index, when tSIR is -10 dB.

One thing to note is that the 32-th subframe experiences the high SFER peak in case of *front*. This is because OFDM data symbol decoding failure due to the increased

ICI. To be more specific, we calculate the average amplitude and phase error of the known pilot sequence in OFDM data symbols after phase correction and channel compensation while receiving A-MPDUs. Fig. 4.12 shows the average normalized pilot error vector magnitude (pEVM) and error vector phase (pEVP) according to OFDM data symbol index, when tSIR is -10 dB. The disappearance of time-domain interference during the reception of the 99-th OFDM data symbol causes an amplitude distortion of 0.1 and a phase rotation of around 10 degrees on average, thus leading to decoding performance degradation of data subcarriers in the I-Q plane. As a result, when time-domain interference exists temporarily within one FFT window, the corresponding OFDM symbol appears to pass through the different wireless channel.

In summary, we have shown that time-domain interference causes AGC failure such as high quantization error or clipping. Interestingly, if *AGC level changes during A-MPDU reception*, such problems can be easily solvable. Especially, since 1) the desired signal does not overlap with time-domain interference on the frequency domain, and 2) subframes can be individually acknowledged by using BlockAck, real-time AGC allows a receiver to be able to decode remaining subframes with low quantization error without clipping.

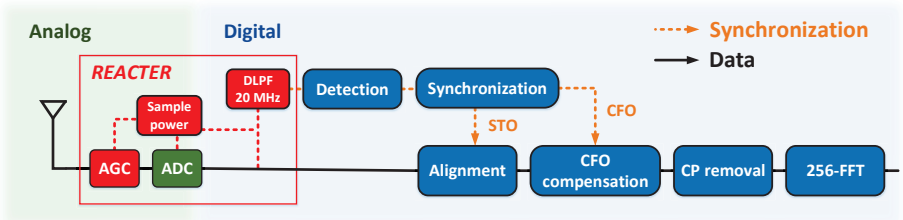

Figure 4.13: Structure of *REACTER*. Digital time-domain samples pass DLPF of 20 MHz for packet detection and synchronization. Based on clipping feedback from ADC and the measured time-samples power, AGC level is adjusted in real-time.

4.3.4 Structure of *REACTER*

In this section, we propose a receiver architecture for eliminating the impact of time-domain interference, based on the observations in Sections4.3.2 and 4.3.3. Through the extensive simulations, we have found two important intuitions: 1) Utilizing DLPF extracting the primary channel for synchronization solves undesirable receive locking problem, enhances packet detection and synchronization performance against time-domain interference, guarantees sufficient performance in the meaningful SNR region, and enables the receiver to reuse the existing hardware block with low complexity. 2) Real-time AGC level adjustment during A-MPDU reception enhances the decoding performance by reducing quantization error and clipping when the strong time-domain interference signal overlaps with the desired packet partially on the time-domain.

Consequently, we propose *REACTER*, a receiver architecture for WLAN receiver for eliminating the impact of time-domain interference to improve the detection, synchronization, and decoding performance.

Fig. 4.13 illustrates the entire structure of *REACTER*. In the digital domain, ADC output (i.e., digital time-domain sample) flows simultaneously into the data path and synchronization path. Following the synchronization path, time-domain samples are firstly filtered to extract the primary 20 MHz channel, and then, detection and synchronization are conducted using the output of DLPF, in order to estimate STO and CFO not affected by time-domain interference.

After acquiring the accurate synchronization, if time-domain interference appears or disappears during the reception of data symbols, AGC level should be adjusted, to minimize quantization error and clipping in the analog domain. To precisely find the appropriate AGC level in real-time, we adopt time-domain sample power, P_n, of the time-domain samples from $n-L$ to $n-1$ as follows:

$$P_n = 10 \cdot \log \sum_{k=0}^{L-1} \left(r_{n+k-L}\right) \left(r^*_{n+k-L}\right), \tag{4.2}$$

where L is the size of moving window for power measurement.

In case the strong time-domain interference signal suddenly comes in the middle of A-MPDU subframes, clipping can occur in ADC circuit. When clipping is detected at time index n, *REACTER* calculates P_{n+L} after receiving the next L samples, to measure the increased power due to time-domain interference. AGC level then decreases by $P_{n+L} - P_n$, resulting in the power of the time-domain sample being bounded within the dynamic range of ADC.

Algorithm 1 Real-time AGC

Update P_n and P_{n-L} for the n-th time-domain sample
if $clipping$ **then**
  Wait for the next L samples
  $Decrease$ AGC level by $P_{n+L} - P_n$
else
  if $P_{n-L} \geq P_n + \beta_{dB}$ **then**
    $P_{max} = P_{n-L} - P_n$
    for the next L samples ($i = 1$ **to** L) **do**
      $P_{max} = \max(P_{max}, P_{n-L+i} - P_{n+i})$
    end for
    $Increase$ AGC level by P_{max}
  end if
end if

On the other hand, the disappearance of time-domain interference signal during A-MPDU reception leads to unnecessarily high quantization error at ADC as explained in Section 4.3.3. In order to detect a sudden decrease of sample power, we continuously compare P_n with P_{n-L} as follows:

$$P_{n-L} - P_n \geq \beta_{dB}, \tag{4.3}$$

where β_{dB} denotes a buffering threshold, blocking an unwanted increase of AGC level caused by a small difference in average power. In case (4.3) satisfies, *REACTER* increases AGC level by the maximum power difference, P_{max}, defined by

$$P_{max} = \max_{1 \le i \le n} P_{n-L+i} - P_{n+i}, \tag{4.4}$$

so that ADC can operate in the optimal range without causing unnecessary clipping. Algorithm 1 summarizes the operation of real-time AGC in *REACTER*.

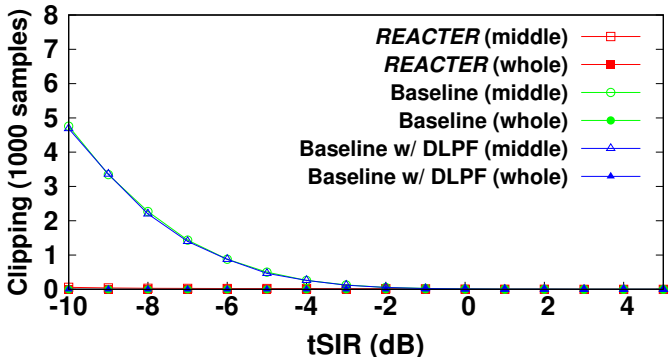

(a) Number of clipping during reception of an A-MPDU.

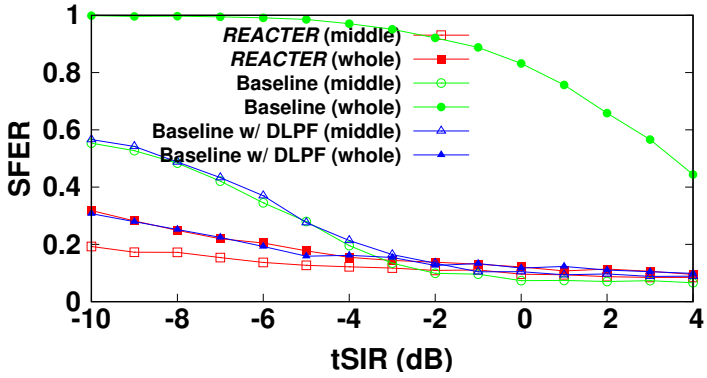

(b) SFER results.

Figure 4.14: SFER and the number of clipping events for according to tSIR, when time-domain interference partly or entirely overlaps with the desired A-MPDU.

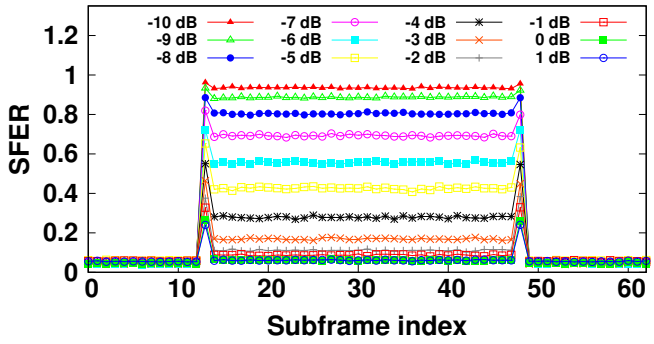

(a) Average SFER of *Baseline*.

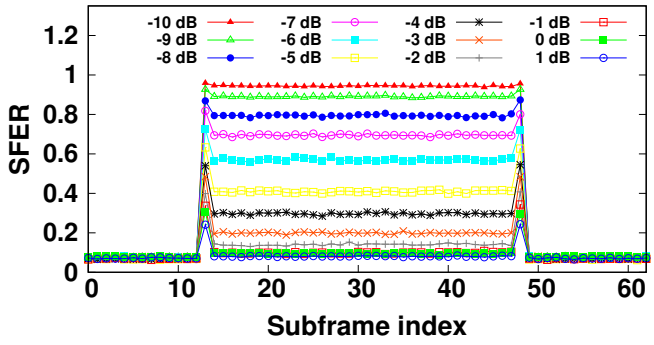

(b) Average SFER of *Baseline w/ DLPF*.

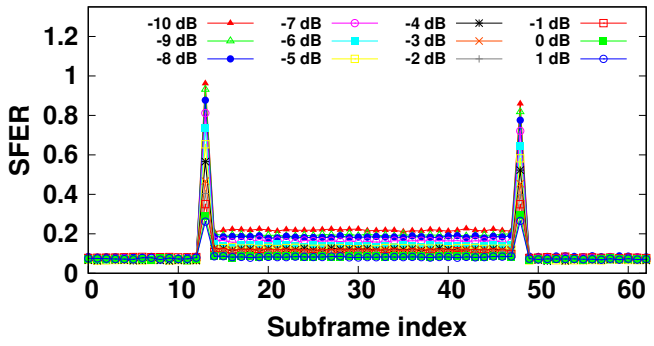

(c) Average SFER of *REACTER*.

Figure 4.15: Average SFER according to subframe index, when time-domain interference partly overlaps with the desired A-MPDU from the 13-th subframe to 48-th subframe.

4.4 Performance Evaluation

In this section, we comparatively evaluate the performance of *REACTER* under a wide range of tSIR, implementing *REACTER* into IEEE 802.11ac link-level simulator. We consider the same simulation environment as used in Section 4.3.3.

Fig. 4.14 shows the average SFER and the average number of observed clipping in a single A-MPDU. Time-domain interference overlaps on the time-domain with 1) the entire A-MPDU subframes (*whole*), or 2) the A-MPDU subframes only in the middle i.e., from the 13-th subframe to 48-th subframe (*middle*). We compare *REACTER* with the baseline 802.11ac of 80 MHz OCW, with and without 20 MHz DLPF for detection and synchronization.

When the time-domain interference signal entirely overlaps with the desired A-MPDU (*whole*), *Baseline* shows the worst performance due to packet detection and synchronization failure as shown in Fig. 4.14(b), where SFER is close to 1 for tSIR of below -4 dB. Since *Baseline w/ DLPF* and *REACTER* use 20 MHz RCF to extract the primary 20 MHz channel, packet detection and synchronization are not affected by the time-domain interference signal. However, quantization error slightly degrades the SFER performance gradually as tSIR decreases inevitably.

On the other hand, when time-domain interference comes in the middle of the A-MPDU (*middle*), clippings occur, thus leading to high SFER as demonstrated in Figs. 4.15(a)and 4.15(b). To suppress clipping, *REACTER* firstly observes whether clipping occurs in ADC circuit and adjusts AGC level by $P_{n+L} - P_n$ while receiving A-MPDU in real-time. It is worth to note that, assuming the latency of AGC circuit is approximately 4 μs, it takes totally 8 μs to observe clippings and reduce AGC level appropriately. Consequently, *REACTER* allows SFER to remain stable, only affected by quantization error due to reduced AGC level from the 14-th subframe as shown in Figs. 4.15(c) and 4.14(b). Moreover, after the 48-th subframe, *REACTER* lowers quantization error by recovering AGC level, based on the sample power difference as explained in Section 4.3.4.

4.5 Summary

In this chapter, we have verified that using DLPF extracting the primary 20 MHz channel significantly enhances the packet detection and synchronization performance when time-domain interference overlaps with the desired packets's preamble. Moreover, we have also observed that time-domain interference causes AGC failure, resulting in high quantization error and clipping at ADC, which degrades the reception performance. Therefore, we propose *REACTER*, a receiver architecture for eliminating time-domain interference in WLAN receiver, fully complying with 802.11 specification. Our extensive simulation using IT++ based IEEE 802.11 link-level simulator shows that *REACTER* enhances the reception performance significantly, by completely eliminating the impact of time-domain interference. We expect that *REACTER* will highly benefit the heterogeneous 5 GHz network, where the time-domain interference problem might be severer due to IEEE 802.11ax or LTE-LAA in the future.

Chapter 5

Concluding Remarks

5.1 Research Contributions

In this dissertation, we have addressed robust MAC and PHY layer strategies to enhance the achievable throughput by overcoming the existing real-world limitations in IEEE 802.11 WLANs. Detailed contributions of the dissertation are as follows.

In Chapter 2, we have built a *caudal noise* model and identified the cause of caudal loss. Based on our observation, we develop *STRALE*, achieving up to 2.9× higher throughput compared to the default setting of 802.11 in mobile environments, based on extensive simulations and prototype measurement. The significant growth of mobile WLAN devices will lead to the increase of the degree of mobility and hidden interferences, and hence, *STRALE* will highly benefit the future large-scale WLANs. We also envision *STRALE* to be applicable to any commercial 802.11 devices and to enhance the performances of high bandwidth-requiring applications such as file transfer and video streaming/conference on mobile devices.

In Chapter 3, we have verified that using bandwidth less than OCW might cause packet detection and synchronization failure, undesirable receive locking problem, and AGC failure due to time-domain interference not overlapping with the incoming desired signal on frequency domain. To solve this problem, we develop *RECONN*,

which intelligently adapts OCW using the frequency-domain information at receiver side. *RECONN* fully complies with 802.11 MAC and requires no hardware modification. Our prototype implementation in commercial 802.11ac devices demonstrates that *RECONN* achieves up to 1.85× higher throughput compared to baseline 802.11ac, by completely eliminating time-domain interference. We expect that *RECONN* will highly benefit the future large-scale and heterogeneous 5 GHz network, where the time-domain interference problem might be severer in the future.

In Chapter 4, we have shown that time-domain interference deteriorates packet detection and synchronization performance, causing undesirable receive locking problem. Moreover, since AGC is conducted during L-STF reception, time-domain interference overlapping with L-STF signal causes very low AGC level, thus leading to high quantization error at ADC. On the other hand, when time-domain interference comes in the middle of desired packet reception, the analog signal can exceed the dynamic range of ADC so that clipping can occur, thus leading to signal distortions. To cope with the observations, we develop *REACTER*, a receiver architecture for eliminating the impact of time-domain interference, fully complying with the 802.11 specifications. *REACTER* improves packet detection and synchronization performance using DLPF, and conducts real-time AGC during A-MPDU reception to reduce quantization error and to prevent clipping at ADC. Therefore, *REACTER* can be applied immediately upon the reception of the desired packets, without incurring any protocol overhead and latency. Our extensive simulations under a wide range of scenarios show that *REACTER* enhances the reception performance significantly by completely eliminating the impact of time-domain interference.

5.2 Future Work

Based on the results of the dissertation, there are several new research directions which require further investigation. We highlight some of them as follows.

First, regarding *STRALE*, our future work will include exploitation of *STRALE* in a variety of environments such as vehicular/vessel communication systems, where user mobility essentially is intensified.

Second, regarding *RECONN*, we will extend our work to provide more reliable packet reception, using power saving features during OCW switching. Moreover, coexistence of our work with emerging technologies such as LTE-LAA and IEEE 802.11ax, which support non-contiguous channel bonding and OFDMA structure, needs to be considered in order to maximize the benefit.

Finally, regarding *REACTER*, prototype implementation for feasibility verification of *REACTER* should be considered. Then, a study on MCS control to overcome time-domain interference problem will be included in our future work.

Bibliography

[1] IEEE 802.11ac, *Part 11: Wireless LAN Medium Access Control (MAC) and Physical Layer (PHY) specifications: Enhancements for Very High Throughput for Operation in Bands below 6 GHz*, IEEE Std., Dec. 2013.

[2] S. Byeon, K. Yoon, O. Lee, W. Cho, S. Oh, and S. Choi, "MoFA: Mobility-Aware Frame Aggregation in Wi-Fi," in *Proc. ACM CoNEXT*, Dec. 2014.

[3] O. Lee, W. Sun, J. Kim, H. Lee, B. Ryu, J. Lee, and S. Choi, "ChASER: Channel-Aware Symbol Error Reduction for High-Performance WiFi Sstems in Dynamic Channel Environments," in *Proc. IEEE INFOCOM*, May 2015.

[4] O. Lee, J. Kim, and S. Choi, "WiZizz: Energy Efficient Bandwidth Management in IEEE 802.11ac Wireless Networks," in *Proc. IEEE SECON*, Jun. 2015.

[5] IEEE 802.11ax-2016, *IEEE Proposed TGax draft specification, IEEE P802.11ax/D0.4*, IEEE Std., Aug. 2016.

[6] *Evolved Universal Terrestrial Radio Access (E-UTRA), Physical Layer Procedures (Release 13), document 3GPP TS36.213 V13.2.0*, 3GPP, Jun. 2016.

[7] B. Ginzburg and A. Kesselman, "Performance Analysis of A-MPDU and A-MSDU Aggregation in IEEE 802.11n," in *Proc. IEEE Sarnoff Symposium*, May 2007.

[8] X. He, F. Li, and J. Lin, "Link Adaptation with Combined Optimal Frame Size and Rate Selection in Error-Prone 802.11n Network," in *Proc. IEEE ISWCS*, Oct. 2008.

[9] K.-T. Feng, P.-T. Lin, and W.-J. Liu, "Frame-Aggregated Link Adaptation Protocol for Next Generation Wireless Local Area Networks," *EURASIP Journal on Wireless Communications and Networking*, vol. 10, Jun. 2010.

[10] O. Lee, J. Kim, J. Lim, and S. Choi, "SIRA: SNR-aware Intra-frame Rate Adaptation," *IEEE Commun. Lett.*, vol. 19, no. 1, pp. 90–93, 2015.

[11] S. I. Kim, H. S. Oh, and H. K. Choi, "Mid-amble Aided OFDM Performance Analysis in High Mobility Vehicular Channel," in *Proc. IEEE Intelligent Vehicles Symposium*, Jun. 2008.

[12] O. Bejarano, E. W. Knightly, and M. Park, "IEEE 802.11ac: From Channelization to Multi-User MIMO," *IEEE Commun. Mag.*, vol. 51, no. 10, pp. 84–90, Oct. 2013.

[13] E. Perahia and M. X. Gong, "Gigabit Wireless LANs: An Overview of IEEE 802.11ac and 802.11ad," in *Proc. ACM SIGMOBILE*, Sep. 2011.

[14] M. Park, "IEEE 802.11ac: Dynamic Bandwidth Channel Access," in *Proc. IEEE ICC*, Jun. 2011.

[15] M. X. Gong, B. Hart, L. Xia, and R. Want, "Channel Bounding and MAC Protection Mechanmsim for 802.11ac," in *Proc. IEEE Globecom*, Dec. 2011.

[16] L. Deek, E. Garcia-Villegas, E. Belding, S.-J. Lee, and K. Almeroth, "Joint Rate and Channel Width Adaptation for 802.11 MIMO Wireless Networks," in *Proc. IEEE SECON*, Jun. 2013.

[17] J. Herzen, R. Merz, and P. Thiran, "Distributed Spectrum Assignment for Home WLANs," in *Proc. IEEE INFOCOM*, May 2013.

[18] S. Jang, K. G. Shin, and S. Bahk, "Post-CCA and Reinforcement Learning based Bandwidth Adaptation in 802.11ac Networks," *IEEE Trans. Mobile Comput.*, vol. PP, no. 99, pp. 1–14, May 2017.

[19] L. Deek, E. Garcia-Villegas, E. Belding, S. J. Lee, and K. Almeroth, "Intelligent Channel Bonding in 802.11n WLANs," *IEEE Trans. Mobile Comput.*, vol. 13, no. 6, pp. 1242–1255, Jun. 2014.

[20] B. A. H. S. Abeysekera, M. Matsui, Y. Asai, and M. Mizoguchi, "Network Controlled Frequency Channel and Bandwidth Allocation Scheme for IEEE 802.11a/n/ac Wireless LANs: RATOP," in *Proc. IEEE PIMRC*, May 2014.

[21] S. Jang and S. Bahk, "A Channel Allocation Algorithm for Reducing the Channel Sensing/Reserving Asymmetry in 802.11ac Networks," *IEEE Trans. Mobile Comput.*, vol. 14, no. 3, pp. 458–472, Jun. 2014.

[22] B. Bellalta, A. Checco, A. Zocca, and J. Barcelo, "On the Interactions Between Multiple Overlapping WLANs Using Channel Bonding," *IEEE Trans. Veh. Technol.*, vol. 65, pp. 796–812, 2016.

[23] A. Faridi, B. Bellalta, and A. Checco, "Analysis of Dynamic Channel Bonding in Dense Networks of WLANs," *IEEE Trans. Mobile Comput.*, vol. 16, no. 8, pp. 2118–2131, Aug. 2017.

[24] C. Kai, Y. Liang, T. Huang, and X. Chen, "To Bond or not to Bond: An Optimal Channel Allocation Algorithm For Flexible Dynamic Channel Bonding in WLANs," in *arXiv:1703.03909v2*, Mar. 2017.

[25] J. Fang and I. T. Lu, "Efficient channel access scheme for multiuser parallel transmission under channel bonding in IEEE 802.11ac," *IET Communications*, vol. 9, no. 13, pp. 1591–1597, 2015.

[26] W. Wang, F. Zhang, and Q. Zhang, "Managing Channel Bonding with Clear Channel Assessment in 802.11 Networks," in *Proc. IEEE ICC*, May 2016.

[27] S. Byeon, C. Yang, O. Lee, K. Yoon, and S. Choi, "Enhancement of Wide Bandwidth Operation in IEEE 802.11ac Networks," in *Proc. IEEE ICC*, Jun. 2015.

[28] R. Karmakar, S. Chattopadhyay, and S. Chakraborty, "Channel Access Fairness in IEEE 802.11ac: A Retrospective Analysis and Protocol Enhancement," in *Proc. ACM MobiWac*, Nov. 2016.

[29] V. P. G. Jimenez, M. J. F.-G. Garcia, F. J. G. Serrano, and A. G. Armada, "Design and implementation of synchronization and AGC for OFDM-based WLAN receivers," *IEEE Trans. Consumer Electron.*, vol. 50, pp. 1016–1025, 2004.

[30] P. Singerl and C. Vogel, "A Fast and Accurate Automatic Gain Control for a Wireless Local Area Network Receiver," Tech. Rep., Oct. 2005.

[31] O. Jeon, R. M. Fox, and B. A. Myers, "Analog AGC Circuitry for a CMOS WLAN Receiver," vol. 41, pp. 2291–2300, 2006.

[32] T. M. Schmidl and D. C. Cox, "Robust Frequency and Timing Synchronization for OFDM," *IEEE Trans. Commun.*, vol. 45, pp. 1613–1621, 1997.

[33] S. Chang and B. Kelley, "Time Syncorhonization for OFDM-based WLAN Systems," *IET Electron. Letters.*, vol. 39, pp. 1024–1026, 2003.

[34] A. Troya, K. Maharatna, M. Krstic, E. Grass, U. Jagdhold, and R. Kraemer, "Efficient Inner Receiver Design for OFDM-based WLAN Systems: Algorithm and Architecture," vol. 6, pp. 1374–1385, 2007.

[35] D. Wang and J. Zhang, "Timing synchronization for mimo-ofdm wlan systems," in *Proc. IEEE WCNC*, Mar. 2007.

[36] The Network Simulator 3 – *ns*-3. http://www.nsnam.org/.

[37] Ath9k: Atheros Wireless Driver, http://wireless.kernel.org/en/users/Drivers/ath9k/.

[38] *STRALE* source code, https://github.com/pathetique/STRALE.git.

[39] IEEE 802.11, *Part 11: Wireless LAN Medium Access Control (MAC) and Physical Layer (PHY) specifications*, IEEE Std., Mar. 2012.

[40] E. Perahia and R. Stacey, *Next Generation Wireless LANs: Throughput, Robustness, and Reliability in 802.11n*, 1st ed. Cambridge University Press, 2008.

[41] IEEE P802.11 WLANs, *TGn Channel Models*, IEEE 802.11-03/940r4, May 2004.

[42] HostAP: IEEE 802.11 AP, IEEE 802.1X/WPA/WPA2/EAP/RADIUS Authenticator, http://hostap.epitest.fi/hostapd/.

[43] Intel WiFi Link 5300, http://www.intel.com/products/wireless/adapters/5000/.

[44] Iperf: TCP/UDP Bandwidth Measurement Tool. http://dast.nlanr.net/Projects/Iperf/.

[45] Linux 802.11n CSI Tool, http://dhalperi.github.io/linux-80211n-csitool/.

[46] A. Bhartia, Y.-C. Chen, and L. Qiu, "Harnessing Frequency Diversity in Wi-Fi Networks," in *Proc. ACM MobiCom*, Sep. 2011.

[47] R. Steele, *Mobile Radio Communications*, 1st ed. IEEE Press, 1995.

[48] Yin, W., Bialkowski, K., Indulska, J., and Hu, P., "Evaluation of MadWifi MAC Layer Rate Control Mechanisms," in *Proc. IEEE IWQoS'10*, Jun. 2010.

[49] Linux Wireless Tools, http://linuxwireless.org/.

[50] D. Tse and P. Viswanath, *Fundamentals of Wireless Communication*, 1st ed. Cambridge University Press, 2005.

[51] D. Halperin, W. Hu, A. Sheth, and D. Wetherall, "Predictable 802.11 Packet Delivery from Wireless Channel Measurements," in *Proc. ACM SIGCOMM*, Sep. 2010.

[52] L. Hentilä, P. Kyösti, M. Käske, M. Narandzic, and M. Alatossava, MATLAB implementation of the WINNER Phase II Channel Model ver1.1, http://www.ist-winner.org/phase_2_model.html.

[53] R. Anwar, K. Nishat, M. Ali, Z. Akhtar, H. Niaz, and I. A. Qazi, "Loss Differentiation: Moving onto High-Speed Wireless LANs," in *Proc. IEEE INFOCOM*, May 2014.

[54] M. Heusse, F. Rousseau, G. Berger-Sabbatel, and A. Duda, "Performance Anomaly of 802.11b," in *Proc. IEEE INFOCOM*, Apr. 2003.

[55] I. Tinnirello and S. Choi, "Temporal Fairness Provisioning in Multi-Rate Contention-Based 802.11e WLANs," in *Proc. IEEE WoWMoM*, Jun. 2005.

[56] National Instrument, "LabVIEW Communications 802.11 Application Framework White Paper," NI, Technical Report, 2015.

[57] M. Morelli, C. C. J. Kuo, and M. O. Pun, "Synchronization Techniques for Orthogonal Frequency Division Multiple Access (OFDMA): A Tutorial Review," *Proceedings of the IEEE*, vol. 95, no. 7, pp. 1394–1427, 2007.

[58] V. P. G. Jimenez, M. J. F.-G. Garcia, F. J. G. Serrano, and A. G. Armada, "Design and Implementation of Synchronization and AGC for OFDM-based WLAN Receivers," *IEEE Trans. Consumer Electron.*, vol. 50, pp. 1016–1025, 2004.

[59] R. Gummadi, D. Wetherall, B. Greenstein, and S. Seshan, "Understanding and Mitigating the Impact of RF Interference on 802.11 Networks," in *Proc. ACM SIGCOMM*, Aug. 2007.

[60] IT++. [Online]. Available: http://itpp.sourceforge.net/

[61] IEEE P802.11 WLANs, *TGac Channel Models*, IEEE 802.11-09/308r12, Mar. 2010.

[62] J. Proakis and M. Salehi, *Digital Communications*, 5th ed. McGraw-Hill Education, 2007.

[63] M. J. M. Pelgrom, *Analog-to-digital conversion*, fisrt ed. Springer, 2013.

[64] M. Yoshioka, M. Kudo, T. Mori, and S. Tsukamoto, "A 0.8 V 10b 8OMS/s 6.5 mW Pipelined ADC with Regulated Overdrive Voltage Biasing," in *Proc. IEEE ISSCC*, Feb. 2007.

[65] B.-M. Min, P. Kim, D. Boisvert, and A. Aude, "A 69 mW 10 b 80 MS/s pipelined CMOS ADC," in *Proc. IEEE ISSCC*, Feb. 2003.

[66] T. Jiang and Y. Wu, "An Overview: Peak-to-average Power Ratio Reduction Techniques for OFDM Signals," *IEEE Trans. Broadcast.*, vol. 54, pp. 256–268, 2008.

초 록

스마트폰과 태블릿 PC 등의 휴대용 장치의 폭팔적인 성장에 힘입어, Wi-Fi로 흔히 알려진 IEEE 802.11 표준 기반 무선랜(WLAN, wireless local area network)은 낮은 비용으로 높은 전송률을 지원하면서, 일상생활에서는 없어서는 안될 중요한 기술로 자리매김 하고 있다. 이러한 두드러진 기술적 성장과 보급을 통해 최근 무선랜의 물리 전송 계층(PHY, physical layer)은 송수신에서 여러 개의 안테나를 사용하는 다중 입력 다중 출력 (MIMO, multi-input multi-output) 시스템, 20 MHz 단위의 채널을 여러 개 묶어서 사용하는 채널 결합 (channel bonding) 기술 등을 지원하면서, 5 GHz 주파수 대역에서 단일 사용자에게 Gb/s 에 이르는 높은 수율을 제공하고 있다. 또한, 매체접근제어 (MAC, medium access control) 계층의 효율을 극대화하는 핵심 기술로써, IEEE 802.11 표준은 여러 MAC 프로토콜 데이터 단위 (MPDU, MAC protocol data unit)를 결합하여 전송하는 프레임 결합기술(A-MPDU, aggregate MPDU)을 정의하고 PHY 와 MAC에서 발생하는 오버헤드를 효과적으로 줄여나가고 있다.

본 학위논문에서는 실사용 수율 증대를 위해 다음과 같은 세 가지 전략을 고려한다. (1) 이동성 인식 PHY 전송률 및 A-MPDU 길이 제어, (2) 수신기 구동 채널 폭 (OCW, operating channel width) 적응, (3) 주파수 영역에서 수신해야하는 신호와 중첩되지 않는 시간영역 간섭 (time-domain interference) 제거를 위한 수신 구조.

첫째, 휴대용 장치에서 생성되는 모바일 데이터 트래픽 볼륨의 상당한 증가로 인해 무선랜 통신 환경이 변화하고 있다; 단일 프레임 수신 기간 동안 무선랜

채널 상태가 더 이상 코시-정적 (quasi-stationary)이 아니다. 특히, 채널이 점진적으로 변해가는 환경에서, 프레임 전송 지속 시간을 크게 증가시키는 A-MPDU의 사용으로 인해 프리엠블에서 획득한 채널 상태 정보(CSI, channel state information)가 A-MPDU 의 뒷부분을 성공적으로 디코딩하기에 더이상 유효하지 않다. 본 학위논문에서는 이 문제를 해결하기 위해, 광범위한 측정을 통해서 이동성을 고려한 무선 채널 동역학을 분석하고, 이동성이 A-MPDU 수신에 어떤 영향을 미치는지 상세히 조사하기 위해 I-Q 평면에서의 잡음 벡터와 이동성의 영향을 나타내는 모델을 제안한다. 또한 모델 및 실측 기반의 분석을 토대로, 우리는 쉽게 구현 가능하면서도, 표준을 준수하고 이동성을 인식하여 PHY 전송률과 A-MPDU의 길이를 적응적으로 조절하여 사용하는 *STRALE* (standard-compliant and mobility-aware PHY rate and A-MPDU length adaptation) 기법을 개발한다. IEEE 802.11ac Network Simulator 3 (ns-3) 기반의 다양한 실측과 상용 IEEE 802.11n 장치를 활용한 프로토타입 구현 기반의 광범위한 실측을 통해 *STRALE*가 IEEE 802.11 표준에 따른 고정된 A-MPDU의 길이 설정과 비교하여, 최대 2.9배의 높은 수율을 제공하는 것을 입증한다. *STRALE*는 구현이 용이하고, 송신기에서의 간단한 장치 드라이버 업데이트를 통해 모든 종류의 플랫폼에 쉽게 적용될 수 있다.

둘째, IEEE 802.11ac는 필수 기능으로 20, 40 및 80 MHz의 대역폭 송수신을 지원하고, 선택적으로는 160 MHz 대역폭을 제공한다. 이러한 넓은 대역폭을 사용하여 패킷을 송수신하기 위해서 802.11ac 장치는 고속 푸리에 변환 (FFT, fast Fourier transform) 크기, 즉 구동 채널폭(OCW, operating channel width)이라 불리는 기저대역의 대역폭의 크기를 증가시킬 필요가 있다. 그러나 우리는 실험결과를 통해, 수신기의 구동 채널폭을 변경하지 않고 대역폭을 적응적으로 사용하면, 주파수축에서 원하는 신호와 겹치지 않는 시간 영역 간섭 간섭으로 인해 성능이 크게 저하되는 다양한 상황을 검증한다. 본 학위논문에서는 이러한 문제를 해결하기 위해 *RECONN* (Receiver-driven operating channel width adaptation), 구현이 용이하고 표준을 준수하는 수신기 구동 OCW 적응적 사용 기법을 제안한다. 상업용 802.11ac 장치를 활용한 프로토타입 구현은 *RECONN* 이 시간 영역

간섭을 완전히 제거하여 최대 1.85배 높은 수율을 달성하는 것을 보인다. 본 연구는 802.11ac 시스템에서 시간 영역 간섭 문제를 분석 및 파악하고, OCW 를 적응적으로 사용하여 이를 해결하는 첫 연구 결과이다.

마지막으로, IEEE 802.11ac 환경에서 시간 영역 간섭이 (1) 패킷 탐지 및 동기화 실패, (2) 바람직하지 않은 수신 잠금 문제, (3) 자동 이득 제어 (AGC, automatic gain control) 실패 문제를 유발한다는 관찰에 기초하여, 우리는 *REACTER* (Receiver architecture for eliminating time-domain interference), 시간 영역 간섭의 영향을 완전히 제거하는 수신 구조를 제안한다. *REACTER*는 시간 영역 간섭에 영향을 받지 않는 원하는 프리앰블 신호를 디지털 필터를 활용하여 추출하고, A-MPDU 수신 시간 동안 적응적으로 AGC 레벨을 조절 하여 간섭에 대한 복원성이 우수한 A-MPDU 수신 성능을 제공한다. 우리는 제안한 수신 구조를 IT++ 기반 링크 수준 시뮬레이터를 이용하여 광범위하게 평가하고, 그 결과 *REACTER*가 시간 영역 간섭의 영향을 완전히 제거하여 패킷 수신 성능을 크게 향상시는 것을 보인다.

요약하면, 본 학위논문에서는 두 가지 실재하는 문제를 다양한 시뮬레이션과 광범위한 측정을 통해 검증하고, 나아가 이를 해결하여 수율을 증대시키는 강력한 알고리즘을 제안한다. 기존의 상업용 802.11n/ac 장치에서 프로토타입을 구현함으로써, 제안된 알고리즘이 IEEE 802.11 MAC를 완전히 준수하고 PHY 수정을 필요로 하지 않음을 보여줄 뿐만 아니라, 간단한 장치 드라이버 업데이트를 통해 다양한 하드웨어 플랫폼에 쉽게 적용될 수 있다는 것을 검증한다. 또한 매우 낮은 비용과 복잡성을 달성하면서도, 동시에 근본적으로 시간 영역 간섭의 영향을 제거하여 광대역 전송에서의 수신 성능을 크게 향상시키는 새로운 수신 구조를 제안한다.